Field Observations and Laboratory Simulation of the Lifted Temperature Minimum

A Thesis

Submitted for the Degree of

DOCTOR OF PHILOSOPHY

in the Faculty of Engineering

by

MUKUND V.

ENGINEERING MECHANICS UNIT
JAWAHARLAL NEHRU CENTRE FOR ADVANCED SCIENTIFIC RESEARCH
(A Deemed University)
Bangalore – 560 064

AUGUST 2008

To Appa and Amma

DECLARATION

I hereby declare that the matter embodied in the thesis entitled "**Field Observations and Laboratory Simulation of the Lifted Temperature Minimum**" is the result of investigations carried out by me at the Engineering Mechanics Unit, Jawaharlal Nehru Centre for Advanced Scientific Research, Bangalore, India under the supervision of Prof. K. R. Sreenivas and that it has not been submitted elsewhere for the award of any degree or diploma.

In keeping with the general practice in reporting scientific observations, due acknowledgment has been made whenever the work described is based on the findings of other investigators.

Mukund V.

CERTIFICATE

I hereby certify that the matter embodied in this thesis entitled "**Field Observations and Laboratory Simulation of the Lifted Temperature Minimum**" has been carried out by Mr. Mukund V. at the Engineering Mechanics Unit, Jawaharlal Nehru Centre for Advanced Scientific Research, Bangalore, India under my supervision and that it has not been submitted elsewhere for the award of any degree or diploma.

Prof. K. R. Sreenivas
(Research Supervisor)

Acknowledgements

This thesis would be incomplete without an expression of gratitude to the many people, who directly or indirectly, made it possible. I thank,

My parents. I owe them more than I could possibly express. They encouraged me to pursue a career in research in spite of a lot of well meant advice that came their way, to stop me from making such a 'serious mistake'. I will always value that.

My wife Sanju. None of this would have been possible without her support, encouragement and love. She sacrificed a lot so that that I could pursue my PhD. And always had to put up with my disappearing for considerable lengths of time, and at odd hours, to conduct my field observations. There must have been countless occasions when I told her that I was very busy just then, but surely would be quite free after a couple of weeks. She has waited for over six years, with patience and good humor, for those two weeks to pass.

Prof. K.R. Sreenivas, my thesis advisor. His expertise in experiments and remarkable physical insights were crucial for my work. I especially value the freedom, both intellectual and otherwise, that he gave me for carrying out my work.

Prof. Narasimha, for taking a keen interest in my work. His comments and suggestions gave direction to the work.

Prof. Vasudeva Murthy and Prof. J. Srinivasan, for many insights and discussions regarding my work.

The Chairman, Dept. of Aerospace Engineering, IISc, for allowing me use of the airfield for the field observations, and the airfield room to stow away the experimental paraphernalia.

Srikrishna Badiger, who assisted me during the initial year during which field observations were made.

Mallappa, who helped me during the final, more arduous stage of the field observations. He also assisted in the laboratory simulations.

Punit, who designed the laboratory setup, which, with a few modifications, was used in my work. And for some nice times in JNC.

Vanaja Kumar, my mother-in-law, who has helped me in so many ways. She especially came down to Bangalore during the final week of thesis writing to help around in the house so that I could just concentrate on writing the thesis. She also

went through portions of the thesis.

N. Selvakumar, my father-in-law, for the constant support and encouragement. He also assiduously went thorough a pre-final draft of the thesis.

Ananya, my daughter, all of two and a half years old, and my stress buster.

Anand, my brother. For, well, being my brother.

Mani. I cannot thank him enough. I had a great time in JNC when he was around. On numerous occasions, he took time off from his own problem to help me out in the field.

Faraz, for helping me out in the field on many occasions even though he was extremely busy with his own work at JNC. And for some really profound and entertaining discussions.

Prof. Meulenberg, visiting professor, Dept. of Physics, IISc, for going out of the way to make emissivity measurements for me. And some nice scientific discussions besides.

Prof. Leclercq, IEMN, Lille, France, for generously and promptly sending me a couple of microradiometers for use in the field experiments.

Murugan, for help relating to some work in the field.

Vivekanand. His help in the last year, in numerous matters both scientific and extra-scientific, was invaluable.

Sameen, for some stimulating discussions, and advice.

Vinod, Shreyas, Pinaki and Kaushik. Probably characters as diverse as these are difficult to get within a small unit like ours. Besides assisting me in several matters, they made my stay at JNC immensely enjoyable.

Arokiyanathan, technician at the workshop, who went beyond the call of duty in helping me out with the machining, often suggesting ideas that have worked wonders.

Prof. Poston and Prof. Vaidya for some splendid lectures and discussions on subjects close to my heart.

Ratul, Rajapandiyan, Harish, Anubhab, Vineetha, Shankar, Debranjan, Ponnulakshmi, Ashish and others at JNC, who have besides helping me on numerous occassions, have made my stay at JNC far more enjoyable than it would otherwise have been.

Contents

Abstract

The present work is concerned with a peculiar vertical temperature distribution that sometimes develops over the ground during calm and clear nights. After sunset, typically an inversion profile is expected to form, in which a minimum in the vertical temperature profile occurs at the ground. However, on calm and clear nights, a temperature profile often develops, where the minimum of temperature occurs a few decimeters above the ground. This phenomenon, first reported by the Indian agro-meteorologist Ramdas in 1932, is identified by various names like 'The Lifted Temperature Minimum', 'The Elevated Temperature Minimum', 'The Ramdas Effect', etc. The lifted minimum is characterized by its height and intensity, the height of the minimum simply being the height above the ground at which the minimum occurs, while the intensity of the minimum is the difference between the ground temperature and the minimum temperature.

In 1993, a model (the VSN model) was proposed, which for the first time, gave a satisfactory explanation for the phenomenon, and also predicted the dependence of the height and intensity of the minimum on various parameters, including surface parameters like ground emissivity and ground cooling rate. It makes the prediction that the lifted minimum cannot develop for a surface emissivity of exactly unity. For calculating the radiative fluxes, this model used a broadband flux emissivity scheme in which the flux emissivity of air is taken only as a function of water vapor path length. In an independent work, a robust radiation code was developed to accurately predict near surface radiative cooling rates. A band model was used to calculate the radiative fluxes. Unlike the flux emissivity model mentioned before, the band model takes the absorption coefficient to be a function not only of water vapor path length, but also of pressure, temperature and wave number. This band model code also predicts a lifted minimum profile for a certain range of the surface parameters. In particular, it allows for a minimum formation even for a surface emissivity of unity. Both flux-emissivity model and band-model indicate that the

lifted temperature minimum occurs due to the interaction of radiative heat transfer with other modes of heat transfer. In this sense, the lifted temperature minimum is an example of a broader class of problems in which radiation plays an important role in determining the temperature distribution and heat transfer in a participating medium. Examples include heat transfer in stellar atmospheres, and glass melts in furnaces.

The present work involves field observations and laboratory simulations of this phenomenon. The field observations were carried out in an airfield situated within the campus of the Indian Institute of Science, Bangalore, India. The field observations were carried out especially with a view to address the role of the surface parameters: surface cooling rate, and surface emissivity. To address the role of these parameters, a circular concrete patch (9 meters in diameter) was laid in the airfield to serve as a reference surface. This could be considered as a high emissivity, low cooling rate surface. This concrete patch was then modified to obtain three other surfaces: (1) a surface with low emissivity and low cooling rate, (2) a surface with high emissivity and high cooling rate, and (3) a surface with low emissivity and high cooling rate. Observations were then carried out on these surfaces. Quantities measured include: the temperature at various heights, ground temperature, wind speed, humidity and net radiation. The dependence of the phenomenon on wind speed, turbulence levels, and the surface parameters is demonstrated. In particular, it is observed that lower surface emissivity results in more intense minima, while a higher ground cooling rate results either in formation of a very weak lifted minimum very close to the ground, or an inversion profile, with the minimum temperature occurring at the ground. The temperature data are also used to estimate near surface temperature gradients and the infrared flux divergence. Wherever possible, the results are compared with the VSN and band models.

If the phenomenon can be reproduced in the laboratory, it can be studied in a more controlled manner than would be possible in field observations. Now, in the atmosphere, at night, the air layers in the inversion layer interact radiatively with a cold radiation source, the effective sky temperature on clear nights, being about 15-20 °C lower than the near surface temperatures. In this sense, the inversion decouples the convection/conduction and radiation boundary conditions. In typical laboratory experiments involving two parallel plates with a temperature difference being maintained between them, it is because of the lack of such a decoupling that

a strong radiative influence on the temperature profiles is not seen. Moreover, with such a set up, if a stable temperature profile is established in the test section (with the top boundary being maintained at a higher temperature than the bottom boundary), a radiative heating is produced in the gas close to the lower boundary, which cannot result in a lifted minimum profile. Keeping these factors in view, for the laboratory simulations an experimental set up was designed and fabricated in which such a decoupling is achieved. In the present experiments an easily measurable influence of radiative effects on the base temperature profiles is observed. This experimental set up is useful in investigating a variety of problems involving conduction or convection in a radiatively participating medium; for example, the role of radiation in stabilizing unstable layers.

Using this set up, lifted minimum profiles are obtained in the laboratory. The experiments show the necessity of a low temperature radiative source in producing the lifted minimum. It is also shown that a lower emissivity for the 'ground' surface results in more intense minima, in agreement with the field observations.

This thesis is structured as follows:

Chapter 1: In this chapter, the phenomenon of the 'Lifted Temperature Minimum' is introduced. The previous work done on the lifted minimum, both observations and theory, is surveyed. Finally, the motivation for, and objectives of the present work are discussed.

Chapter 2: This chapter deals with manner in which the field observations were carried out. Details of the observation site, surface modifications and instrumentation are included.

Chapter 3: The results of the field observations are discussed in detail here.

Chapter 4: The laboratory simulations are considered in this chapter. The literature relating to the simulations is surveyed. This is followed by a discussion of the laboratory set up, after which the results obtained in the laboratory are discussed.

Chapter 5: The conclusions resulting from this work are presented.

List of Figures

List of Tables

CHAPTER 1

INTRODUCTION

The near surface vertical distribution of air temperature in the atmosphere is an important aspect of studies in agricultural and boundary layer meteorology. Typical clear weather temperature profiles are shown in figure 1.1. Though there is some dependence on local conditions, the profiles shown in the figure are typical of many parts of the world. The ground surface is a much stronger absorber and emitter of radiation than air. Hence, during the day time, with clear skies, the ground absorbs radiation much more strongly than the air above it, resulting in the ground being hotter than the overlying air layers. The resulting temperature profile is shown in figure 1.1 as profile-a. The temperature decreases rapidly with height in the lowest layers, with very high gradients in the first few centimeters. This is followed by the convective mixed layer, in which the temperature changes very little, and at greater heights, the temperature follows a more or less constant lapse rate. Similarly, at night time, one would expect the ground to cool faster than the air above it, resulting in a temperature profile with a local minimum of the temperature occurring at the ground. Such an inversion profile is shown in figure 1.1 as profile-b. However, about seventy years ago, Ramdas & Atmanathan (1932) reported temperature profiles on calm clear nights in Pune and other stations in India, which showed that the minimum temperature did not occur at the ground as in profile-b, but a few decimeters above the ground as in profile-c. This phenomenon is often called the 'Lifted Temperature Minimum', henceforth abbreviated to lifted minimum. Other names such as 'Raised minimum', 'Elevated minimum', 'Ramdas effect', etc. have also been used in the literature to describe this. Shown

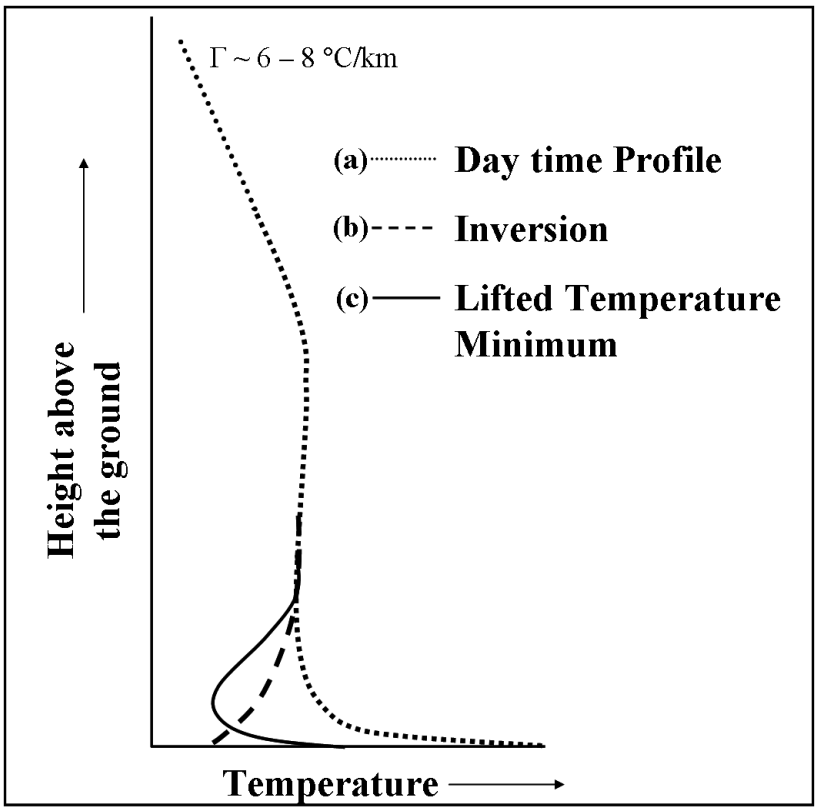

Figure 1.1: A schematic representation of vertical temperature profiles in the atmosphere. Typically, after sunset, an inversion profile is expected to form, with the minimum temperature on the ground. But on calm and clear nights, a 'lifted temperature minimum' profile often forms in which the minimum temperature occurs a few decimeters above the ground.

in figure 1.2 is a closer view of the lifted minimum profile. The lifted minimum may be characterized by two parameters: its height and intensity. The intensity of the minimum is the difference between the ground temperature and the minimum temperature. The height of the minimum is simply the height at which the minimum temperature occurs. Also shown in figure 1.2 are typical values of the height and intensity of the minimum as reported in the observations of Ramdas.

An understanding of the nocturnal air temperature distribution near the ground is important for several reasons. The temperature field near the ground is an im-

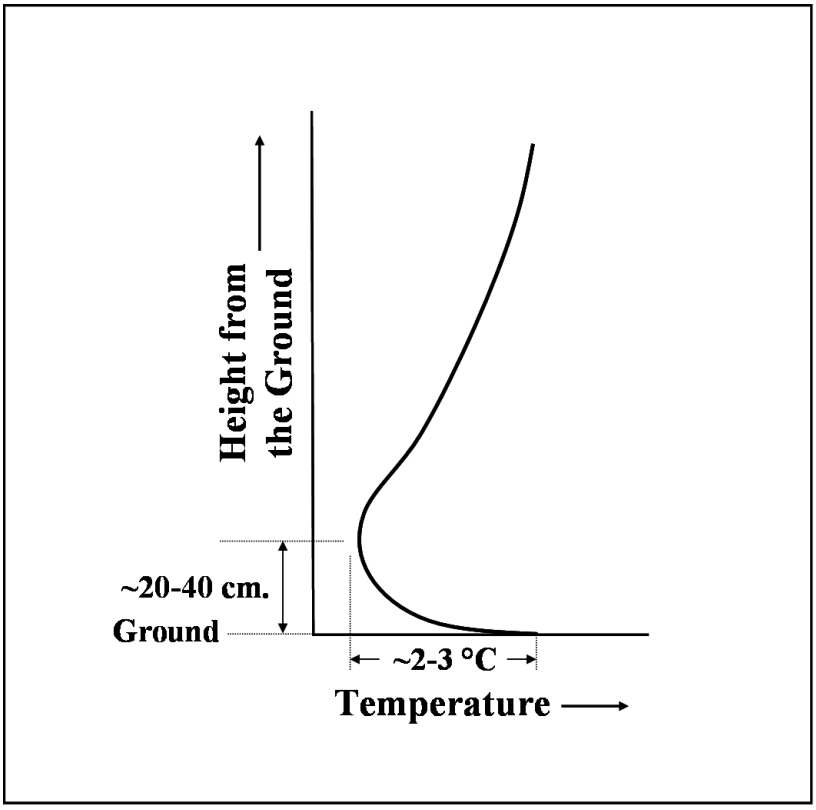

Figure 1.2: Detail of the Lifted Minimum. The height at which the minimum temperature occurs is called the height of the minimum, while the difference between the ground temperature and the minimum temperature is called the intensity of the minimum. Also shown are typical values of height and intensity as reported by Ramdas (1932).

portant factor in determining the environment in which crops grow, influencing for example, the formation of fog and frost. In fact, this was the motivation for the observations made by Ramdas & Atmanathan (1932). Lake (1956a) quotes studies showing that in tomato plants, frost first affects fruit well above ground, as the temperature at a few tens of centimeters above the ground can be below freezing even when the temperatures at the ground and screen height (4 ft or 1.22 m) are well above freezing. Another study (Yamada & Takahashi (2004)) examines the influence of the lifted minimum on frost damage to flower buds. The difference

between the temperature at screen height and right at the ground has other repercussions. For example, there is a need for more accurate radiation calculations in climate models as climate problems are sensitive to small changes in radiation quantities (Warner & Ellingson (2000)), but as Garratt (1995) has shown, the relation between the temperature right at the surface and at screen or model height can significantly affect infrared global radiant flux estimates. The phenomenon should also be important for retrieval of correct surface temperatures from remotely sensed satellite data, especially as temperatures are required with increasing degrees of accuracy for global climate modeling. Finally, an understanding of even a singular phenomenon in a field, advances our basic knowledge in the area as a whole.

As will be discussed in later sections, the observations as well as theoretical work on this phenomenon indicate that the lifted minimum profile occurs basically due to a distortion of the basic inversion profile by a strong radiative cooling near the ground. Also, the air layers below the minimum point are unstably stratified, and radiation plays a role in stabilizing this layer. Thus, the phenomenon is basically due to an interaction of radiation with the other forms of heat transfer. In this sense, this lifted minimum is only an example of a broad class of problems in which radiation plays an important role in determining the heat transfer and temperature distribution in a participating medium.

Insights gained from the study of the phenomenon can be carried over to such problems. Examples include heat transfer in stellar atmospheres and glass melts in furnaces. In glass melts for example, it desirable to maintain a uniform temperature in the molten glass. Radiative effects (with the molten glass as the participating medium) have to be taken into account to ensure this. It is interesting to speculate that something very similar to the lifted minimum phenomenon may be occurring in the problem of coronal heating (Aschwanden (2004)) in the sun. This is a

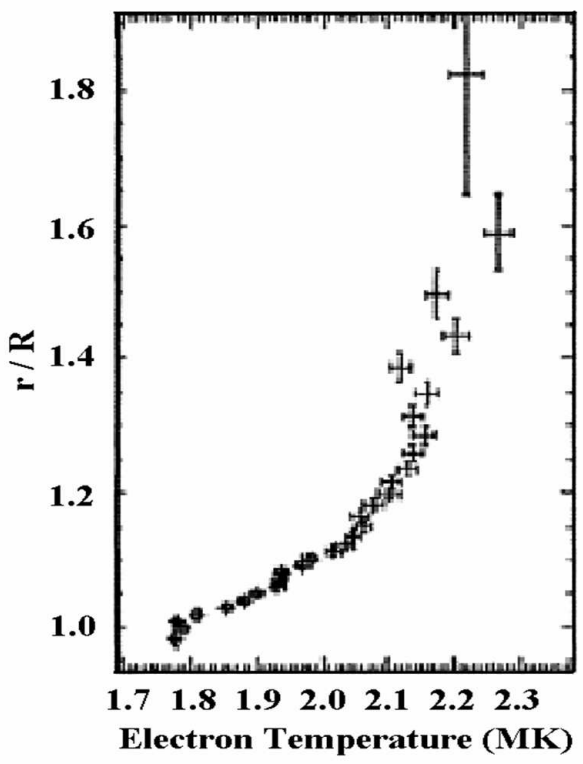

Figure 1.3: Experimentally determined temperature profile in the sun's corona showing coronal heating.

long outstanding problem in solar physics which relates to the question of why the temperature of the Sun's corona is millions of kelvin higher than that of the surface (see figure 1.3). The high temperatures require energy to be carried from the solar interior to the corona by non-thermal processes, because the second law of thermodynamics prevents heat from flowing directly from the solar photosphere, or surface, at about 5800 kelvin, to the much hotter corona at about 1 to 3 million K (parts of the corona can even reach 10 million K).

1.1 Historical Overview

1.1.1 Observations

As mentioned earlier, the first report of the LTM was made by Ramdas and Atmanathan in 1932, based on their observations at four Indian stations, namely Pune, Agra, Madras and Bhadrachalam. Their reports were received with skepticism for two main reasons. In the first place, the prevailing view was that on clear nights, an inversion always developed above the ground, with the temperature minimum at the ground. This view had the support of observations, though temperature measurements were not usually made below the screen height of 4 feet (around 1.2 meters). Secondly, with a LTM profile, the air layer immediately next to the ground (called the Ramdas layer) would be unstable. Taking typical observed values of 2°C and 30 cm for the height and intensity of the minimum, gives a Rayleigh number of about 10^6 for the Ramdas layer. As the critical Rayleigh number for the onset of convection is around 1000 (depending on boundary conditions), the layer should be unstable, and vigorous convection should destroy such a profile, even assuming that it had arisen as a transient. So, it was believed that faulty instrumentation or advection of colder air from the environs was the cause of the reported profiles. This was in spite of the fact that further work by Ramanathan & Ramdas (1935) had led to the conclusion that the effect was not due to advection. More observations by researchers like Lake (1956a) and Raschke (1957) and Oke (1970) removed any remaining doubts about the phenomenon.

Raschke (1957) carried out a series of careful and thorough measurements at Pune, India. He also made some measurements on the bare and flat top of Chaturshringi hill at Pune, where advection could not have been present. Based on his

observations, he distinguished between three types of temperature profiles near the ground (see figure 1.1): (i)The normal radiative type (usual inversion), occurring on clear nights with wind having the minimum on the ground, (ii) Special radiation type (LTM), with the minimum some height above the ground, occurring on calm and clear nights. (iii)Advective type, with the temperature minimum some height above the ground, occurring on clear or cloudy nights whenever there was advection of colder air from the environs. In his observations, whenever the LTM profiles occurred, the wind speed at a height of 20 centimeters above the ground, as a rule, was less than a threshold value of about 50 cm/s. If the wind speed exceeded this threshold value, then the lifted minimum was replaced by a normal inversion, with the minimum temperature being at the ground. If the wind velocity fell below this value, then the air layers near the ground cooled within a few minutes relative to the soil surface and a minimum temperature moved up in height. The typical height of the minimum was between 1 cm. to a few decimeters above the surface. The LTM profiles were marked by large temperature fluctuations at a height of about 1 m. (and to a lesser extent, at a height of 10 m.). Such fluctuations were not present in the other two types of temperature distributions. Raschke could get rid of the lifted minimum by vigorously waving a thin plywood sheet nearby, suggesting that the phenomenon is sensitive to turbulent transport. After the waving was stopped, the lifted minimum reappeared in less than a minute.

Oke made his observations at a couple of sites at Ontario, Canada. He found that on flat bare soil, the lifted minimum was usual whenever the skies were clear and wind speed at a height of 25 cm. was less than 1 m/s. The height of the minimum ranged from a few centimeters up to 50 cm., while intensity often exceeded 3°C. On the other hand, rough bare soil (obtained by harrowing the soil surface), showed only infrequent and uncertain indications of development of a lifted mini-

mum. The height of the minimum never rose above 2.5 cm. and its intensity never exceeded 0.2°C, even with wind speeds lower than 40 cm/s. This again indicates that the phenomenon could be suppressed by increased turbulent transport.

Other observers of the phenomenon include Albani (1951), Brawand & Kohnke (1952), Fleagle & Badgley (1952), Jenny (1953), Szakály (1957), Funk (1960), Nijliks & Moldau (1960) and Lützke (1960). Kondratyev (1972) remarks "Temperature minimum at heights of 3-15 cm. above the earth's surface are observed in different parts of the globe and over different underlying surfaces. The most recent experiments of this kind prove that this temperature minimum can occur in the absence of advection and phase transformation of water, which were previously considered responsible for its development".

1.1.2 Theory

Till the work of Vasudeva Murthy *et al.* (1993), there was no satisfactory explanation of the phenomenon. Though Lettau (1979) has suggested turbulent convection to be the mechanism, most investigators (Lake (1956a), Lake (1956b), Raschke (1957), Oke (1970), Kondratyev (1972)) believed radiation to be the cause of the lifted minimum. But none of the earlier attempts to explain the lifted minimum were entirely satisfactory. Zdunkowski (1966) followed up a suggestion that a haze layer above the ground could lead to the strong radiative cooling that might explain the phenomenon. However, to produce the lifted minimum, Zdunkowski had to assume values of turbulent diffusivity which were *less* than the molecular value by a factor of up to 18. Moreover, no evidence of a haze layer has been found during many of the observations of the phenomenon (e.g Raschke (1957), Oke (1970)). Computations of Coantic & Seguin (1971) show a maximum in the radiative flux

divergence profiles at a height of order of 10 cm., and they suggest that this could be responsible for the lifted minimum. However, they assumed a monotonic temperature profile in their calculations, and hence it is not clear if such a maximum in the radiative flux divergence would remain in the non-monotonic profile characteristic of the lifted minimum. They also did not have any direct computations of height or intensity of the minimum to compare with observations. Further, they assumed steady state conditions, as assumption that is not valid in the atmospheric boundary layer in early mornings, late evenings or nights (see e.g Kondo (1971)).

As mentioned, Vasudeva Murthy *et al.* (1993) were the first to propose a self-consistent model (the VSN model) for the phenomenon that appears to be in good agreement with observations. They considered energy balance near the ground, with the radiative fluxes being modeled by the flux emissivity method (e.g. Liou (1980)), which is a simple model for longwave radiation which assumes the absorption coefficient to be a function of optical path length only. They solved the full coupled air-soil problem in which the ground temperature $T_g(t)$ comes out as part of the solution. They also used an alternative but equivalent approach in which the ground temperature is specified as

$$T_g(t) = T_{g0} - \beta\sqrt{t} \tag{1.1}$$

where β is given by

$$\beta = \frac{2R_N}{\sqrt{\pi\rho c\kappa}} \tag{1.2}$$

where R_N is the net radiation near the ground, ρ, c and κ are respectively the density, specific heat capacity and thermal conductivity of the soil or subsurface material.

This equation was first derived by Brunt (1941) by solving the heat equation in the soil subject to a constant heat flux boundary condition at the soil surface and an initial condition that at zero time (usually sunset), the entire soil is at uniform temperature T_{g0}. It must be noted that it is assumed that the entire flux from the surface is radiative, conductive and convective fluxes (either free or forced) being ignored. It is also assumed that there is no condensation or evaporation at the surface and the initial condition is that of an isothermal ground.

As can be seen, β depends inversely on the square root of the thermal conductivity and heat capacity of the soil or subsurface material, and directly on the net radiation. Following VSN, we shall refer to β as the ground cooling rate (though its units are $K/h^{-1/2}$. Vasudeva Murthy *et al.* (1993) demonstrated that this approach gives results in excellent agreement with the coupled air-soil model and has the advantage of being simpler and easier to interpret.

However, as will be seen from the field observations, the temperature gradients just above the surface during a lifted minimum can be quite high. Hence, circumstances arose in our observations where the conductive fluxes cannot be ignored. Hence, for the present work, it will be appropriate to include conductive fluxes in the above formulation. Provided the other assumptions are satisfied, there will be no change in equation 1.1, but equation 1.2 will be replaced by

$$\beta = \frac{2(R_N + C)}{\sqrt{\pi \rho c \kappa}} \tag{1.3}$$

where $C = \kappa_{air} \partial T / \partial z$ is the conductive flux from the soil.

Here, κ_{air} is the thermal conductivity of air.

It follows from equation equation 1.1 that the instantaneous ground cooling rate at any time after sunset is given by:

$$\frac{dT}{dt} = -\frac{\beta}{2\sqrt{t}} \tag{1.4}$$

The crux of the results obtained by Vasudeva Murthy *et al.* (1993) can be stated as follows. If the ground emissivity ϵ_g is not unity then there can be a huge radiative cooling just above the ground. If the ground cooling rate β is not too high, a negative radiation slip or temperature discontinuity at the ground can result, with the air just above ground being cooler than the ground. Diffusion then smears the discontinuity into the lifted minimum profile. Thus the VSN model predicted a lifted minimum for values of ground emissivity ϵ_g not too close to unity, and for reasonably low values of the ground cooling rate β. The importance of the surface parameters ϵ_g and β had not been fully appreciated before. In particular, though some investigators(e.g Lützke (1960), Raschke (1957) and Oke (1970)) had realized the importance of the ground thermal conductivity (which influences β), the ground emissivity ϵ_g which plays a crucial role in the VSN model, had not been considered in previous explanations. The authors go further in giving the dependence of height and intensity of the minimum on ϵ_g and β.

Narasimha & Vasudeva Murthy (1995) provide further physical insight into the phenomenon. In their paper, the authors, using the VSN model, provide a detailed discussion of the energy budget near the ground. They show that the net cooling rate near the ground is due to the small difference between two dominant terms, representing respectively radiative upflux from the ground and from the air layers just above the ground. They demonstrate that the energy balance near the ground is very delicate and needs careful handling.

Ragothaman *et al.* (2001) used the VSN model to study the dynamical behavior of the lifted minimum. Consistent with observations, they found that both

the height and intensity of the minimum can evolve. The evolution is strongly influenced by the surface parameters ϵ_g and β, again highlighting the important role played by these surface parameters in the problem. Depending on the values of these parameters, the lifted minimum if it appears after sunset, can exhibit monotonic growth, near steady state or growth followed by collapse. They also analyzed the effect of a 'wind perturbation' or 'gust' through their model. Simulations revealed that the gust rapidly (over a time of order of 20 s) destroyed the lifted minimum. After the gust was stopped, there was a rapid reemergence of the lifted minimum over a time of order 10 - 20 s. This is in line with the observations of Raschke upon waving a plywood sheet. But though the lifted minimum was reestablished quickly, full recovery to the pre-gust temperature distribution took a much longer time, of the order of an hour. They concluded that after cessation of the gust, evolution took place on two disparate time scales: a fast process (over times of order of 10-20 s) characterizing a quick radiative adjustment during which the lifted minimum reemerges, followed by a slow diffusive process (of the order of 10^3 s), during which the no-gust distribution is eventually attained.

The importance of surface parameters ϵ_g and β is again brought out in the work of Ragothaman *et al.* (2002). Based on numerical simulations of the nocturnal inversion they showed that both the depth and intensity of the inversion, as also their evolution, is strongly affected by ϵ_g and β, and that it is essential to take proper account of surface properties in modeling the evolution of the nocturnal boundary layer. They suggest that the highly variable results on inversion parameters reported in the literature may be due to site dependent surface characteristics whose influence had till then been largely ignored, but would need explicit attention in future field observations and models.

Varghese *et al.* (2003a) presented a new code that employed a novel numerical

scheme for making precise estimates of longwave fluxes and cooling rates near the surface of the earth. The band model was used to calculate the radiative fluxes. Unlike the flux emissivity model mentioned before, the band model takes the absorption coefficient to be a function not only of water vapor path length, but also of pressure, temperature and wave number. They found that as the surface emissivity ϵ_g departs from unity, the cooling rates rise dramatically near the surface, and the effect of ϵ_g is noticeable up to heights of nearly 1 km. The band model implementation of the VSN model by Varghese (2003b) shall henceforth be simply called as the band model, while the original VSN model with the flux emissivity scheme shall be referred to as the flux emissivity model. Varghese found that the band model does reproduce the lifted minimum but the intensity of the minimum was much lower, and the height greater than that predicted by the flux emissivity model, as well as typically observed values. Interestingly, the band model predicts a lifted minimum profile even for ground emissivity ϵ_g exactly equal to unity, which was not permitted in the flux emissivity model.

1.2 Motivation and Objectives of Present Work

The VSN model has shown the importance of surface parameters ϵ_g and β, and predicted the dependence of height and intensity of the lifted minimum on these parameters. But none of the reported observations provide data on these parameters. Also, observations (e.g. Oke (1970)), seem to indicate considerably high gradients near the ground, but no definite statements can be made due to poor vertical resolution of temperature measurements near the ground.

The primary aim of the present work is to make detailed field observations of the lifted minimum with high spatial resolution of the vertical temperature profile,

especially near the ground, and with special emphasis on the surface parameters ϵ_g and β. These observations would also generate a body of data that can be used to compare against predictions of theories or models of the nocturnal, near surface thermal environment.

Also, as the VSN model suggests, if the lifted minimum is due to an simple interaction between radiation and conduction, it ought to be possible to simulate the phenomenon in the laboratory. If this can be done, it confers a great advantage, as in the laboratory, unlike field observations, parameters governing the phenomenon can be varied independently and in a controlled manner. The physical insight that can be gained from such a study can be then transferred to the atmospheric situation, or other problems where radiation plays an important role. Hence, another aim of the present work is to investigate the possibility of obtaining the lifted minimum in the laboratory.

CHAPTER 2

FIELD OBSERVATIONS: SET UP

Introduction

In this chapter, the manner in which the field observations were carried out, including the observation site and instrumentation is discussed in detail. Section 2.1 deals with the observation site, with subsection 2.1.1 dealing with the various ways in which the observational surface was modified. In section 2.2, the instrumentation used and the manner in which the data was acquired is described. The chapter concludes with section 2.3, in which a typical observational run is described.

2.1 Observation Site

The observations were made at the airfield situated in the campus of the Indian Institute of Science, Bangalore, India (13°01′33″ N, 77°33′55″E). At a suitable location in the airfield, a circular concrete patch, about 2.5 cm. thick and 9 m. diameter, was laid. The finishing of the surface was done with a thin layer of fine cement, to obtain a surface that was perfectly plane and smooth. This area consisting of the concrete patch shall henceforth be referred to as the 'observation site'. An aerial view of the airfield and the observation site (obtained from Google earth) is shown in figure 2.1. A closer view of the observation site is shown in figure 2.2.

Most of the observations were made during the winter, when the prevailing wind blows from the north-east, though a few observations were made just before

Figure 2.1: Aerial view of observation site at the airfield situated in the campus of the Indian Institute of Science, Bangalore, India.

Figure 2.2: A photograph of a closer view of the concrete patch which constitutes the observation site. Also seen is the central mast on which the temperature sensors were mounted.

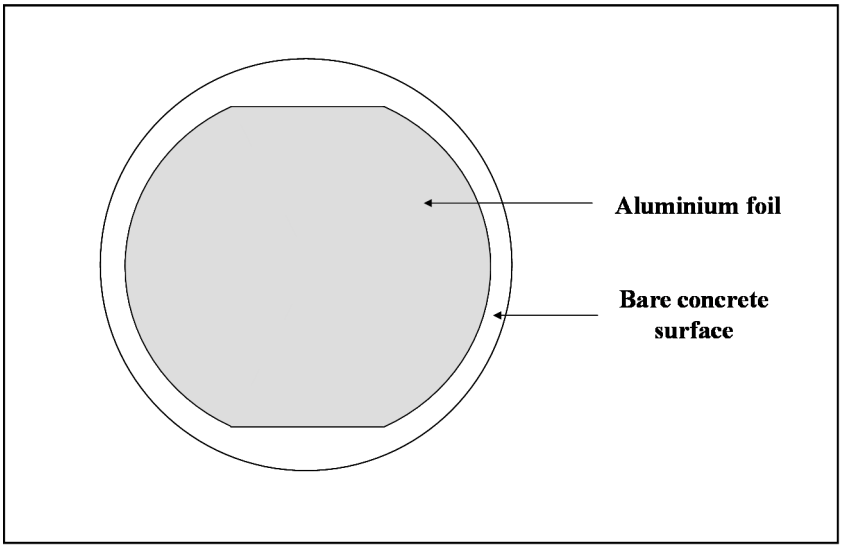

Figure 2.3: Schematic of the manner in which the concrete patch was covered with aluminium foil.

the monsoons set in, when the prevailing wind is south-westerly. Around the observation site, other than patches of dry grass , the ground was flat and bare, for a distance of about 30 meters along the north and south, and for about 100 meters and 200 meters along the east and west directions respectively. Additionally, whatever grass was present, was completely scraped off over a certain distance from the edge of the observation site. This distance varied from about 10 m in the north and north-east directions (the upwind direction for most of the observations) to about 5 m in the south and south-westerly directions. Thus the area just surrounding the site consisted of bare, highly compact soil.

One of the chief aims of the observations is to investigate the effect of the ground cooling rate and emissivity on the lifted minimum. The ground cooling rate will vary from day to day depending on the total amount of solar radiation received during the day, the clarity of the sky at night, etc., but the range of variation is not high. To obtain cooling rates that are significantly different requires an

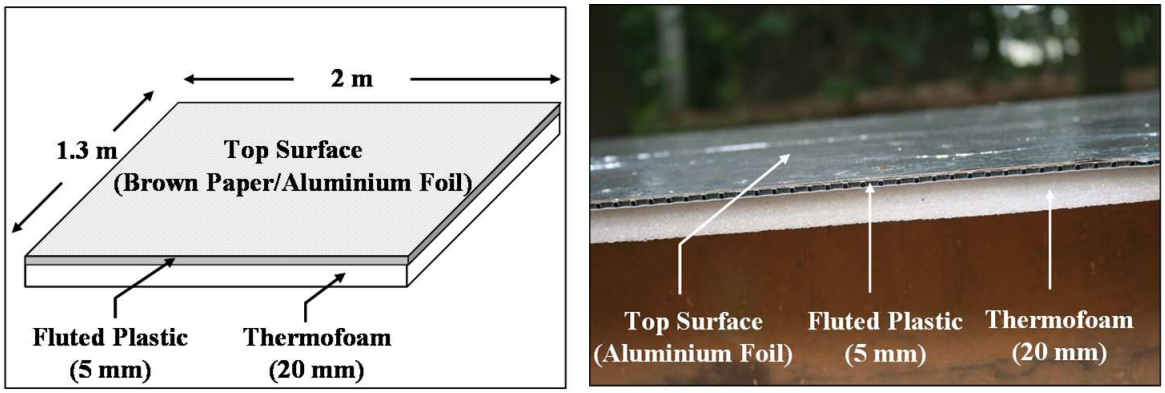

Figure 2.4: (a)A schematic of an individual panel. The thermofoam has a low heat capacity and thermal conductivity. The fluted plastic sheet provides rigidity to the panel. The fluted plastic is then covered either with brown paper (high emissivity) or aluminium foil (low emissivity). (b) A photograph of an individual panel with aluminium foil as the top surface

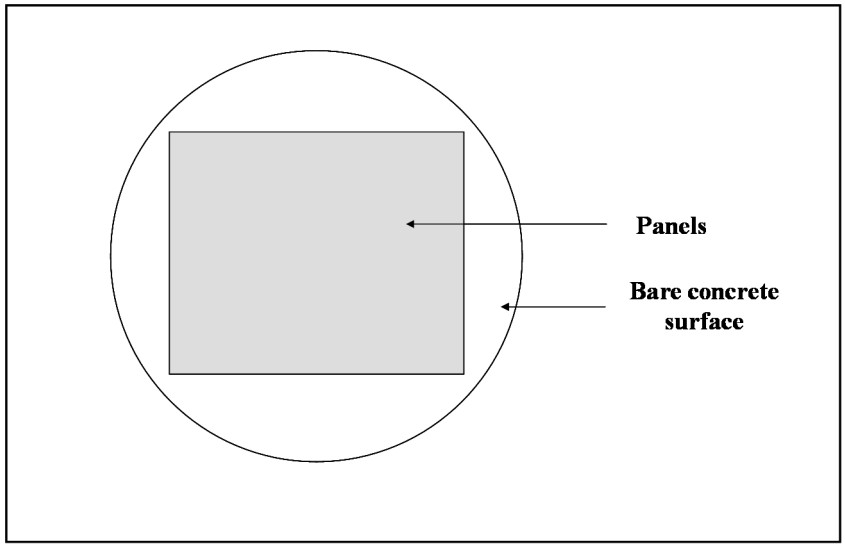

Figure 2.5: Schematic of the manner in which the concrete patch was covered with the panels

Figure 2.6: A photograph showing the manner in which the concrete patch was covered with panels having aluminium foil as the top surface

active modification of the surface. The surface emissivity can only be varied by a modification of the surface.

Hence, the observations were made directly over the concrete surface, or with the concrete surface modified in a variety of ways, in order to get low and high values of both the surface emissivity and surface cooling rate. These modifications shall now be described.

2.1.1 Surface modification

The observations over concrete served as the baseline case against which to compare observations over the other surfaces to be described in this section. The concrete surface has a high surface emissivity (~ 0.9). To study the effect of emissivity then,

one would be required to modify the surface to obtain a low emissivity surface. The cooling rate of concrete is typically comparable to that of highly compacted soil, and it is not easy to get cooling rates that are drastically lower. Hence the surface modifications to change the ground cooling rate have to be done in the direction of increasing the ground cooling rates. Then, in comparison, the concrete surface will be considered as a low cooling rate surface. Thus, the concrete surface is a high emissivity, low cooling rate surface. This was then modified so as to obtain other surfaces with all the various combinations of high and low values for the emissivity and ground cooling rates.

One modification consisted of putting strips of aluminium foil (which possesses a low emissivity) over the concrete patch, with an intervening thin film of water, to provide good thermal contact. Food grade aluminium foil of about 20 μm thickness was used. About 70% of the central portion of the patch was thus covered in a manner shown in figure 2.3. This surface will henceforth be simply called as the 'aluminium on concrete' surface. Due to the high reflectivity of aluminium in the infrared, this surface has a low ground emissivity ϵ_g. As the thermal inertia and conductivity of the concrete surface is not affected by this procedure, the cooling rates of this surface will be expected to be comparable to that of the concrete surface. That this is so will be seen shortly, when observed cooling rates will be presented. This surface is thus a high emissivity, low cooling rate surface.

Another modification was done by placing rectangular panels on the concrete patch. Each panel was 2 m. by 1.3 m. and consisted of a fluted plastic sheet (5 mm thick) stuck on top of a thermofoam sheet (about 20 mm. thick) as shown in figure 2.4(a). The fluted plastic was used to give strength and rigidity to the structure. This was necessary as stands bearing sensors would have to be placed on the panels. Either plain brown paper(which has a high emissivity) or aluminium

foil (which has a low emissivity) was then pasted on top of the plastic sheet (see figure 2.4(a). A photograph of a single such panel with an aluminium top surface is shown in figure 2.4(b). The panels were then placed over the central portion of the concrete patch as shown in figure 2.5, covering an area of about 6m. by 4m. A photograph of such an arrangement in the field, made with panels topped with aluminium foil is shown in figure 2.6.

The surface obtained by placement of panels with brown paper as the top will be referred to simply as the thermofoam surface. Due to the brown paper top, this surface will have a high emissivity ϵ_g. The fluted plastic has a low heat capacity and the upward heat flux through the ground is reduced due to the insulating thermofoam. This will tend to increase the surface cooling rate. Thus, the surface obtained by placing panels with brown paper will be a high emissivity, high cooling rate surface.

The surface obtained by placement of panels with aluminium foil as the top surface will henceforth be called as the 'thermofoam with aluminium' surface. The cooling rate of this surface will be comparable to that of the themofoam surface, but with a lower emissivity due to the reflective aluminium top. Hence the 'thermofoam with aluminium' is a low emissivity, high cooling rate surface.

Table 2.1 is a summary of these surface modifications, the names by which they will henceforth be referred, and their emissivity and cooling rate properties.

Now we would eventually like to determine β values for these surfaces from the observations, so that comparisons with the VSN model may be made. This can be done by either directly fitting a straight line to a plot of ground temperature versus square root of the time, or inferring β from the time and instantaneous ground cooling rates (see eqn 1.4). Unfortunately, this is not straightforward. The equations 1.1, 1.3 and 1.4 are based on some assumptions: No free or forced con-

Surface modification	**Appellation**	**Surface property**
Bare concrete patch	Concrete	High emissivity Low cooling rate
Aluminium foil spread on the concrete patch	'Aluminium on concrete'	Low emissivity Low cooling rate
Concrete patch covered with panels having brown paper as the top surface	Thermofoam	High emissivity High cooling rate
Concrete patch covered with panels having aluminium foil as the top surface	'Thermofoam with aluminium'	Low emissivity High cooling rate

Table 2.1: A table summarizing the various ways in which the original concrete patch was modified, the name by which each surface will be referred to in the subsequent sections, and their emissivity and cooling rate properties.

vective fluxes (which implies no wind) and an isothermal ground at some initial time t, and constant net radiation. These assumptions are not always satisfied in practice. Let us take the simplest case of the concrete surface (which is very similar to a bare soil surface). The assumption of an initial isothermal ground is well approximated at some time around sunset. With clear skies, the net radiation is also more or less constant throughout the night, even though this is not true immediately after sunset and just before sunrise. The addition of conduction fluxes does not change the picture qualitatively, but with the rather high near surface temperature gradients during lifted minimum the value of β may be slightly different from that given by equation 1.2 or 1.3. But the presence of wind results in a deviation from the $\sqrt{t}$ behavior, though the deviation may not be perceptible at low wind speeds. Also, as will be shown in the next chapter, sudden changes in wind speed causes transients in the ground cooling rate, during which the cooling rate may temporarily show huge changes. At such times, the $\sqrt{t}$ behavior does not hold good. Also, if the wind settles to a more or less constant, but drastically

different value, so does the ground cooling rate. The ground cooling observed at a particular time during the observations also depends on the previous cooling history. If due to wind or presence of clouds, if the cooling rate at an earlier time were greater or lower than given by the equations 1.1 to 1.3, the cooling at a later time could be correspondingly lower or greater and apparently not agree with the β values derived from equation 1.2. With the high cooling rate surfaces, these issues become more serious due to the low heat capacity and conductivity of the top layer of corrugated plastic and thermofoam. The cooling rates with different wind speeds will be drastically different, and in particular, very different from the no wind case. Changes in wind speed cause more dramatic changes in ground cooling rate as compared with the concrete surface. In addition, the high cooling rate surfaces cool so rapidly, that the net radiation is no longer constant. For example, by the time the measurements were started over the thermofoam surface, the net radiation values were about 25 W/m^2, where as, just before covering the surface with panels, the net radiation would be typically around 100 W/m^2. Clearly, the thermofoam has cooled so rapidly as compared to say, the concrete surface, that the net radiation values have fallen to this low value. This can be confirmed by noting that the surface temperatures over thermofoam are much lower than that over the concrete surface for similar experimental conditions.

Also, these high cooling rate surfaces were obtained by putting rectangular panels over the concrete surface (as explained in the previous section). This process was generally finished well after sunset, and hence there is no well defined initial time at which the isothermal ground condition is satisfied. This problem is also there with the 'aluminium on concrete' surface, where the process of laying the aluminium in strips, all the while ensuring that there was a film of water underneath, took about 4-5 hours.

Due to these reasons, either a $\sqrt{t}$ behavior may not be valid, or the values of β obtained from a $\sqrt{t}$ fit may not agree with the theoretical β obtained from equations 1.1, 1.3 and 1.4. In particular, the instantaneous cooling rates at a given time as obtained from observations may be radically different from that predicted from equation 1.4. This is especially true of the high cooling rate surfaces. In fact, in view of the above discussion, it may not be appropriate to apply Brunt's formula for cooling and associate a β with these surfaces.

Though even without estimates of β, a qualitative comparison with VSN model is certainly possible, a more quantitative comparison would certainly be desirable. To this end, an observed and a theoretical β value is estimated.

The observed β was obtained from a linear fit to a plot of the ground temperature versus $\sqrt{t}$, t = 0 being the time of sunset. For many of the observational runs over the concrete and 'aluminium on concrete' surfaces, a good linear fit, and hence a β value could be obtained. Cases where it was not possible to obtain a good linear fit over the entire observation period have not been considered. As discussed above, for the high cooling rate surfaces, the concept of β, as defined by equations 1.1- 1.3, is not meaningful. This is also borne out by the observations: no reasonable linear fit over the entire observation period could be obtained for a plot of the ground temperature versus $\sqrt{t}$. However, for sake of completeness, an observed β is calculated for these surfaces also. In such cases, periods *within* an observational run are identified, in which the plot of ground temperature versus $\sqrt{t}$ is linear in an average sense, though typically there are large fluctuations in the ground cooling rate even within such periods. A separate β is identified for each such period. This gives a range of β values for a given observational run, instead of a unique β value. Examples of such estimates will be given in the next chapter.

A theoretical estimate of β is made directly from equation 1.3, using the material

properties of the surface, and the *observed* values of net radiation. Again, for the sake of completeness, the theoretical β estimates will be carried out for the high cooling rate surfaces also. Even here, there are two main issues that have to be addressed. The first issue is that, as mentioned earlier, the net radiation is not constant, but decreases (very rapidly at first and then more slowly, till it asymptotes to a constant value). This again implies lack of $\sqrt{t}$ behavior, or equivalently, that the beta in equation 1.1 is not constant. However, as the net radiation drops more or less constant by the time the observations begin, the final observed value of the net radiation will be used for the calculations. It may be noted that, especially for the thermofoam surface, this is much lower than the usual value of net radiation over natural surfaces.

The other issue has to do with the layered construction. The high cooling rate surfaces have a top layer of 25 mm thickness with low heat capacity and conductivity, and an underlying deep concrete/soil layer which has a high heat capacity and thermal conductivity. It is not immediately clear what thermophysical properties have to be used in defining β. In principle, for such a layered situation, the $\sqrt{t}$ cooling law is again not valid. The initial cooling rate is determined only by the properties of the top layer. But as the cooling penetrates well into the bottom layer, the cooling rate starts changing to reflect the thermal properties of the bottom layer. Hence, the time after which departures from a β value determined by properties of the top layer become significant is directly proportional to the depth of this top layer. In our case, rough calculations as well as numerical simulations show that the effect of the second underlying layer is not significant till about 3-4 hours after the initial time. Even after that, departures from the cooling rates as determined by the thermal properties of the top layer are less than about 20 % for another 3-4 hours. However, given the fact that the β values estimated for the

high cooling rate surfaces are not very meaningful, it will be sufficient to use the thermophysical properties of the top layer to estimate β theoretically.

Table 2.2 summarizes the calculations of β for the various surfaces. As the β is anyway supposed to be a rough estimate, the thermophysical properties are taken from tables. As mentioned earlier, the net radiation values are taken from observations. The net radiation values of course vary a little from day to day (even with clear skies); hence representative values are taken. For example, with the aluminium over concrete surface, the net radiation values vary from about 10 to 30 W/m^2. So, a mean, representative value of 20 W/m^2 is chosen. As the observations are made at night when, with clear skies, the net radiative flux is upwards (loss from the surface), in this thesis, fluxes directed upwards will be taken as positive. Similarly, a representative value for the conductive flux is taken. For the 'aluminium on' concrete surface, the conductive fluxes are *higher* than the net radiative flux. For this surface at least, inclusion of the conductive flux in Brunt's formula (see equations 1.1, 1.3 and 1.4) is essential.

The observed β values are also presented. For the thermofoam and 'thermofoam with aluminium' surfaces, the lower range of observed β values has a negative value, which indicates a warming. This is because on these surfaces, there were distinct periods (typically associated with changing wind speed) during which the surface temperature actually increased with temperature for some time. Such warming periods are also noticed over the concrete or 'aluminium on concrete' surface. But in these cases, the warming rate is relatively less and the rise in ground temperature is very small. Such periods are relatively short as compared to the total observation time. Hence, the linear fit to obtain β is not affected. On the other hand, the warming rates over the thermofoam and 'thermofoam with aluminium' surfaces are much higher, and periods for which the warming occurs can be a considerable

Material	$\boldsymbol{\rho}$	**c**	$\boldsymbol{\kappa}$	$\boldsymbol{R_N}$	**C**	**Theoretical β**	**Observed β**
Concrete	2300	900	1.4	100	10	4.3	3 — 7
'Aluminium on concrete'	2300	900	1.4	20	50	2.8	2 — 4
Thermofoam	100	1000	0.03	25	3	33	-4 — 18
'Thermofoam with aluminium'	100	1000	0.03	25	10	43	-28 — 46

Table 2.2: A table summarizing the calculations of β for the various surfaces. The β value is calculated from 1.3, using the observed value of net radiation and the thermophysical properties of the surfaces. Also shown is the range of observed β values for the various surfaces, obtained by a fit to the data. The negative values of observed β for the thermofoam surfaces, indicate periods of surface warming.

fraction of the observation period.

For the concrete and 'aluminium on concrete' surfaces, the agreement between theoretical and observed β values is as good as can be expected from such estimates. Note that for the 'aluminium on concrete' surface, the agreement would have been poorer if the conductive fluxes had not been taken into account. For the high cooling rate surfaces (thermofoam and 'thermofoam with aluminium'), the range of observed β values is huge. Also, especially for the 'thermofoam with aluminium' surface the agreement between observed and theoretical β values is poor. This again underscores the fact that Brunt's formula does not yield good predictions for the cooling rates for these surfaces.

In spite of the fact that a β value cannot be associated with observations on the thermofoam and 'thermofoam with aluminium' surfaces, occasionally for brevity, these surfaces will be referred to as high β surfaces. This only implies that it is surface which has a high cooling rate, and would under similar conditions, cool faster than the concrete surface.

2.2 Instrumentation

In this section, the instrumentation used in the field observations is discussed. Other than temperature sensors to measure the vertical profile of temperature, a wind sensor to measure the wind speed, and a humidity sensor were used in all the observations reported here. These sensors were mounted on a central mast (figure 2.2). In addition, sensors used in many, though not all observations include: a net radiation sensor, two different kinds of radiometers to measure upwelling or downwelling fluxes, and a separate wind sensor to measure vertical air currents. It must be mentioned here that articles placed at the observation site were not safe from theft or damage. Hence, the observational set up had to be designed in such a way that all the equipment, including the central mast or the panels (in the case of surface modification), could be brought from a nearby room, unpacked and assembled in the evening within a relatively short time, and again packed and taken away in the morning after the observations. As the power for active devices was supplied by a portable, off line UPS, it was also important that the sensors (or any other equipment used in the set up) consumed as little power as possible. These considerations, along with limited funds, was an important factor in the choice of sensors, the way in which they were mounted, etc.

2.2.1 Temperature Sensors

For measuring the quantities of our interest like the height and intensity of the minimum, or the ground cooling rate, it is sufficient to know relative temperatures (for example, temperature relative to some reference); sensitivity and stability were more important than accuracy in measuring absolute temperatures. Fast response times would be preferred due to short radiative time constants. On the other hand,

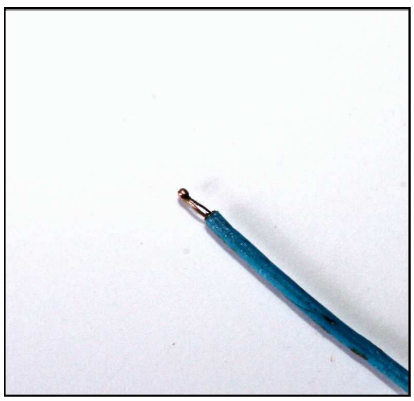

Figure 2.7: A photograph of the end of a single T type (copper-constantan) thermocouple sensor, showing the thermocouple wires fused in the usual fashion, with the copper and constantan wires exposed at the end of the covering sheath, and then fused to form a small bead of a diameter of around 0.6 mm.

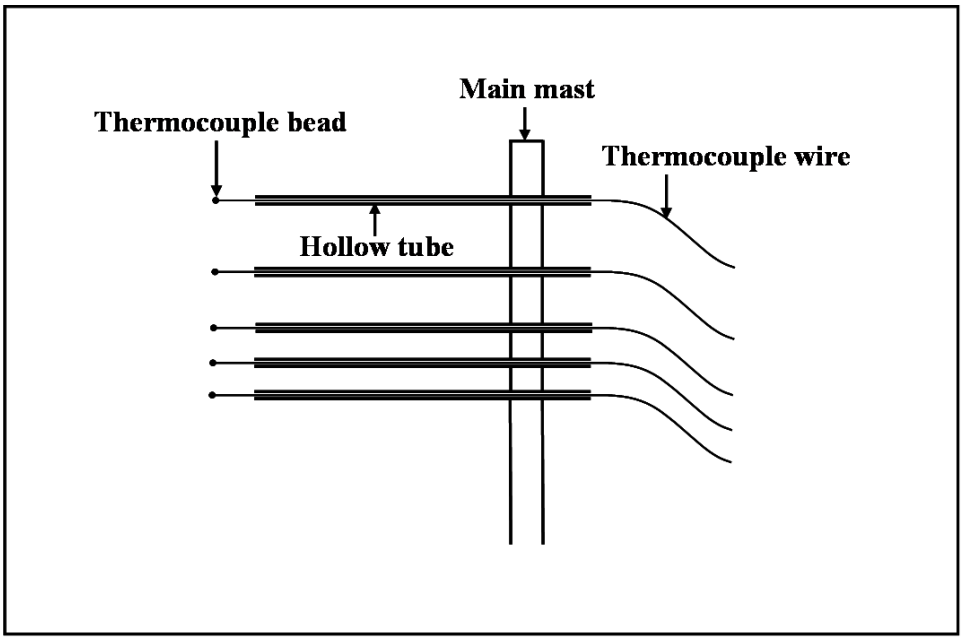

Figure 2.8: A schematic showing the manner in which the thermocouples were mounted on the main mast. The thermocouples were inserted into hollow aluminium tubes which were then together inserted into holes that had been bored into the mast for this purpose.

the sensor needs to be rugged enough for our purposes. The thermocouple was chosen as the temperature sensor because it meets our requirements and is inexpensive. Copper Constantan (type T) thermocouple was used and has a high sensitivity and stability in the temperature range of our interest. Fine gauge wires will result in fine 'beads' or thermocouple junctions, which are necessary for quick response and for reducing the radiation error of the temperature sensor. But very fine wires would be too fragile for our purposes. As a compromise, 0.25 mm. thermocouple wires (gauge 32) were used. All the thermocouple used in the measurements were cut from a single reel of thermocouple wire to ensure the same calibration constants for all the thermocouples. For measuring temperatures close to the ground (heights less than 6 cm.) a special stand was made, which will be described shortly. For measuring the profile at greater heights, 17 to 20 thermocouples were used. These were fused in the usual fashion, with the copper and constantan wires exposed a little at the end of the thermocouple wire, and then fused to form a small bead of diameter 0.6 mm. as shown in figure 2.7. These were mounted on the mast with the help of hollow stainless steel tubes as shown in figure 2.8, with the thermocouples being inserted into the hollow tubes, which were then inserted into holes drilled in the mast. The highest point of measurement was 160 cm.

As mentioned earlier, observations of Oke (1970) indicated rather large temperature gradients near the ground. Preliminary observations made by us indicated that, near the ground, at least with the first 3-4 millimeters, measurements at every millimeter would be needed to adequately capture the gradients. Also, as for every observation session, the sensors were set up from scratch, the arrangement for these near surface measurements should be such that the sensors can be quickly and accurately set up at the desired heights. It was difficult to achieve these aims with our thermocouple wires fused in the usual fashion. Hence a separate arrangement

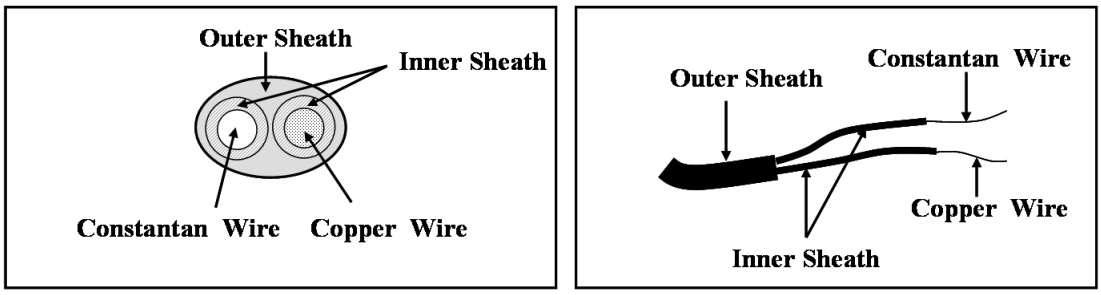

(a) (b)

Figure 2.9: A schematic showing the inner teflon sheath that individually covers the copper and constantan wires and the outer teflon sheath which holds the insulated copper and constantan wires together.

was devised for the near surface measurements.

The thermocouple wire consisted of individual sheaths for the copper and constantan wires, enclosed in an outer sheath as shown in figure 2.9. The outermost sheath of the thermocouple wire was stripped off for some length, keeping the individual sheaths around the copper and constantan wires intact. The copper and constantan wires were then laid along a straight line (approaching from opposite directions) with their tips touching as shown schematically in figure 2.10(a) and fused (butt welded) at the point of contact. This results in a junction which is of the same thickness as that of the individual wire, being 0.25 mm. A photograph of such a junction is shown in figure 2.10(b).

A frame was fabricated from aluminium. In the laboratory, these butt welded thermocouple wires were stretched across the frame in two rows (figure 2.11). The rows were separated by about a centimeter. Their heights were monitored with a traveling microscope, and the heights of the junctions were adjusted and permanently fixed (by fixing the wires to the frame) at the desired heights, relative

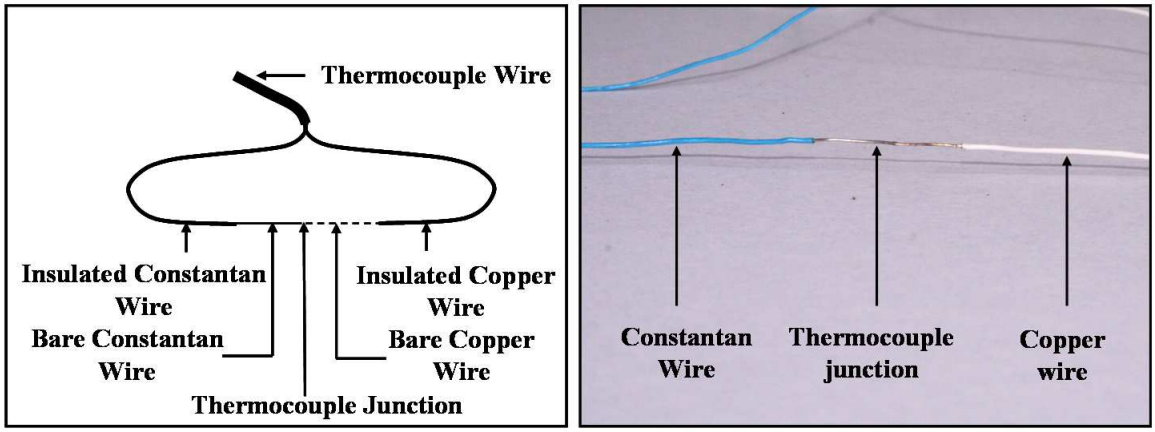

(a) (b)

Figure 2.10: Illustration of the manner in which thermocouples were butt welded for use in high resolution measurements near the surface. The outermost sheath of the thermocouple wire was stripped off for some length, keeping the individual sheaths around the copper and constantan wires intact. The copper and constantan wires were then laid along a straight line (approaching from opposite directions) with their tips touching as shown schematically in figure 2.10 (a) and fused (butt welded) at the point of contact. This results in a junction which is of the same thickness as that of the individual wire, being 0.25 mm.

to a plane surface. The aluminium frame was provided with leveling screws. In the field, these screws were adjusted such that one thermocouple junction in each row (say the highest) was at the desired height with respect to the ground. The construction ensured that all the other junctions were automatically at the desired heights. The heights of the near surface junctions were chosen to be 1, 2, 3, 4, 6, 8, 15, 30 and 50 millimeters.

For measuring the ground temperature, thermocouples fused in the usual fashion were used, but with the difference that just after fusing, when the beads were

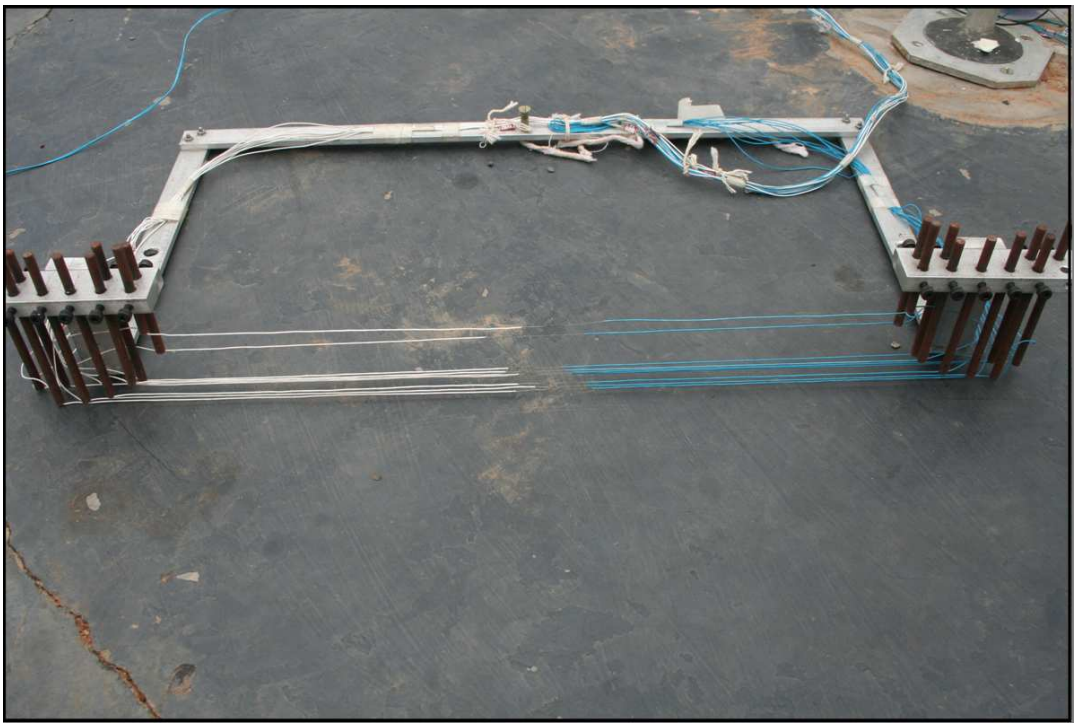

Figure 2.11: A photograph of the stand which was designed to measure near surface temperature profiles with high precision. The butt welded thermocouples were stretched across the stand in two parallel rows, the rows being about a centimeter apart.

still soft, they were beaten into thin discs with a thickness of 0.25 mm. These were then taped to the ground, with a little conducting paste underneath them, as shown in figure 2.12. On some occasions, on top of the tape that was used to stick the ground sensors in place, and directly over the position of the disc shaped thermocouple junction, a small piece (about 3 mm by 3 mm) of a 1 mm thick, thermally insulating tape was stuck. This was done to reduce convective cooling of the junction from the top surface, but no differences in ground temperature could be discerned with this additional precaution.

In order to investigate certain temperature fluctuations (to be discussed in the next chapter), in addition to the above mentioned sensors, two more temperature

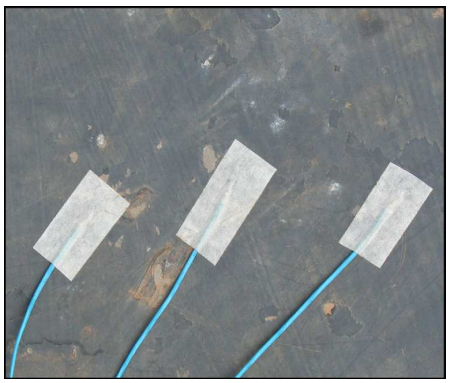

Figure 2.12: A photograph of the manner in which ground temperature was measured using thermocouples.Disc shaped thermocouples (thickness of 0.25 mm) were taped to the ground with a little conducting paste underneath them.

sensors were used. These were thermocouples fused in the usual manner, and mounted on separate stands on diametrically opposite sides of the mast, at heights ranging from 10 to 20 cm. The horizontal seperation between these sensors was kept as large as possible, consistent with the fact that they should be well within the boundary of the observational surface, so as to avoid effects due to sudden change of surface characteristics. Thus, the distance between these sensors varied from about 6 m. for the bare concrete surface to about 3 m. for the thermofoam and 'thermofoam with aluminium' surfaces, whose spatial extent was smaller.

All the thermocouple sensors had a common reference junction. This reference junction was kept embedded in a metal block. This block was placed in an insulated box, so that its temperature, and consequently, that of the reference junction changed very slowly. The temperature of the reference junction was monitored with a thermistor embedded in the same metal block. The thermistor used was a Resistance temperature curve matched negative temperature coefficient thermistor, with an accuracy of 0.1 °C.

Care was taken to ensure as accurate temperature readings as possible. The

thermocouples were calibrated at the beginning of every season. The calibration was carried out in the lab in a hot water bath. On a couple of occasions, the thermocouples in the field (using the same connectors, wires, insulation box, etc. as used for the actual observations), were immersed in a beaker of well stirred water. All the thermocouples agreed to within 0.05° of each other. This puts an upper bound on the inter sensor error due to the particular arrangement used (like differences in temperatures at the thermocouple junctions, etc). A note must be added on the radiation error. The radiation error of temperature sensors is an important aspect of field measurements. Sensors are usually shielded to minimize the radiation error. In the present case, this is impractical due to number of sensors, vertical distance between near surface sensors and temporary nature of the set up. Also, shielding will tend to reduce response times whereas quick response times are desirable due to small radiative time constants. However at night time, for fine sensors like those used here, the radiation errors are quite small (see, for example Fritschen & Gay (1979) and Raschke (1954)). In our case for example, the error is less than about 0.5 °C for the extreme case of zero wind. In any case, the radiation errors will be more or less the same for all the sensors, and hence it will merely result in an offset for the entire temperature profile, which will not affect quantities of our interest like intensity and height of the minimum.

2.2.2 Wind Sensors

The lifted minimum is adversely affected by turbulent transport, with the lifted minimum being replaced by an usual inversion whenever the wind speed exceeded a threshold value. Oke (1970) found this threshold to be about 100 cm/s at a height of 25 cm. while Raschke (1957) quoted a value of about 50 cm/s at a

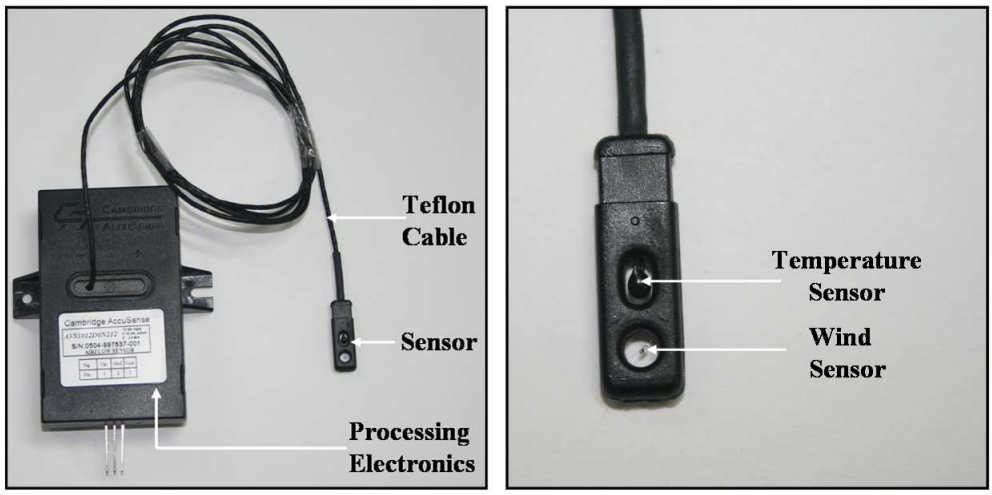

(a) (b)

Figure 2.13: (a) The wind sensor shown along with the processing electronics. (b) Close up of the sensor showing the thermistors used to measure the wind speed and ambient temperature.

height of 20 cm. above the ground. Hence our interest would mainly be in the low wind regime. The wind sensor chosen for the observations should be sensitive and accurate at low velocities. It would be desirable if the sensor could give some idea of the turbulence levels, as the turbulent transport also affects the phenomenon. The sensor should be rugged, portable, and easy to install and uninstall within a short duration. As we were also interested in examining vertical air currents very close to the ground arising from convective instabilities, the sensor should not be bulky so as to avoid disturbing the air flow or modifying the near surface thermal environment. A model (AVS 1012DON212) from the AVS 1000 series air velocity sensor manufactured by Accusense (a part of Degree Controls Inc.) was chosen As it satisfied these requirements.

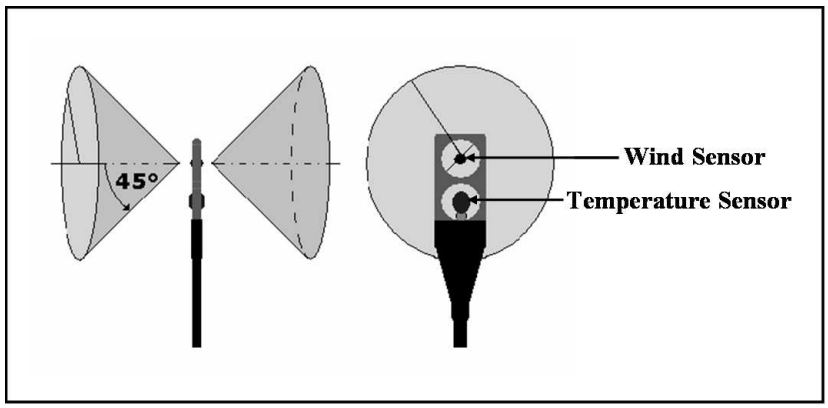

Figure 2.14: The acceptance angle of the wind sensor. As long as the sensor makes an angle of less than 45° with the wind direction, the error will not exceed 2% compared to a reading taken with the sensor head perpendicular to the airflow.

The AVS Sensor Series uses thermal anemometer technology, which measures heat loss from a heated wire or bead. Two thermistors in the sensor head (figure 2.13) detect airflow and ambient temperature simultaneously. The airflow reading is then compensated for temperature and linearized with the help of a microprocessor, and made available as the output. The microprocessor and other processing electronics is contained in a small casing (7 cm. by 5 cm. by 1.5 cm.), connected to the sensor head by a thin teflon cable (figure 2.13). The sensor is specifically designed to measure low velocities accurately, the model chosen by us having a measuring range of 0 - 2.5 m/s, with an accuracy of $\pm$ 5 cm/s. Readings below 15 cm/s however, cannot be considered accurate due to free convection effects arising from the heated thermistor. It has a response time of 100 ms. which is good enough to give some idea of the turbulence levels. The sensor head has an extremely low profile (about 7 mm wide and 3 mm deep), with a thin (1 mm) teflon cable, providing minimal obstruction to the airflow and can be used for the vertical air current measurements with a negligible effect on the near surface conditions. The sensor has a low angular dependence on direction of wind, with an acceptance angle of

45°. (This means that as long as the sensor makes an angle of less than 45° with the wind direction, the error will not exceed 2% compared to a reading taken with the sensor head perpendicular to the airflow, as shown in figure 2.14). The entire unit is lightweight (less than 40 g including the casing containing the electronics), and yet rugged and can withstand shock and vibration. One such sensor was mounted directly on the mast with the help of a hollow aluminium rod. Though the sensor has a high acceptance angle, care was taken to mount the sensor as perpendicular to the wind flow direction as could be determined, and this alignment was checked periodically, and if necessary, adjusted during the course of observations. In some of the observations, a similar (but separate) unit was used to try and measure any vertical air currents. This was mounted on a small stand, and placed about mid-way between the mast and the edge of the observation area. The sensor head was aligned to be parallel to the ground, and at a height ranging from 10 to 20 cm.

The calibration of the wind sensor was done at Accusense using panametrics flowmeter GP68022-1001-0, S/N 604, and a calibration certificate provided along with the sensor. The relation between wind speed and sensor voltage is given by

$$W = 0.25V$$

Here V is the sensor voltage (in volts) and W is the winds speed in m/s.

The calibration at Accusense is one of an unbroken chain of calibrations traceable to National Institute of Standards and Technology(NIST). Verification of this traceability is performed by Accusense at regular intervals.

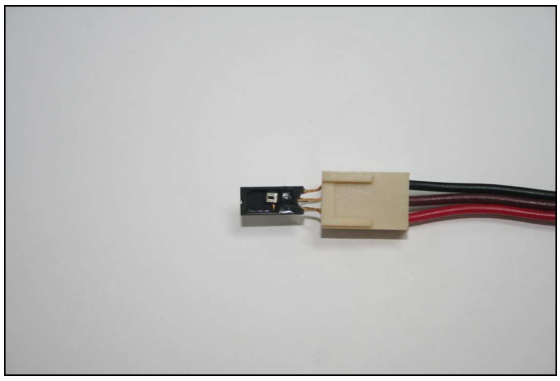

Figure 2.15: A photograph of the capacitance based humidity sensor (Honeywell make) used in the observations.

2.2.3 Humidity Sensor

The HIH-3610 series humidity sensor manufactured by Honeywell, was used in our observations (figure 2.15). The sensor uses a a laser trimmed thermoset polymer capacitive sensing element with on-chip integrated signal conditioning, and is available in a molded plastic housing with a thermoplastic cover. The sensing element's multilayered construction provides excellent resistance to wetting, dust, dirt, oils, and common environmental chemicals. The sensor directly detects changes in relative saturation (which is a measure of the relative humidity) as a change in sensor capacitance, with fast response, high linearity and excellent long term stability. The sensor is small (about 10 mm by 5 mm) and light (a few grams), inexpensive and has a power consumption of only 1 mW. The output of the sensor is converted into a relative humidity reading by means of a sensor specific equation:

$$RH = (vhum - 0.89)/0.0307$$

where RH is the relative humidity and $vhum$ is the output (in volts) of the sensor. Though the temperature effect for the sensor is small, the relative humidity

so obtained is then corrected for temperature effects using a sensor independent equation provided by the manufacturer:

$$TrueRH = RH/(1.0546 - 0.00216T)$$

where T is the temperature in °C, and $TrueRH$ is the corrected relative humidity The sensor provides a relative humidity accuracy of ±2% over the entire range of relative humidity from 0% to 100% (non condensing). The sensor was mounted on the main mast at the same height as one of the thermocouples. The temperature reading obtained from this thermocouple was then used to convert the relative humidity readings into absolute humidity. The sensor comes calibrated (in the form of a sensor specific equation), and is very stable, with the drift typically being less than 1% Rh in 5 years. Nevertheless, some simple checks were done to see if any drift had occurred. Three numbers of the same sensor model were procured at the same time, with only one being used in the field, with the others being kept as a standby or used for laboratory experiments. They initially agreed to within 1.5 % RH of each other. They were compared at regular intervals. The three sensors never disagreed by more than 2% during the entire period of observations. This was take to indicate that, with a high degree of probability, no measurable drift had occurred. The RH readings obtained in the field were often compared with the readings of the RH sensor on the roof top of the Center for Atmospheric and Oceanic Sciences, in the campus of the Indian Institute of Science, barely a kilometer from the airfield where the observations were being carried out. They always agreed to within ±5%, with any disagreement not getting significantly worse over the years in which the field observations were made. These checks were taken as sufficient for the kind of accuracy desired in the humidity readings.

2.2.4 Radiation Sensors

There are two important areas in the field observations where radiation measurements could provide valuable information. One is connected with the observation that, for the lifted minimum clear skies seem to be necessary (Ramdas & Atmanathan (1932), Raschke (1957)). Thus, the effective sky temperature (or more precisely, difference between sky and surface temperatures) seems be an important parameter in the problem. A radiometer (pyrgeometer) can be used to measure to measure downwelling fluxes, which then gives an idea of the effective sky temperature. For example, the presence of clouds, which affects the phenomenon under study, will be indicated by increased downwelling fluxes. The other point is that, according to the VSN model, the lifted minimum is basically caused by radiative cooling, there being a large radiative flux divergence just above the ground. This flux divergence is mainly due to the upwelling radiation, the downwelling radiation not changing much near the surface. One can attempt to measure this divergence by traversing a radiometer near the ground to obtain a vertical profile of the net radiation. This can either be a net radiometer, or a pyrgeometer measuring upwelling fluxes. The changes in radiative flux, at least according to the predictions of the VSN model, can be quite small. For example, according to the predictions of VSN, for ground emissivity = 0.8 and water vapor mixing ratio = 0.005, the flux divergence just above the ground is about 20 W/m^3, falling to about 5 W/m^3 at a height of 10 cm , and practically zero above abut 30 cm above the ground. This means that the radiative flux itself changes by about 2-3 W/m^2 from the just above ground to a height of about 30 cm. and by less than 0.5 W/m^2 from a height of 10 cm. to 30 cm. Such small changes are very difficult to measure, but if at all they are to be measured by traversing a radiometer, then the first measuring sta-

tion should be as close to the ground as possible (where the gradients are higher), possibly as low as 1 cm., so that the total change in radiative flux is comparatively larger, and hence more reliably measurable. So, the radiometer construction should be such that it enables the sensing element to be placed within a centimeter or so from the ground. Also, the radiometer should be as small as possible (at least in horizontal extent), lest it modifies the radiative environment when placed so close to the ground. At the same time, the radiometer should be as sensitive as possible to measure such small changes in radiative flux. Most of the commercially available radiometers, because of their construction or presence of a dome do not allow their placement very close to the ground. Hence, simple and inexpensive, yet sensitive radiometers were designed and fabricated together in the laboratory and used for the field observations. Details of these radiometers are described next.

The net radiometer was of the usual type with the difference between temperatures of two surfaces in radiative equilibrium being measured by a thermopile. The two surfaces or absorber plates are parallel, face opposite directions and the sensor is mounted horizontally so that one of the surfaces is exposed to downwelling sky radiation and the other to the radiation emitted and reflected by the ground surface. Thermoelectric modules manufactured by Melcor were used as a thermopile, with the two surfaces of the module themselves acting as the absorber plates. A thermoelectric module is a semiconductor thermopile and has two thin ceramic wafers with a series of P and N doped bismuth-telluride semiconductor material sandwiched between them. The ceramic material on both sides of the thermoelectric adds rigidity and the necessary electrical insulation. Thermoelectric modules were chosen as they are available off the shelf, inexpensive and have a high Seebeck coefficient. The Seebeck coefficient of a single bismuth-telluride thermocouple is more than 350 μV/°C, which is an order of magnitude more than than a metal

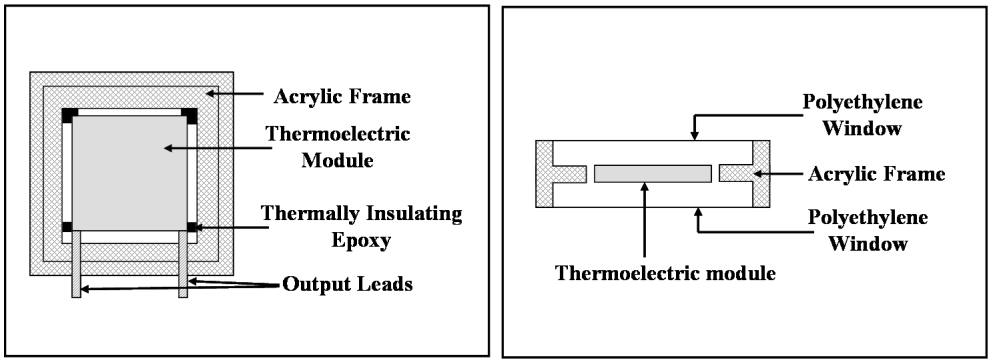

(a) (b)

Figure 2.16: A schematic of the manner in which the net radiometer was assembled (a) Top view showing the peltier module separated from the acrylic frame by a small air gap. (b) Side view showing the polythene windows on either side of the module surface.The spectral response of the sensor is decided solely by the high absorptivity black matte paint (manufactured by Akzo Nobel). According to the information supplied by Akzo Nobel, this paint has an absorptivity of greater than 0.9 in the range of 0.3 - 40 μm.

thermocouple.

Using small thermoelectric modules will result in smaller sensors which would be preferable for near surface measurements. But a smaller sensor will also result in lower sensitivity of the sensor due to lower number of thermocouple junctions. Bearing these points in mind, two different thermoelectric modules were used. One was the CP 0.8-31-06L module, which was the smallest module that was readily available . This measures 12 mm by 12 mm by 3.4 mm, and has 31 junctions. The other was the CP 1.0-127-05L module, which is somewhat larger, being 30 mm by 30 mm by 3.2 mm, and has 127 junctions. Both the surfaces of the thermoelectric module were coated with a black matte paint (with an emissivity of about 0.9 in the range 1 - 40 μm) to maximize the effects of radiation on the energy balance of the surfaces. The module was then fixed inside a acrylic/plexiglass frame as shown

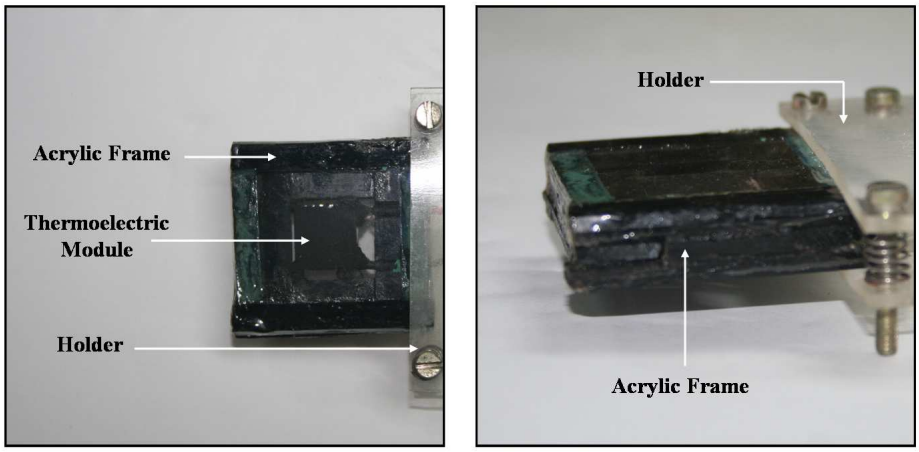

(a) (b)

Figure 2.17: A photograph of the net radiometer along with the holder. (a) top view (b) side view

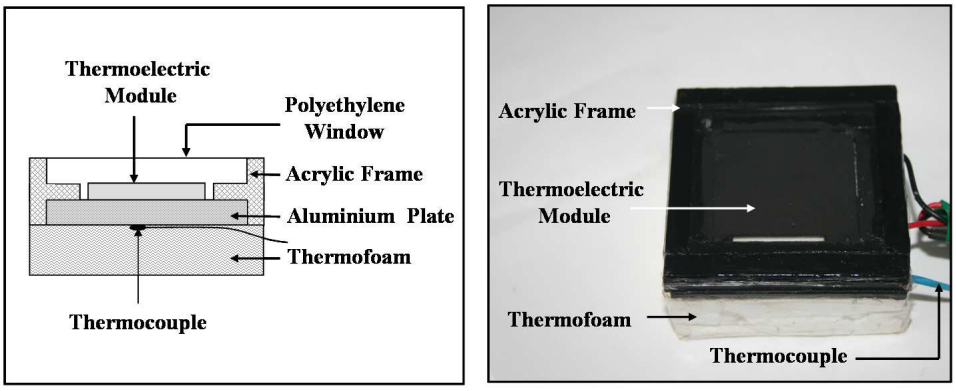

(a) (b)

Figure 2.18: The 'sky sensor' used to measure one sided fluxes (a) Schematic showing the aluminium plate fixed to one of the surfaces of the peltier module, the thermocouple to measure the temperature of the aluminium plate, and the thermofoam to ensure that the temperature of the aluminium plate changes only slowly. (b) A photograph of the sensor.

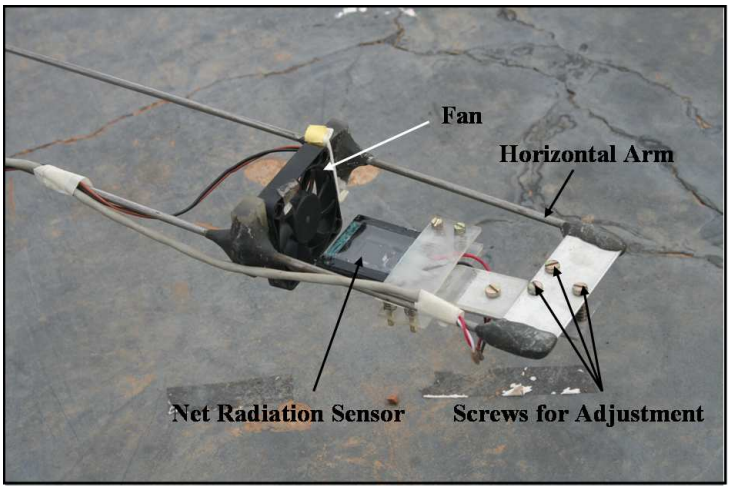

Figure 2.19: Photograph showing the manner in which the net radiometer was mounted in the field. The sensor holder is screwed to a horizontal arm which is in turn fixed to a stand. A fan directs an air stream over the sensor to prevent condensation during low wind speeds.

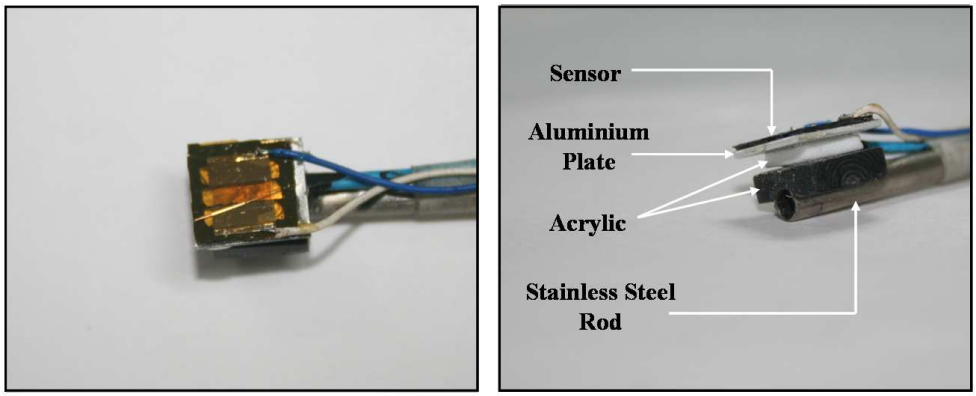

(a) (b)

Figure 2.20: A photograph of the microradiometer used to measure one sided fluxes (a) Top view showing the active surface (b) Side view showing the thin aluminium plate to which the sensor was fixed and the supporting rod.

in figure 2.16. There was a small gap (about 0.5 mm) between the outer edge of the module and the acrylic/plexiglass frame, except at the four corners, where the module was attached to the acrylic/plexiglass frame by means of a thermally insulating adhesive. This was done to thermally insulate the module from the frame, as otherwise it would result in distorted heat flow near the edges of the module. The frame had raised edges across which a polyethylene sheet was stretched to reduce the effects of convection. The distance ℓ of the polyethylene window from the surface of the sensing element has to be carefully chosen. In appendix A, the relationship between the net radiation and temperature difference across the sensor is derived (see equation A-8). It can be seen that for the error terms to be small, ℓ should be large. On the other hand, increasing ℓ decreases the field of view of the sensor, unless the size of the acrylic frame and consequently the sensor is also increased, which may not be desirable for such near surface measurements. $\ell = 3$ mm. was chosen as the optimum for both the sensors. The polyethylene sheet used was ordinary, commercially available food wrap, with a thickness of 25 microns and a transmissivity of 80% in the range of 2 - 20 μm. The final assembled sensor using the smaller thermoelectric module measured 38 mm by 38 mm by 9.4 mm, while the sensor using the larger module was 57 mm by 57 mm by 9.2 mm. The pyrgeometer (figure 2.18) was assembled in a similar way, except that the polythene window was fitted only on one side. On the other side, an aluminium plate, about 45 mm by 45 mm and 3 mm thick was stuck to the surface of the thermoelectric module by a thermally conducting epoxy. A thermocole piece of about 20 mm thickness was attached to the plate. This was done so that the lower surface of the module had a more or less stable temperature and responded only slowly to ambient temperature changes. The temperature of the bottom surface of the module was monitored with the help of a thermocouple fixed to the aluminium plate with help of the thermally

conducting epoxy(figure 2.18 (a)). As a calibration facility was not available, these sensors were calibrated in a simple manner in the laboratory. The details of the procedure followed are given in Appendix B . For use in the field, stands were made, consisting of a thin vertical rod (80 cm tall) fixed on a small horizontal base plate. The base plate was provided with leveling screws. A horizontal arm could slide on the vertical rod, and could be fixed at any desired height. The net radiation sensor was screwed onto the horizontal arm (figure 2.19). The plane of the sensor could be adjusted with the help of three screws provided on the horizontal arm. With the help of these screws and the leveling screws on the base plate, the net radiometer was adjusted to be parallel to the ground surface before commencement of the measurements. A small fan was fixed to the horizontal arm a small distance away from the sensor, with the air stream being directed over the sensor. This was done to prevent condensation on the polyethylene window, especially during calm and clear conditions. The net radiation profile was obtained by traversing the net radiometer in the vertical by means of the sliding arm. The radiometer was kept at a given traverse position (given height above the ground surface) for a period of 2-4 minutes. The average of the readings obtained in this period was considered to be the net radiation flux at that height. As the main objective of these measurements to try and capture the radiative flux divergence just above the ground predicted by the VSN model, the profile measurements were confined to the first 20 - 50 cm. above the ground. Each complete traverse to obtain a single profile took anywhere between 10 to 20 minutes. Hence, care was taken to only consider profiles obtained over a period in which the average wind speed was more or less constant (variation of less than 0.5 m/s) and the downwelling radiation did not change too much (on an average, less than 1 W/m^2), so that spurious flux divergences are not obtained.

As will be discussed in detail in the next chapter, measurements with these

radiometers did not reveal any divergence close to the ground. Assuming such a divergence exists, some reasons why it did not show up in the measurements may be speculated. One of them is that, small as these sensors are, they are still large enough to modify the radiative flux when placed so close to the ground. One could use a smaller sensor to see if the divergence can be picked up. Unfortunately, the smaller of the two net radiometers mentioned above is the smallest one that can be made using off-the-shelf thermoelectric modules. Though smaller custom made modules are available, they are very expensive, and their sensitivity is too low for measuring small changes in flux. Hence it is necessary to use some other kind of sensor. The sensor which was used was a infrared microsensor, developed and fabricated at Institut d'electronique, de microelectronique et de Nanotechnologie (IEMN), Universitié des Sciences et technologies de Lille, France *. These are high sensitivity planar infrared microsensors, and are capable of measuring radiation from one hemisphere. These are made using standard silicon technology, with doped polysilicon thermocouples being used as thermopiles. The sensor construction is such that it has a low influence to convection and can be used without a shield. The sensor used, measured 9 mm by 8 mm (thickness less than 0.3 mm), with a sensitivity of 80 μV/W^2. The sensor was calibrated at the IEMN facility. The sensor was glued on to a 9 mm by 9 mm aluminium plate which acted as a heat sink. A thermocouple to measure cold junction temperature was fixed to this plate. This assembly was stuck to a small acrylic plate (10 mm by 10 mm), and the whole arrangement was fixed to a thin stainless steel rod. The details are shown in figure 2.20. The rod was fixed to a stand similar to the ones used for the net radiometers, and thus the sensor could be traversed vertically for measurement of

*I heartily thank Prof. D. Leclercq at IEMN, Universitié des Sciences et technologies de Lille, France, for promptly sending us two of these sensors to be tried out in our experiments

flux divergence.

2.2.5 Data Acquisition

A HP make programmable data logger (34970A) was used to record and store the data obtained during each observational run. Switching was done by a twenty channel HP make multiplexer module (34901A). Two such modules were used, thus providing a total of forty measurement channels. The thermocouple leads, and the output or power input wires from the other sensors were plugged into a small board placed near the edge of the concrete patch. This board was placed inside a well insulated box to ensure that the thermocouple terminals were all at the same temperature. A cable, also plugged into the board, carried all the sensor signals to the data logger, as well as carrying power for the humidity and wind sensors. A UPS was used to provide power to the data logger, and the wind and humidity sensors. The data logger was programmed to collect the data at regular intervals of time (typically 5-10 seconds), and the data was later transferred to a computer for further analysis. An observer was present throughout the observational period to ensure the safety of the instrumentation, and to maintain notes regarding the conditions during the observations. The observer was stationed about 10 meters away from the edge of the concrete patch to avoid any interference with the phenomenon being observed, and this was also where the data logger, UPS, and other paraphernalia were kept.

2.3 Typical Observational Run

In this section, a brief description is given of the manner which a typical observational run was carried out. For the case of the bare concrete surface, the procedure

was straightforward. As mentioned before, the experimental paraphernalia was brought to the site from a small room (about a hundred meters from the observation site) where they were stored. The mast was fixed in the center and then the sensors were unpacked and deployed as described in the earlier section. All other materials were then removed to a location about 10 meters away from the edge of the concrete patch. The data logger and UPS were also placed here, and this was also where the observer was stationed throughout the observations. The sensors were wired to the data logger and power supplied to those sensors that required it. The data acquisition was then started. This whole procedure usually took about 2.5 to 3 hours for a single person to carry out. Typically, the data was acquired for anywhere between 2 to 3 hours, the acquisition time being limited by the battery backup as well as the memory of the data logger. This concluded a single observational run, after which the equipment was dismantled, packed and taken back to the room until the next observation day. It must be mentioned here that, by the time the observations on the modified surfaces were begun, a laptop was acquired for use in the field. Transferring the acquired data from the data logger to the laptop would free the data logger memory, allowing more data to be recorded. Thus, in conjunction with a larger battery (35 Ah), two observational runs could be made in one night, with an interval of about an hour or so between them to allow for the data to be transferred to the laptop.

For the surface modification involving the panels, the procedure was similar. The panels were first placed on the observation area and the sensors were then deployed as usual. But in the case of the panels with an aluminium foil top ('thermofoam with aluminium' surface), it was important that one did not have to step onto the panels to place the sensors, as any dirt layer on the aluminum foil could drastically reduce its reflectivity. Hence, in this case, all panels except one were

Material	ϵ_g	β	Number of Observations
Concrete	0.90 ± 0.01	4.3	55
'Aluminium on concrete'	0.04 ± 0.02	2.8	12
Thermofoam	0.89 ± 0.01	33	4
'Thermofoam with aluminium'	0.04 ± 0.02	43	2

Table 2.3: A table summarizing the surface properties of the various surfaces used in the experiments.

placed on the concrete patch, so that there was access to the mast. The sensors (both on the mast and otherwise) as well as other sensors were then placed without stepping onto the panels and finally, the remaining panel was put in place. The complete observational set up for the case of the surface modified with panels required two persons and took about 4 hours to complete.

As mentioned before, for the case of the 'aluminium on concrete' surface, a thin layer of water was necessary between the aluminium foil and the concrete to ensure proper thermal contact. The aluminium foil was laid as slightly overlapping strips. In spite of utmost care, there were always a few places where the underlying water would seep onto the top surface of the aluminum foil. If this water is dirty, it can again reduce the reflectivity of the foil. Hence, right in the beginning, the concrete surface was mopped clean. After this, the aluminium foil was laid in strips with a water layer below them. The strips overlapped slightly and were pressed down flat with a roller. As in the case of the panels, it was advisable not to step onto the surface to place the sensors. Hence, a small area was left without the aluminium foil, so that there was access to the mast, and only after all the sensors were in place was that area covered with aluminium foil. The whole set up procedure for this case required two persons and took about 5 hours.

The observations on the concrete surface used in the thesis were made over a period of four years (2004-2007). In each year, the observations were made in

winter and early summer (before the monsoon set in), typically from January to May. The observations on the 'aluminium on concrete' surface were made from March to May, 2006. Thus, the ambient conditions for observations made on these surfaces were not fixed, but covered the wide range encountered during all the observations, e.g varying winds speeds, humidity, etc. The observations on the thermofoam and 'thermofoam with aluminium' surface were made in April 2007.. A summary of the surface modifications, their characteristics and the number of observations carried out on each surface is given in table 2.3. Included are the normal emissivity values [†] for the samples.

[†]I heartily thank Prof. A. Meulenberg, visiting scientist, Dept. of Physics, IISc, Bangalore for making the emissivity measurements.

CHAPTER 3

FIELD OBSERVATIONS: RESULTS

Introduction

In this chapter the results of the field observations will be presented. The chapter is organized as follows: In section 3.1, the manner in which the data was processed, and the methods used to estimate the spatial derivatives of the temperature are presented. The observations made over the concrete surface are presented next in section 3.2. Results include the near surface temperature gradients and the dependence of the intensity of the minimum on wind speed and turbulent intensity. Sections 3.3 to 3.5 deal with the related observations over the modified surfaces. Attempts to measure near surface radiative flux divergence, and estimates of the of the same are discussed in section 3.6. Temperature fluctuations that are observed on calm days forms the topic of section 3.7. The chapter concludes with a summary of the chief results from the field observations.

3.1 Data Processing

As mentioned, the data from the field observations was transferred to a computer for further analysis. The raw data, with some exceptions, was rarely used while analyzing the observations or in the graphs presented here. In this section, a brief overview is given to indicate the way in which the data was processed.

First, the data was passed through a low pass filter. The filter used was a simple moving average, with an averaging window of 5 minutes. In the case of the wind

data, the raw data and the moving average obtained from it was used to calculate the standard deviation of the wind speed, which would serve as a measure of the level of turbulence. Unless otherwise mentioned, the basic quantities (temperature and wind speed), discussed in this chapter are filtered in this manner.

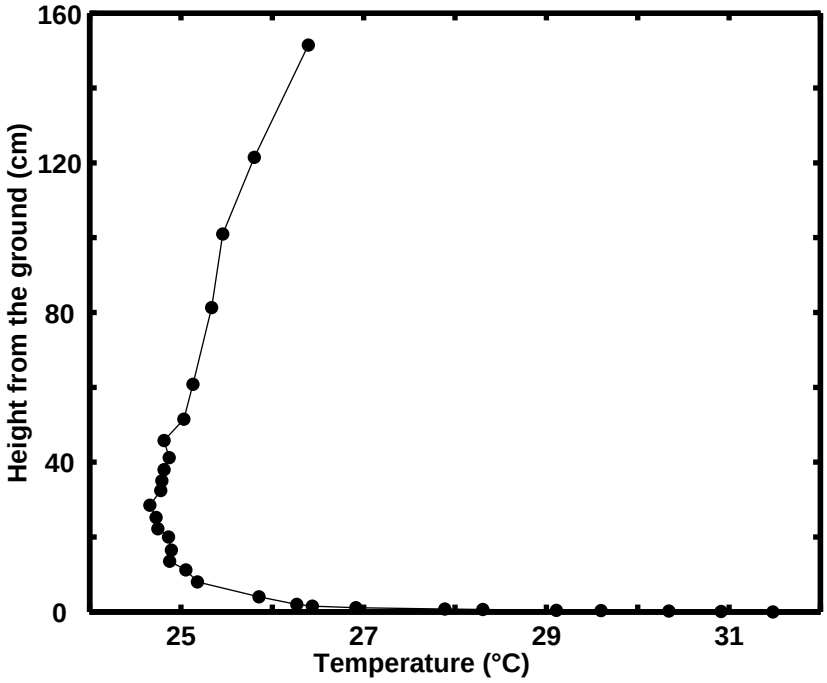

Figure 3.1: A typical vertical temperature profile. The temperature data has been low pass filtered with a simple moving average, with a window of 5 minutes.

Figure 3.1 shows a typical lifted minimum profile. The temperatures on the X axis are filtered as mentioned above. It is seen that there is some noise in the data, and the line joining the data points is far from smooth. This is to be expected as, among other sources of error, there will be systematic errors in measurement of height and temperature. As far as evaluating a quantity like intensity of the minimum is concerned, these errors are quite small and will not make a significant difference. But evaluating the near surface gradients will require the first spatial derivative of the temperature data, and later on (section 3.6) second derivatives of

the temperature profiles will also be used to obtain information on the near surface radiative flux divergence. However, obtaining derivatives from experimental data is unreliable, and even small errors are highly magnified in the process. Currently, the most widely followed procedure for differentiating experimental data is to fit a set of polynomial or spline curves to the data and then to differentiate these curves analytically to obtain the derivatives. Even so, the results cannot be guaranteed to be reliable. In spite of these difficulties, it will clearly be valuable to have at least some idea of the near surface gradients and flux divergences. Hence, two slightly different procedures are used for fitting a smooth curve to the data. A comparison of the derivative values obtained form these two procedures, gives some idea of the errors involved in estimating these quantities.

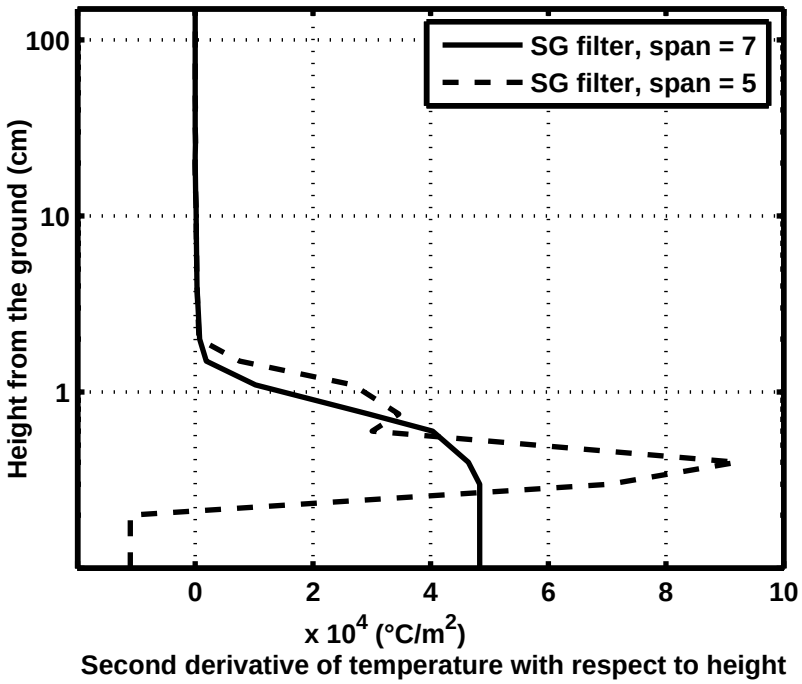

Figure 3.2: A comparison of the second derivative of temperature with respect to height, estimated by a 7 point and 5 point SG filter. The 7 point filter provides a smoother estimate.

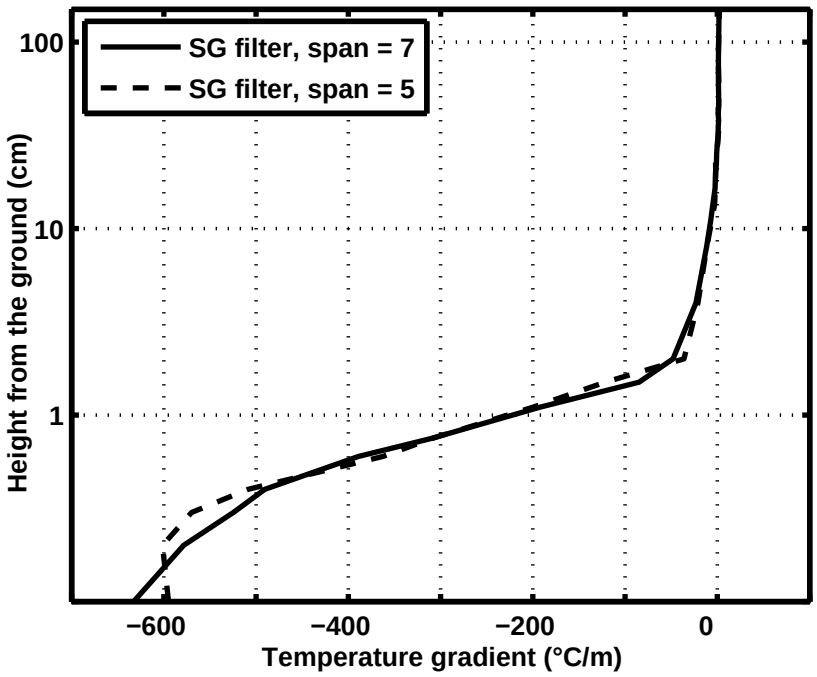

Figure 3.3: A comparison of the first derivative (temperature gradient), estimated by a 7 point and 5 point SG filter. The results agree very well.

In the first procedure, a Savitzky-Golay filter (SG filter) was applied to the data. In this, each point is replaced by a corrected or filtered data point. The method for a one dimensional case (one independent variable x, and one dependent variable y) can be described as follows: to obtain the filtered y value for a particular data point (called the estimation point), a set of contiguous data points (the span) which includes the estimation point is chosen. Usually, the span is odd, so that there are an equal number of points on either side of the estimation point, though this will not be possible near the ends of the data set. Then, a polynomial is fitted to these points in a least squares sense. The value of the polynomial evaluated at the estimation point is the corrected y value. The derivative of the polynomial at the estimation point is taken as an estimate of the derivative of the data at the estimation point. It can be shown that this procedure is equivalent to a weighted moving average

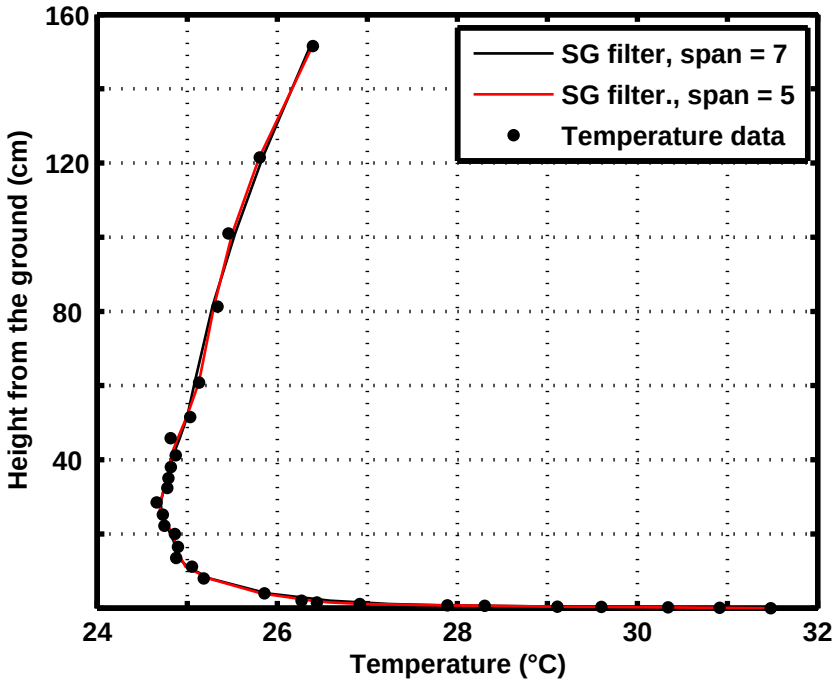

Figure 3.4: A comparison of the temperature profiles (zeroth derivative), estimated by a 7 point and 5 point SG filter, showing very little difference.

(Savitzky & Golay (1964)), with the weights depending only on the x values of the data points. Weights can be obtained for the filtering as well as for the derivatives. This highly simplifies implementation of the procedure. A MATLAB routine was written to implement the Savitzky-Golay filtering. A second degree polynomial was used. For a fit with a quadratic polynomial, the minimum odd span would have 5 points, as a quadratic polynomial would exactly pass through 3 points. However, for our data, a 5 point span did not give the requisite amount of smoothing as compared to a 7 point span, especially for the second derivatives, where small errors would be strongly amplified. In figure 3.2, the second derivative of the temperature with respect to the vertical coordinate, at a given instant, obtained by a SG filter with spans of 5 and 7 points is shown. It can be seen that the derivative obtained with a 5 point span shows a huge jump very near to the surface, going from almost zero

to a very high value and then decreasing to zero. This is due to small errors in the height of the near surface temperature sensors, which are magnified by taking the second derivative. Such non-monotonic behavior is not expected on any theoretical grounds. The second derivative estimated from a 7 point is smoother and seems to 'average out' the near surface jump in the 5 point filter. In cases where the 5 point filter does not exhibit such jumps, the 7 point and 5 point filters agree quite well. But the 7 point filter sometimes tends to underestimate the derivatives as compared to the 5 point filter, with the worst case disagreement being less than 35% just above the surface (heights less than 4 mm). As will become clear when second derivatives are estimated by the second method (to be discussed shortly), the inherent uncertainties involved in finding second derivatives are much higher than 35 %. As one can at best hope to find the order of magnitude of the second derivatives from such data, this discrepancy between 5 and 7 point filters is not serious. The discrepancies are however lesser when estimating the first derivatives (temperature gradients). Shown in figure 3.3 is the temperature gradient (for the same data used for calculating the second derivatives above), by both the 5 point and 7 point SG filters. Needless to add, for the temperature profiles themselves (zeroth order derivatives), the two fits are indistinguishable (figure 3.4). As it achieves desirable smoothing and does not exhibit large near surface fluctuations in the second derivatives, the 7 point SG filter was used in all the calculations. The SG filter is also used to find the intensity and height of the minimum. For each vertical profile, the SG filter is applied. The intensity is simply found by taking the difference between the value of the SG filtered ground temperature and the minimum value of the SG filtered temperature data. The height of the minimum is the height corresponding to this minimum point.

The other procedure consisted of using the *spap2* routine in MATLAB. This

provides a least squares spline fit (LS spline fit) to the data. As the temperature profiles are expected to have a monotonic first derivatives, a quadratic spline was chosen. The number of polynomial pieces to be used for the fit was chosen such that the mean of the residuals was the closest possible to the residuals obtained from the 7 point SG filter for the same data. The derivatives of these least squares splines are then taken as estimates of the derivatives of the data. The splines are also used to find the intensity and height of the minimum. The intensity is simply found by taking the difference between the value of the spline fit at the ground and the minimum value of the spline. The height of the minimum is the height corresponding to this minimum point.

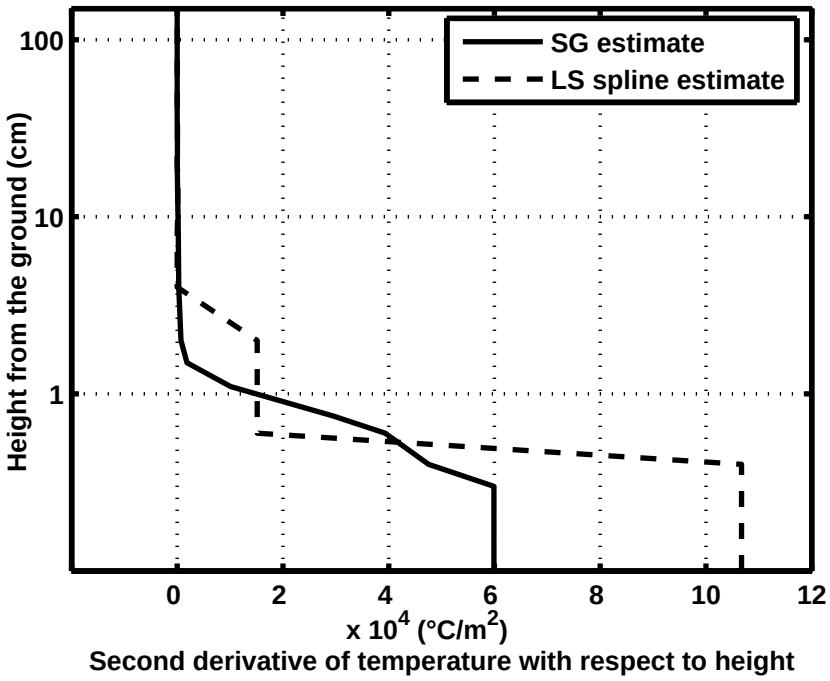

Figure 3.5: A comparison of the estimates of the second derivative of temperature with respect to height from a SG filter and LS spline fit.

To get an idea of the uncertainties involved in derivative estimates (especially for the second derivative), the second derivatives of temperature at a given instant,

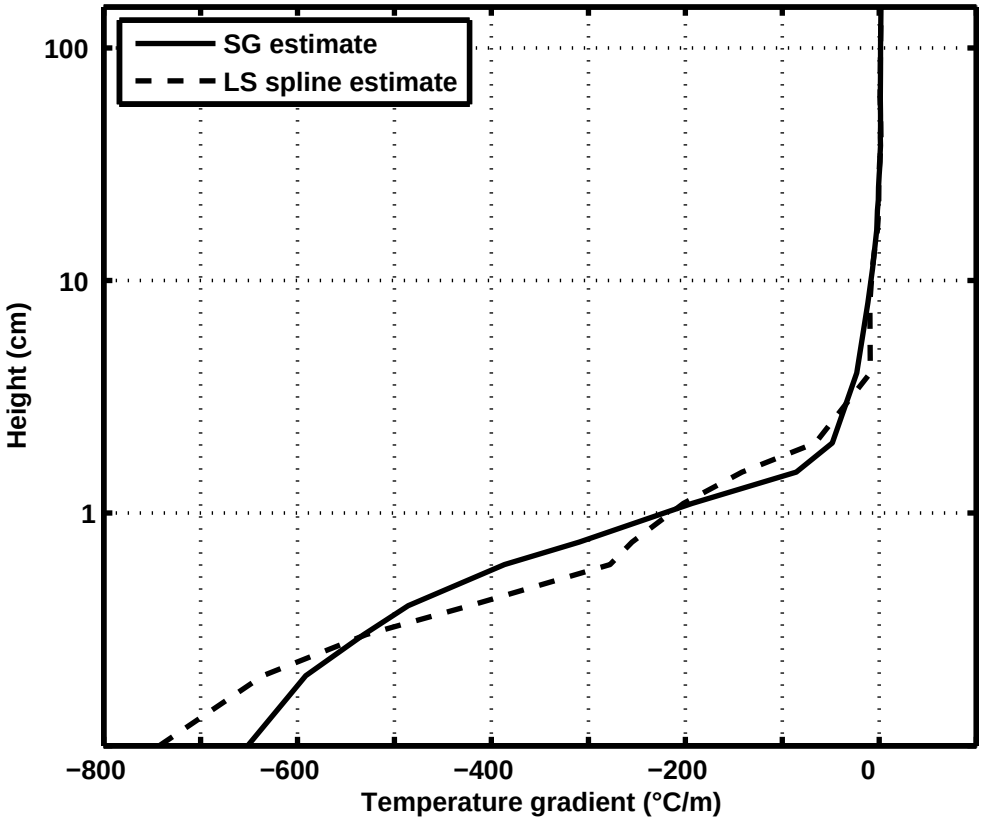

Figure 3.6: A comparison of the estimates of the first derivative of temperature with respect to height (temperature gradient) from a SG filter and LS spline fit.

obtained from the SG filter and LS spline fit are shown in figure 3.5. The data set used is still the same as used in the SG filter examples above. It can be seen that the disagreement is the worst just above the surface, and is almost 50% of the mean of the estimates from the two methods. Typically, the agreement is better than 50% for more than 80% of the total data, though for a small fraction of the data (less than 5%), the disagreement can be as high as 100% of the mean. As shown in figure 3.6, the agreement is much better for the first derivative (temperature gradient). The agreement is better than 10% for about 80% of the consolidated data, and is

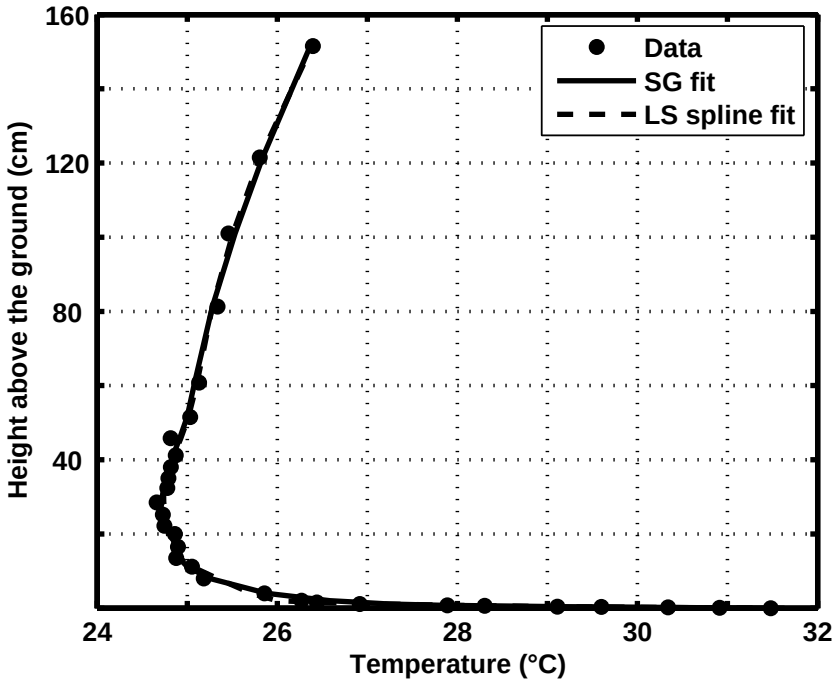

Figure 3.7: A comparison of the filtered vertical temperature profile (zeroth derivative of temperature with respect to height) from a SG filter and LS spline fit.

never worse than 30%. The fits to vertical profile (zeroth order derivative) from these two methods are shown in figure 3.7. Clearly, differences in estimates of quantities like intensity of the minimum by these methods will be insignificant.

Having obtained some idea of the uncertainties involved in derivative estimates, from now on, for the vertical profiles or gradients or second derivatives of temperature, the SG filter (with a seven point span) will be used. The original data points will be omitted in most cases and only the filtered curve will be shown.

3.2 Observations over the concrete surface (high ϵ_g, low β) surface

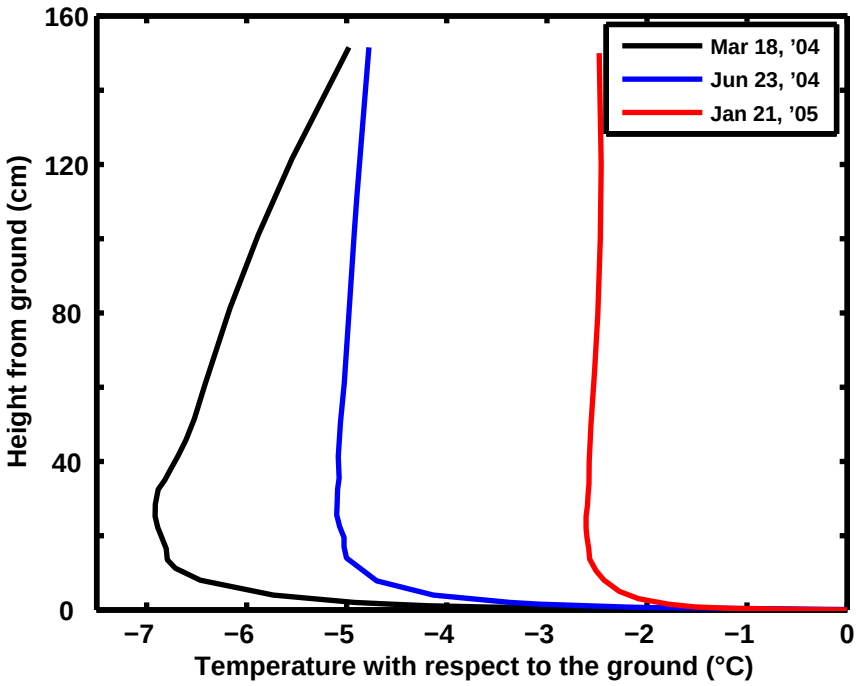

Figure 3.8: Typical lifted minimum profiles obtained over the concrete surface (baseline case). Note the minimum with an intensity of about 7 ^{o}C obtained on Mar 18, 2004.

To begin with, we will present in detail, our observations over the concrete surface, which is a high ϵ_g, low β surface. Observations on this surface, serve as the baseline case with which to compare observations conducted on the other modified surfaces.

Typical vertical temperature profiles with the lifted minimum obtained from our field observations are shown in figure 3.8. These profiles were obtained over the bare concrete surface (high ϵ_g, low β surface). It may be noted that on March 18, 2004, intensity of the minimum was as high as 7 °C. That these minima are not

advective is demonstrated by the fact that in our observations, without exception, the intensity of the minimum increased whenever the wind speed decreased, reaching maximum intensity for wind speeds tending to zero. This will be discussed in the next section.

Dependence on Wind speed

In typical observations over soil, the factor which has the most striking influence on the phenomenon is the wind speed. Previous researchers (Raschke (1957), Oke (1970)) found that the intensity reduced with increasing wind speed, till, above a threshold value (ranging from 50 cm/s to 1 m/s), the lifted minimum profile was replaced by an inversion. Our observations show a similar trend, though there was never a case, even at the highest wind speeds encountered, where an inversion was obtained. In figure 3.9, a time series plot, from data obtained on February 23, 2004 is shown. As will be usual in such plots, the time refers to the time after the start of observations. The top panel shows the average wind speed. The middle panel indicates temperature traces at different heights. For clarity, not all the temperature traces have been shown. In addition, to avoid overlap, the temperature trace of each successive thermocouple (staring at the ground and going upwards), is offset by an an additional 0.5 °C over the previous one. Consequently, except for the ground temperature, the values of the of the other temperature traces do not have actual meaning. Hence, except at one point, actual temperatures are not indicated on the Y-axis. Instead only relative magnitudes are indicated. The bottom most panel indicates the intensity of the minimum. Up until about 70 minutes after the start of observations, the wind speed was low. Around 80 minutes, the wind speed suddenly picked up. At this time, the air layers just above the ground started warming up relative to the ground, the ground cooling

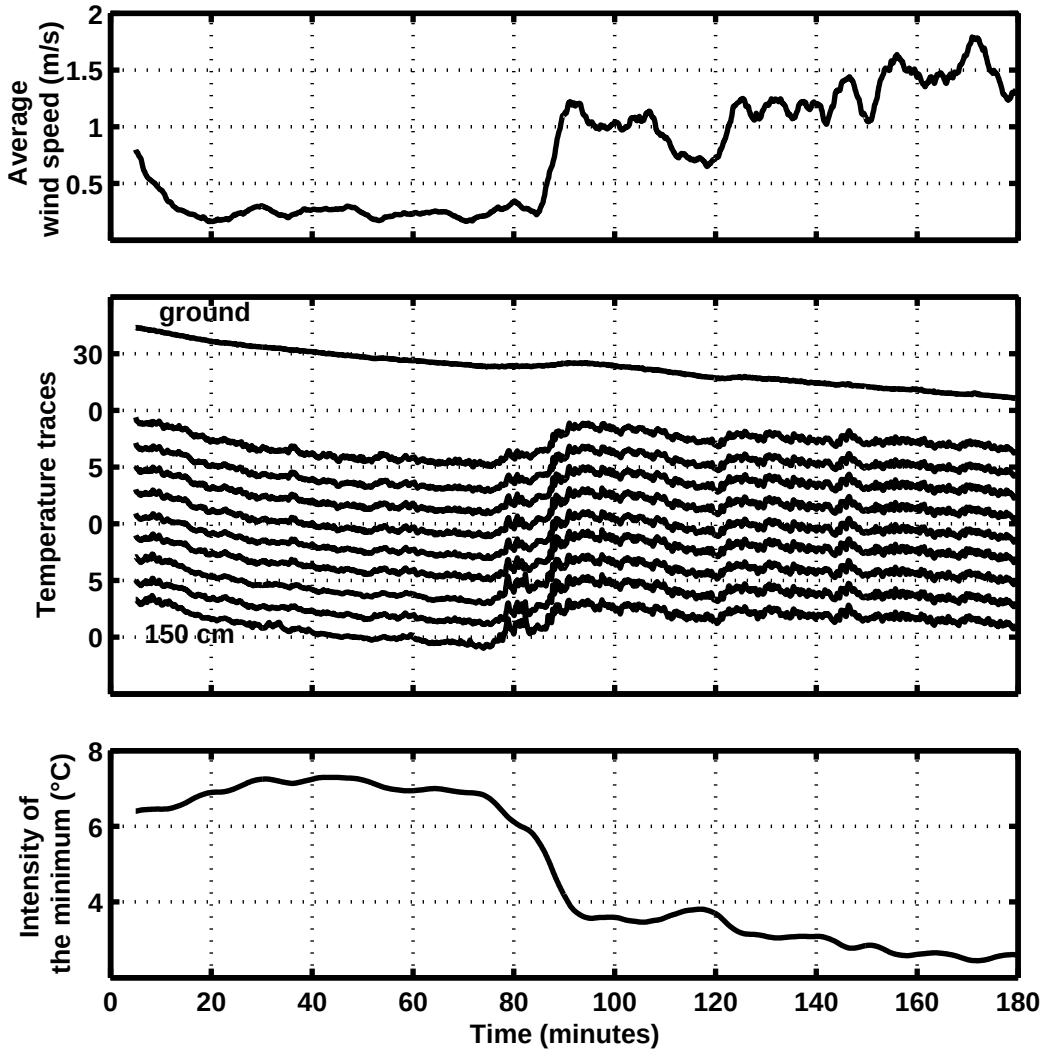

Figure 3.9: Effect of wind speed on the intensity of the minimum (from data obtained on Feb 23, 2004). At around 70 minutes (after start of observations), the wind speed increased rather suddenly. Immediately, the air layers above the ground warmed up relative to the ground and the intensity of the minimum went down.

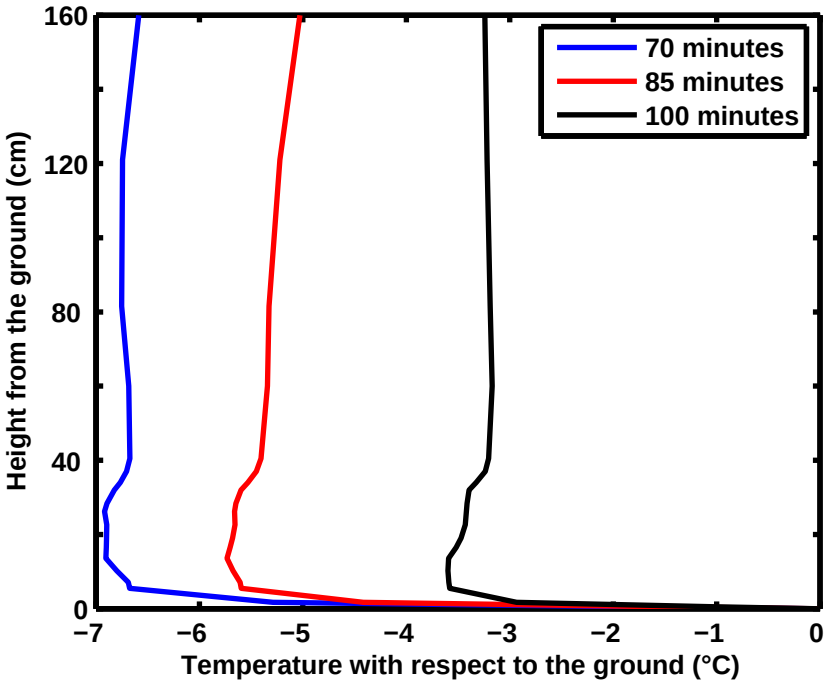

Figure 3.10: Temperature profiles corresponding to data presented in figure 3.9, showing weaker minima associated with higher wind speeds.

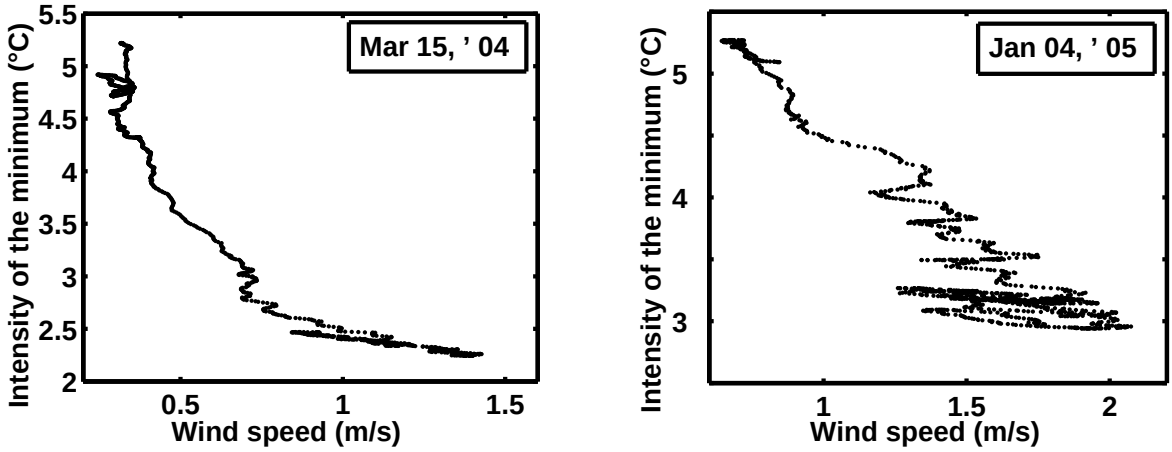

Figure 3.11: Scatter plots of wind speed versus intensity of the minimum, showing the strong dependence of the intensity of the minimum on wind speed. From data obtained on Mar 15, 2004 and Jan 04, 2005.

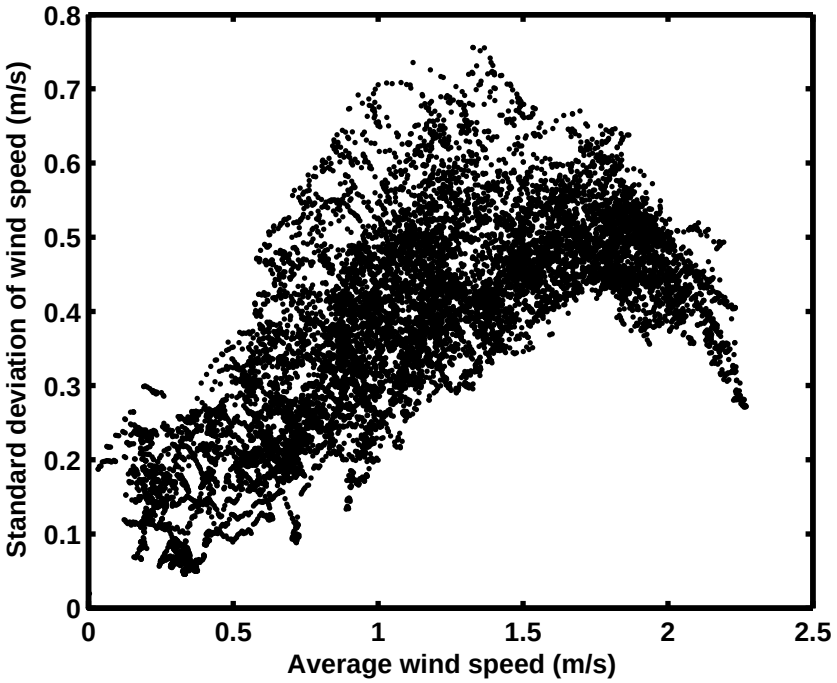

Figure 3.12: A consolidated scatter plot (from all the observations over the concrete surface) of average wind speed versus the standard deviation of the wind speed (representative of the turbulence levels). Higher levels of turbulence are associated with higher wind speeds.

rate being more or less unaffected. Within a few minutes, the intensity of the minimum went down. Profiles corresponding to this data set are shown in figure 3.10. This strong dependence of the wind speed on the intensity of the minimum is also brought out in figure 3.11, where scatter plots of wind speed versus intensity of the minimum are shown from data obtained on two different days. The trend is clear.

Turbulence levels also play an important role in deciding the intensity of the phenomenon. As typically higher wind speeds are associated with higher turbulence levels, this effect is hard to isolate. The high correlation between the average wind speed and turbulent intensity (represented by the standard deviation of the wind speed), is shown in figure 3.12. However, a clear example of the role of turbulence

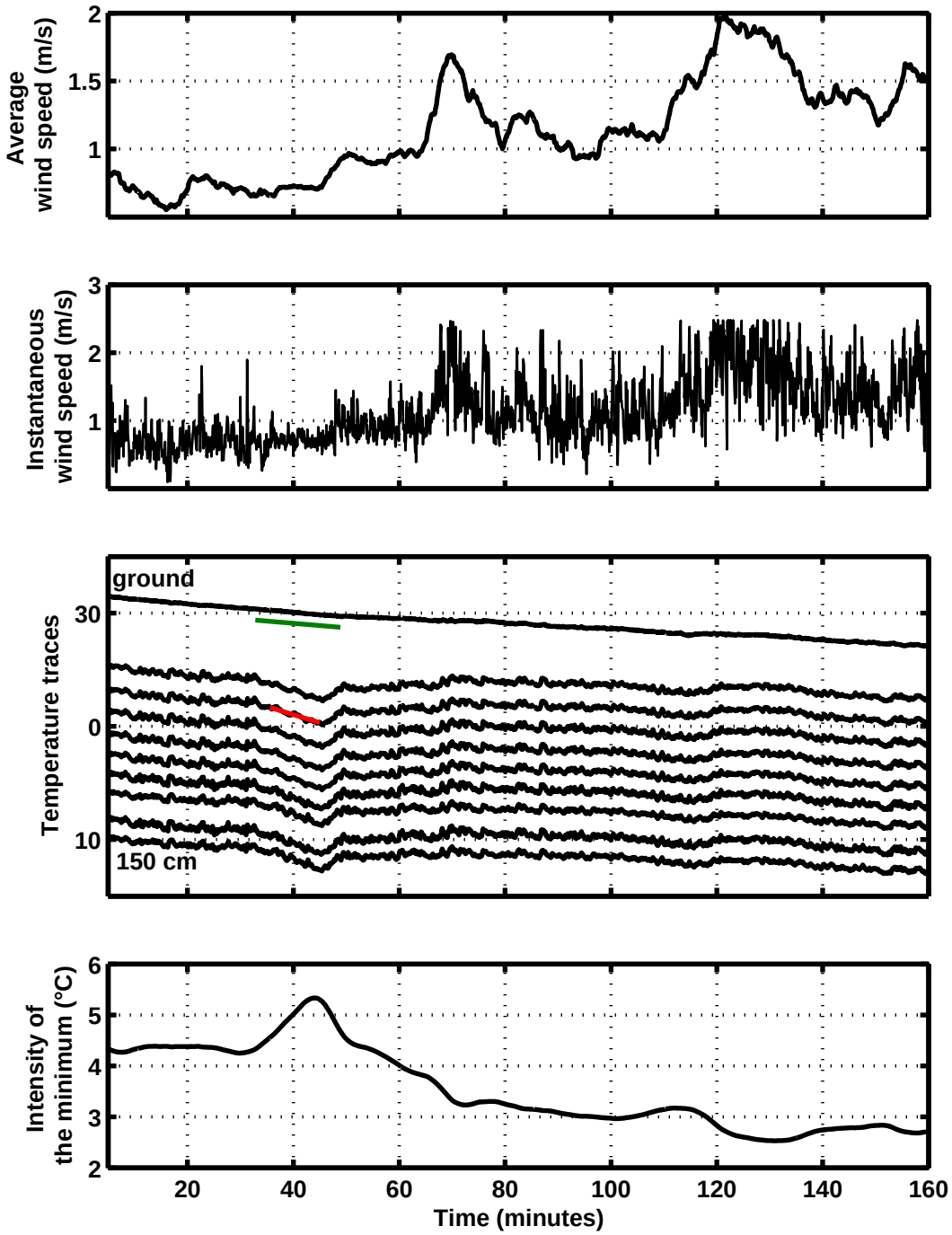

Figure 3.13: Effect of turbulent transport on the phenomenon. The data is obtained from observations on Feb, 28, 2004. Though the mean wind speed was almost constant from 20 to 45 minutes, there was a decrease in the intensity of turbulent fluctuations at about 30 minutes. The air layers above the ground cooled strongly, and the intensity of the minimum increased. It reduced again as both the intensity of fluctuations and mean wind speed picked up.

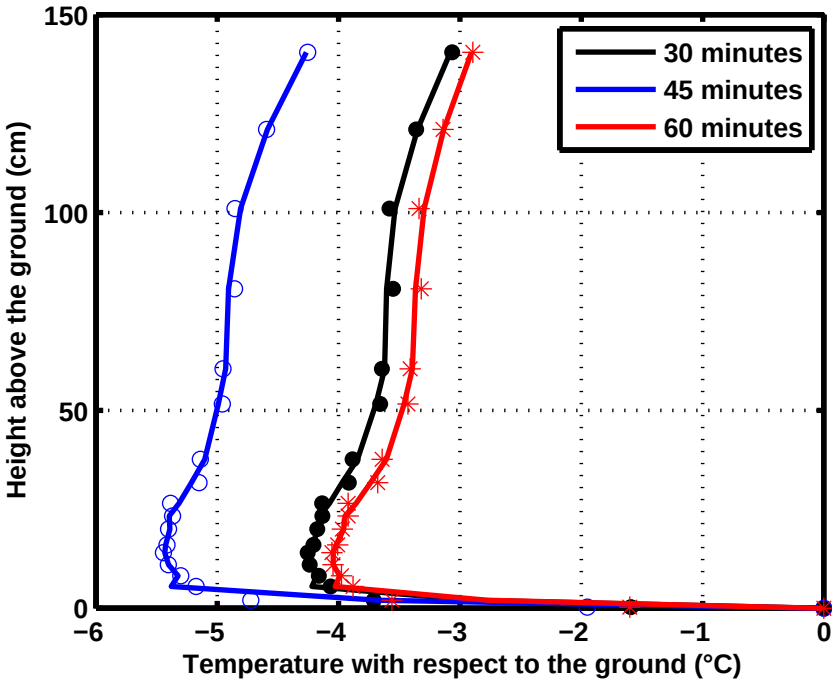

Figure 3.14: Temperature profiles corresponding to data presented in figure 3.13, showing the effect of turbulent fluctuations on the intensity of the minimum. The mean wind speed at the times corresponding to all the three profiles shown is the same, but the intensity of turbulent fluctuations was lower at t = 45 minutes, resulting in a stronger minimum.

levels, is afforded by data collected on Feb 28, 2004. The time evolution of average wind speed, instantaneous wind speed (without the averaging), temperature traces at selected heights and the intensities of the minimum are shown in figure 3.13. From 25 to about 45 minutes after the start of observations, the mean wind speed was more or less constant. However, at about 30 minutes, the intensity of turbulent fluctuations decreased. Immediately, the air layers above the ground started cooling at a faster rate (red line), the ground cooling rate (green line) being unaffected.This led to a rapid increase in the intensity of the minimum as seen in the bottom most panel. The corresponding profiles at 30 and 45 minutes shown in figure 3.14 clearly show the increase in intensity. At around 45 minutes, the intensity of turbulent

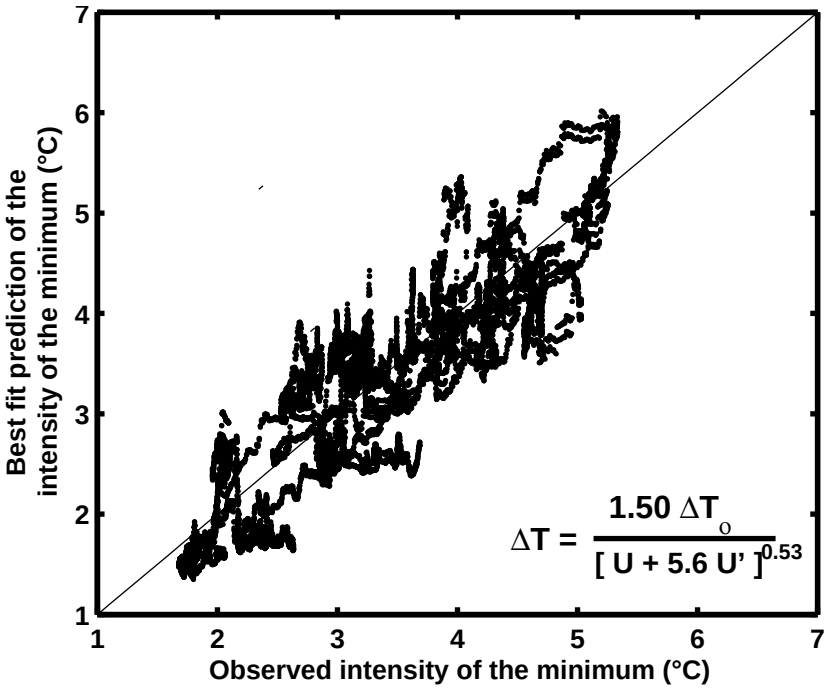

Figure 3.15: A scatter plot of predicted versus observed intensity of the minimum for consolidated data from observations over the concrete surface. The intensity is predicted by seeking a simple functional dependence of the intensity on wind speed and standard deviation of wind speed. The free parameters in the function are obtained by minimizing the difference between predicted and observed intensity values. The coefficient of determination r^2 for the fit is 0.74, while the standard error of the estimate S (root mean square error) is 0.47 ^{o}C.

fluctuations increased. The air layers once again quickly warmed up relative to the ground, and the intensity of the minimum again returned more or less to the value it had before this episode. A profile at 60 minutes is shown in figure 3.14, which has an intensity almost the same as the one at 30 minutes.

Considering the very strong dependence of the intensity of the minimum on the wind speed and standard deviation of wind speed, one could try and see if a simple functional relationship can be found between these variables. A simple dependence was sought of the form

$$\Delta T = a(U + bU')^c \tag{3.1}$$

Here ΔT is the intensity of the minimum, U is the wind speed and U' is the standard deviation of the wind speed.

Values of a, b and c were sought that minimized the difference between the predicted ΔT (from equation 3.1) and the observed ΔT for all the data points from a given observational run. The predictions made from equation 3.1 using the values for a, b and c so obtained were in good agreement with the observed values. Though values of b and c obtained for different observational runs were not too different, the value for a varied considerably. However, it was found that if ΔT was normalized by $\Delta T_\circ$, which is the intensity of the minimum right at the beginning of a given observational run, then the variation in a across observational runs was dramatically reduced. The quantity $\Delta T_\circ$ thus took into account the variations across observational runs arising from other variables like the absolute temperature of the ground, the effective sky temperature, ground cooling rates, humidity etc. The consolidated data from all the observational runs was then considered for a common fit. The consolidated data consisted of the data from all observational runs over concrete in which the measurements for all the relevant quantities were available. The best fit equation obtained for the consolidated data over the concrete surface was

$$\Delta T = 1.50 \frac{\Delta T_\circ}{(U + 5.6U')^{0.53}} \tag{3.2}$$

A scatter plot of the intensity of the minimum predicted from equation 3.2, versus the observed intensity of the minimum, for the consolidated data for the concrete surface, is shown in figure 3.15. The agreement is fairly good across observations.

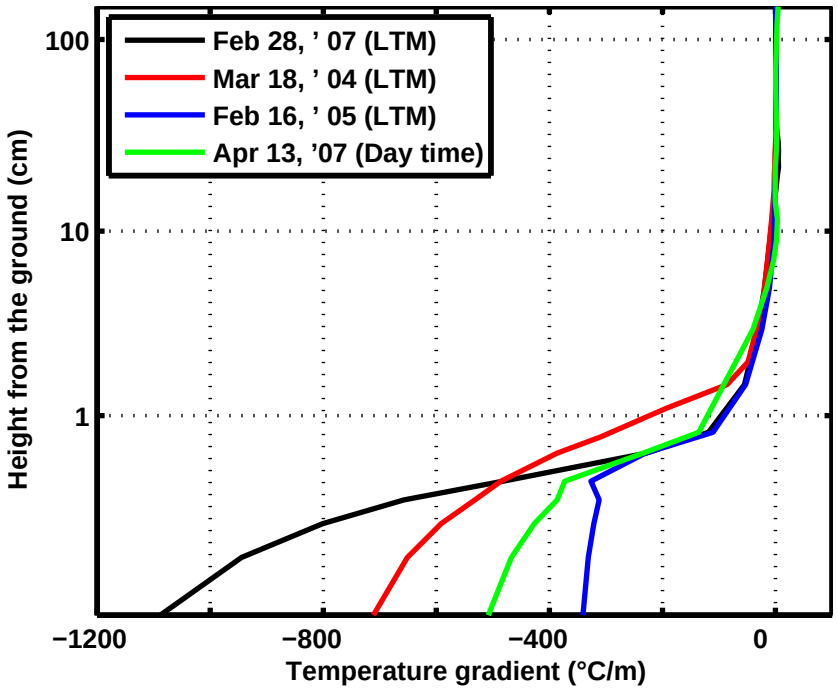

Figure 3.16: Typical near surface temperature gradients for the concrete surface (high ϵ_g, low β surface) during a lifted minimum, as well as during the day time. The gradients during a lifted minimum are surprisingly high, and are comparable to the gradients observed during the day.

Temperature gradients near the surface

During the day time, temperature gradients near the surface are negative and can be quite high in magnitude. For example, (Ramdas & Malurkar (1932)) reported gradients with a magnitude of order of 100 °C/m in the lowest 10 cm which is about ten thousand times the adiabatic lapse rate. Our observations indicate that surprisingly, near-surface gradients during the lifted minimum are of the same order of magnitude as that observed in day time. Temperature gradients near the ground during a lifted minimum obtained from our observations are shown in figure 3.16. The gradients shown in the figure are in low wind conditions (wind speed less than 0.3 m/s). For comparison, a typical day time gradient is also shown. The day time

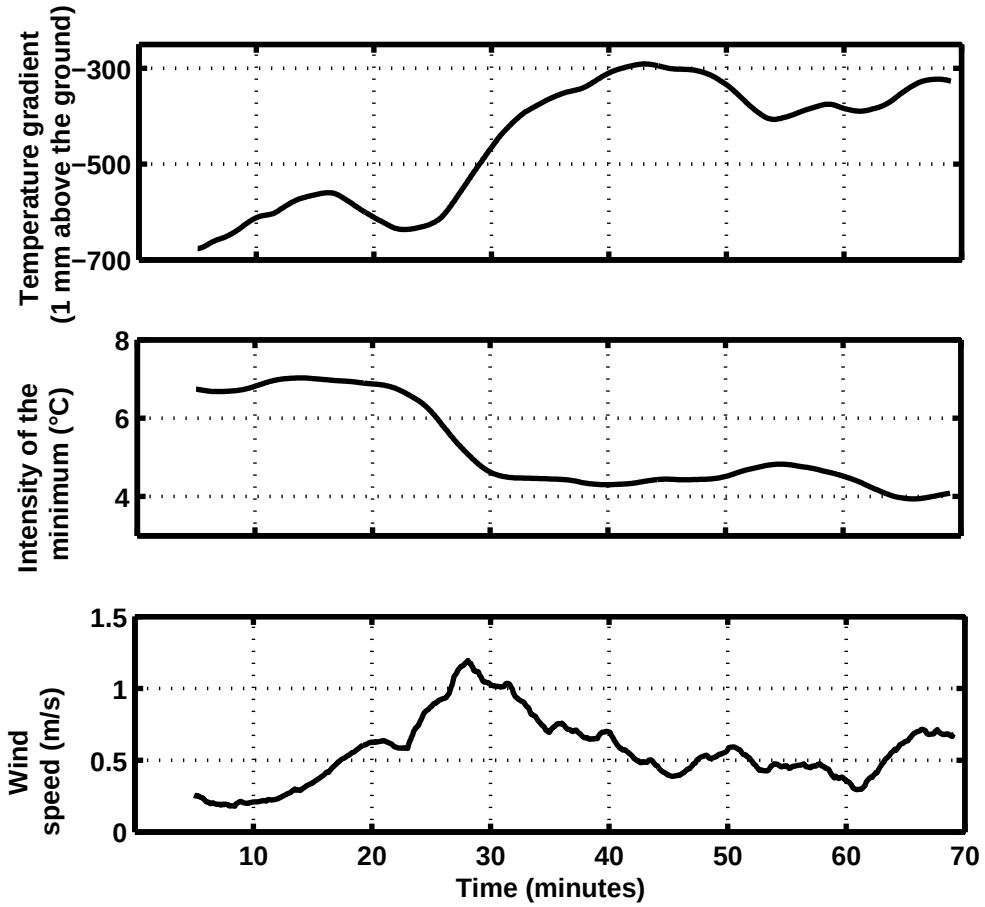

Figure 3.17: Time series plot showing dependence of temperature gradient on the intensity of the minimum. Typically, the near surface temperature gradients increase in magnitude with the intensity of the minimum.

gradient was obtained from similar observations carried out a little before noon (from about 10:00 a.m to 11:00 a.m) day time with shielded thermocouple sensors. It can be seen that the absolute value of the gradients just above the surface during a lifted minimum range from about 300 °C/m to more than 1000 °C/m. This is comparable, if not more than, the day time gradient of around 700 °C/m.

Typically, the gradient increases with increasing intensity of the minimum. In most cases, the wind speed itself does not seem to have a direct effect except in so far as the intensity of the minimum is strongly affected by the wind speed. The

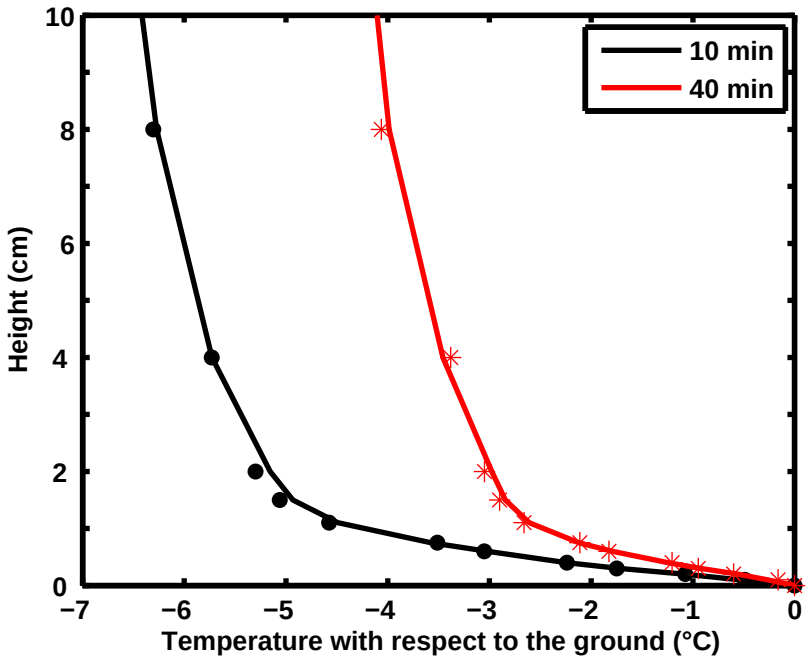

Figure 3.18: Temperature profiles in the first 10 centimeters above the surface, corresponding to the data indicated in figure 3.17, at two different times, again demonstrating that the gradients are typically higher for more intense minima.

time evolution of the gradient at a height of 1 mm, the intensity of the minimum and the average horizontal wind speed are shown in figure 3.17. This data is from observations made on Mar 18, 2004. It can be clearly seen that the near surface temperature gradients increase in magnitude with increase in intensity of the minimum. This is also clear from figure 3.18, where the temperature profiles at two different times are shown.

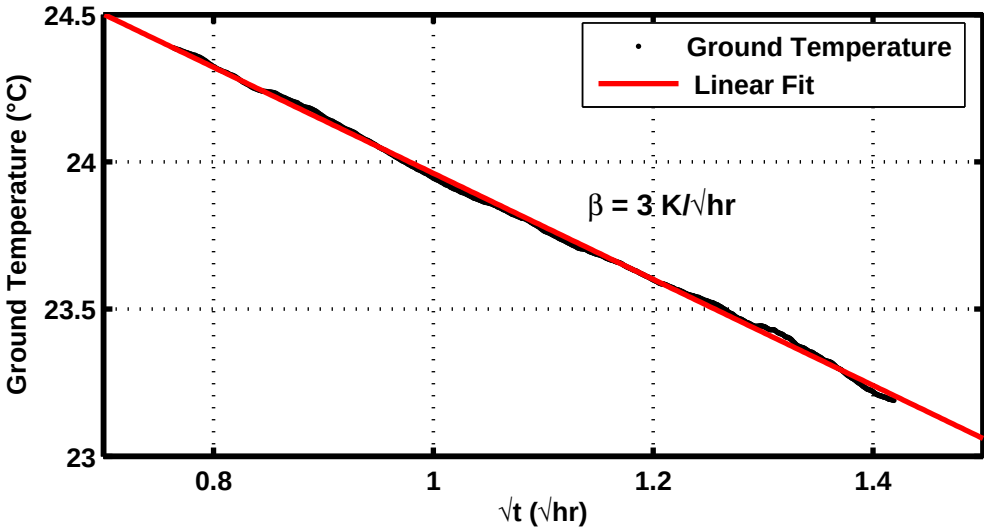

Figure 3.19: Ground cooling rate of the concrete surface(from data obtained on Jan 21, 2005), showing $\sqrt{t}$ behavior.

Effect of humidity

Humidity was monitored throughout most of the observations. The water vapor mixing ratio varied from about 5 - 10 g/kg. Over this range, there appears to be no significant effect of the humidity on the phenomenon, again in agreement with the VSN model.

Comment on β

The ground cooling rate parameter β plays is given considerable importance in the papers discussing the VSN model (Vasudeva Murthy *et al.* (1993), Narasimha & Vasudeva Murthy (1995), Ragothaman *et al.* (2001)). This section will be devoted to a discussion of the observed ground cooling rates in the base case (concrete). In figure 3.19, the variation of ground temperature with time is shown. Though the wind was not low (around 1.8 m/s throughout the observation period), the plot of ground temperature versus $\sqrt{t}$ is fairly linear, with a slope (β) of $3K/\sqrt{hr}$).

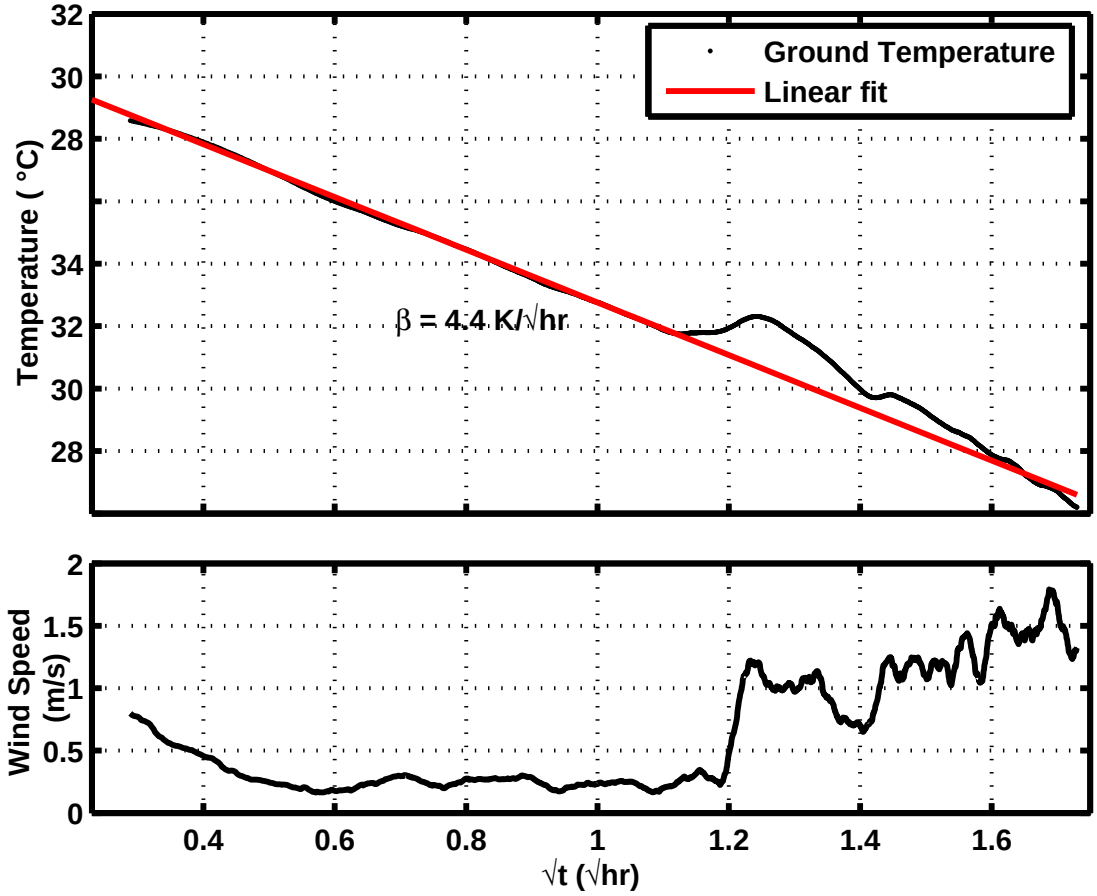

Figure 3.20: Ground cooling rates of the concrete surface (from data obtained on Feb 23, 2004), showing deviation from $\sqrt{t}$ behavior due to wind.

Even when winds are not very low, the deviation from $\sqrt{t}$ is not perceptible (over the period of our observations, which usually last from 2 to 3 hours). However winds are rarely constant throughout the night and under such circumstances, the ground does not cool as $\sqrt{t}$ throughout the observation period. These effects are so pronounced in the case of the high cooling rate surfaces (as will be shown later) as to render the concept of β meaningless. For the concrete surface, this effect can be seen in figure 3.20, where the ground cooling rate on Feb 23, 2004 is shown.

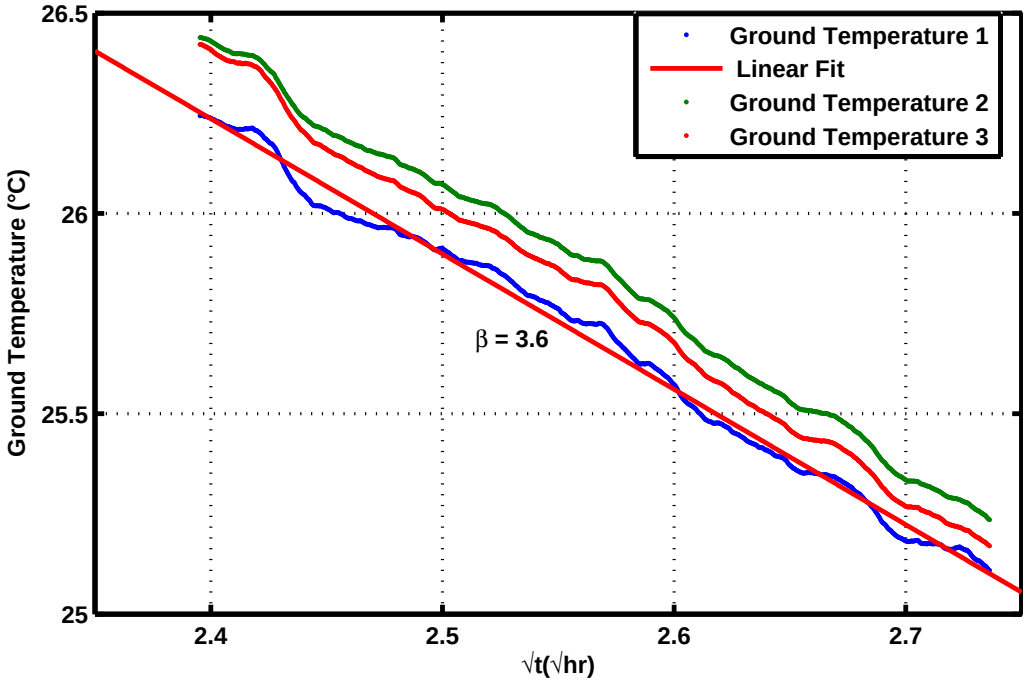

Figure 3.21: Ground cooling rates of the concrete surface (from data obtained on Feb 28, 2007), from the three sensors (spread out over a distance of about 25 cm) that measured the ground temperature. This shows that though there may be small spatial variations in the ground temperature over the concrete patch, the ground cooling rates are more or less the same.

The wind speed is low from the beginning of the observations up to $\sqrt{t} = 1.2\sqrt{hr}$, and a linear fit for this period is shown in the figure, with a β of $4.4K/\sqrt{hr}$. At $\sqrt{t} = 1.2\sqrt{hr}$, there is a sudden increase in wind speed, and there is a transient in the ground cooling rate. The wind settles more or less to a new (though different value), the ground cooling rate settles to a much larger value of β. Thus, there were many cases, even for the concrete surface, where a single β value could not be fitted over even the relatively short observation period of 2-3 hours. Moreover, as discussed by Ragothaman *et al.* (2001), even in the ideal case of a single β value over the night, the minimum could evolve in both height and intensity. Thus, though the concept of the parameter β is definitely useful in understanding the

basic mechanisms involved in the lifted minimum, it is probably of limited value in understanding actual field observations. This would be especially true for a low thermal inertia, low conductivity surface, e.g the sand surface in deserts.

In cases where more than one sensor spread out over a little distance (10 - 30 cm) were used to measure the ground temperature, it was observed that though there were spatial variations in the ground temperature (of the order of 0.1 - 0.5 °C over 10 - 30 cm), the ground cooling rates were more or less identical. An example of this is shown in figure 3.21, from data obtained on Feb 27, 2008.

Overall, the β values obtained from observations range from 3 to 7 $K/\sqrt{hr}$, which is is reasonable agreement with the theoretically derived value of 4.3 $K/\sqrt{hr}$. It must also be remarked that these β values are of the same magnitude as usually observed over soil surfaces by previous researchers (Raschke (1957)).

3.3 Observations on the 'aluminium on concrete' surface (low ϵ_g, low β surface)

This section deals with observations on the 'aluminium on concrete' surface (low ϵ_g, low β surface). Profiles obtained over this surface are shown in figure 3.22. The minima are very intense, with intensities reaching 13 °C. In fact, even with wind speeds above 1.5 m/s, the intensity of the minimum never fell below 9 °C. This is in line with the predictions of the VSN model, which predicts higher intensity of the minimum over a low emissivity surface.

Typical gradients in low wind conditions (wind speeds less than 0.3 m/s) over this surface are shown in figure 3.23. The gradients are much higher than those obtained over the concrete surface.

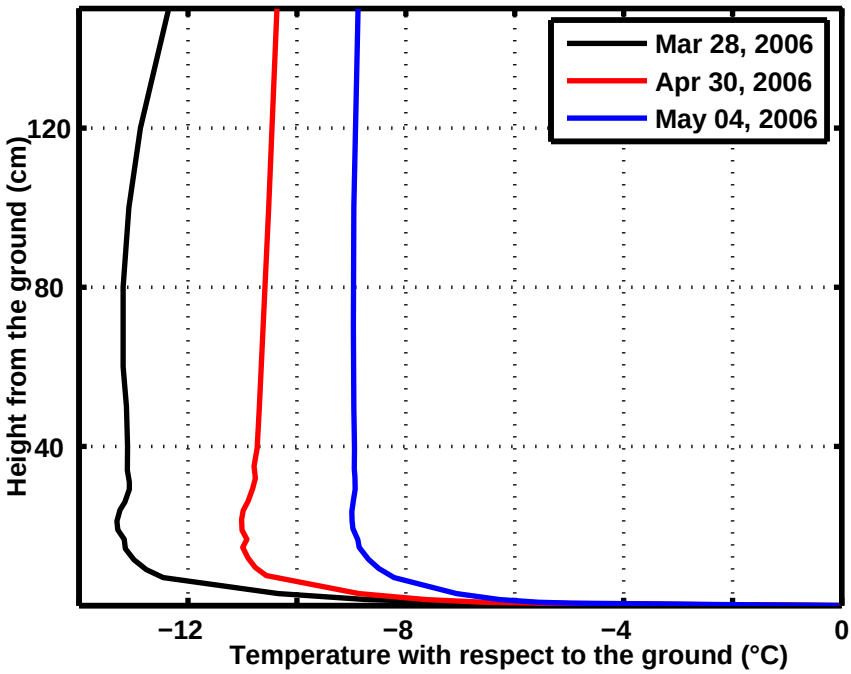

Figure 3.22: Profiles obtained on the 'aluminium on concrete' (low ϵ_g, low β surface) surface. The effect of the low emissivity is to produce intense minima, in agreement with the predictions of the VSN model.

One effect of the low emissivity surface is to reduce the radiative loss from the surface. Measured values of the net radiation range from 10 to 30 W/m^2. This naturally results in a lower cooling rate as compared to the concrete surface. In general, reasonable linear fits can be made over the observation period for most of the observational runs over this surface, with β ranging from 2 - 4 $K/\sqrt{hr}$. This is lower than the cooling rates over concrete (where the range was 3 - 7 $K/\sqrt{hr}$), but not dramatically so, and in fact, there is some overlap in the range of cooling rates for both these surfaces. This is because of the very high near surface gradients in the case of the 'aluminium on concrete' surface, which results in a high conductive flux just above the surface (of the order of 50 W/m^2). Thus, though the radiative loss has decreased, there is a considerable increase in conductive heat loss from the

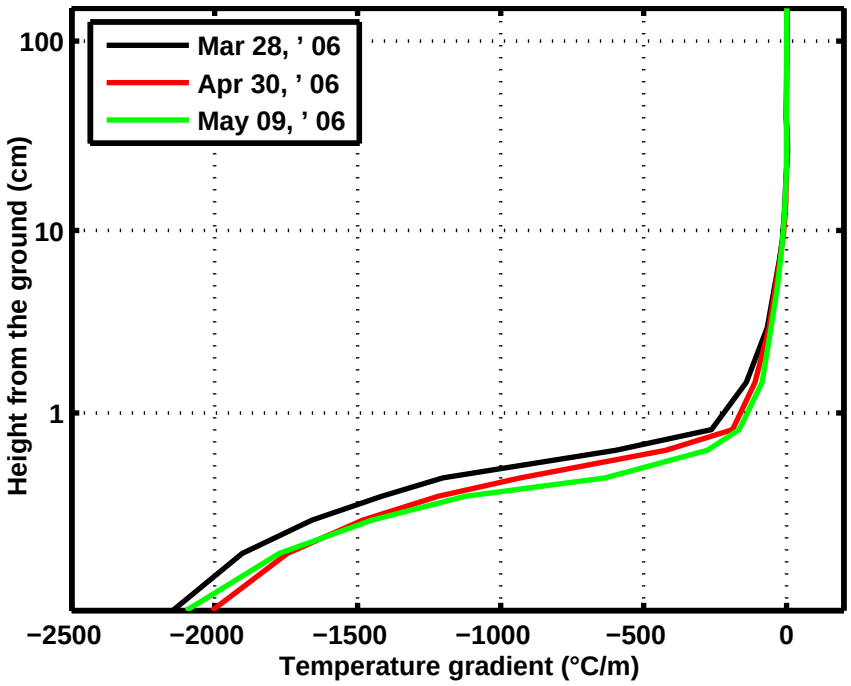

Figure 3.23: Typical near surface gradients obtained on the 'aluminium on concrete'(low ϵ_g, low β surface) surface. The near surface temperature gradients are higher than the base case (concrete surface).

ground. Consequently, the ground cooling rate does not decrease as dramatically as one would expect, and are only slightly lower than the concrete case (see the calculations shown in table 2.2). This lowering of the ground cooling rate can also be seen by comparing the range of ground temperatures obtained from observations over concrete and the 'aluminium on concrete' surfaces. Shown in figure 3.24 is a frequency histogram of ground temperature obtained from all observations over concrete and 'aluminium on concrete' surfaces. The frequency of observations has been normalized by dividing by the maximum frequency, so that the frequencies lie between zero and one. It was preferable to normalize in this manner as the number of data points over the concrete surface are much higher than those over the 'aluminium on concrete' surface. It can be seen that there is an overlap, but in

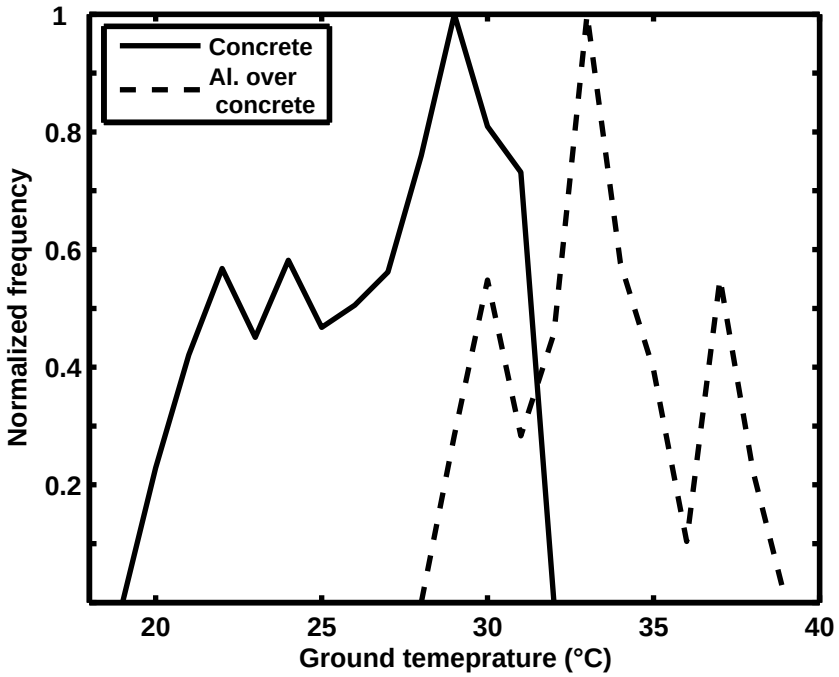

Figure 3.24: A histogram of measured ground temperatures over the concrete (high ϵ_g, low β surface) and 'aluminium on concrete' (low ϵ_g, low β) surfaces. The frequency has been normalized by the maximum frequency to obtain frequencies between zero and one. Though there is an overlap, the ground temperatures are higher in the 'aluminium over concrete' surface as compared to the concrete surface. For the concrete and 'Aluminium on concrete' surfaces, the total number of observations are 15,285 and 6576 respectively, and the maximum frequencies (used in the normalization) are 2157 and 1487 respectively.

general, the ground temperatures obtained from observations over the 'aluminium on concrete' surface are higher than those over the concrete surface. However, the dramatic increase in intensity of the minimum, cannot be attributed to the decreased cooling rates or increased ground temperature alone. In spite of the fact that there is an overlap of cooling rates and ground temperature values, there is no overlap in the intensity of the minimum obtained over these two surfaces. This can be seen in figure 3.25, where the frequency histogram of the intensity of the minimum obtained over the two surfaces is shown. Again, the frequency is normalized by the maximum frequency. This shows that the emissivity, besides lowering the ground cooling rate, plays a direct role in increasing the intensity of

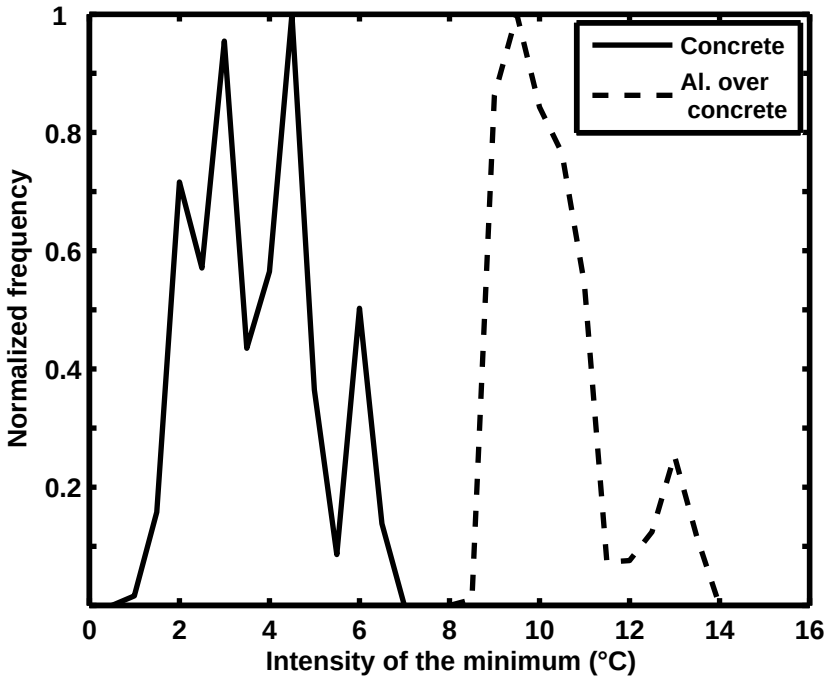

Figure 3.25: A histogram of intensity of the minimum over the concrete (high ϵ_g, low β surface) and 'aluminium on concrete' (low ϵ_g, low β surface) surfaces. The frequency has been normalized by the maximum frequency for the concrete and 'aluminium on concrete' surfaces respectively). In spite of an overlap in the ground cooling rate and ground temperatures, there is no overlap in the intensity of the minimum obtained over the two surfaces. This shows that the ground emissivity plays a direct role in increasing the intensity of the minimum.

the minimum.

The height of the minimum over the 'aluminium on concrete' surface did not differ significantly as compared to the baseline case. Except for emissivites very close to unity (greater than 0.9), the VSN model also does not show any significant effect of emissivity on the height of the minimum.

As a relatively large number of observational runs are available for this surface, one could try to obtain a functional dependence of the intensity of the minimum on the wind speed and standard deviation of wind speed, as was done for the observations over the concrete surface (see section 3.2). Following a similar procedure, a

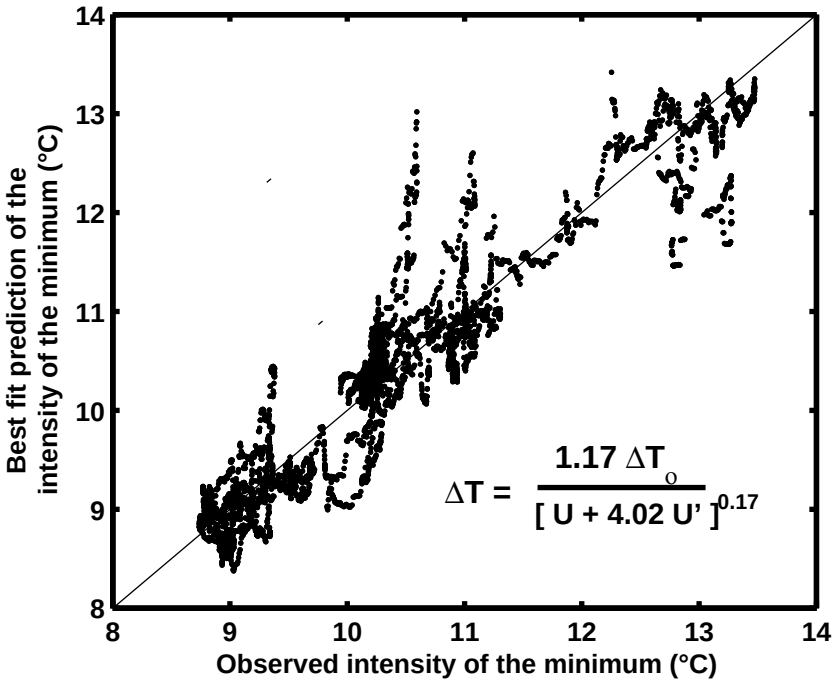

Figure 3.26: A scatter plot of predicted versus observed intensity of the minimum for consolidated data from observations over the 'aluminium on concrete' surface. The intensity is predicted by seeking a simple functional dependence of the intensity on wind speed and standard deviation of wind speed. The free parameters in the function are obtained by minimizing the difference between predicted and observed intensity values. The coefficient of determination r^2 for the fit is 0.62, while the standard error of the estimate S (root mean square error) is 0.72 ^{o}C.

best fit equation was obtained for the consolidated data over the 'aluminium over concrete' surface. The best fit equation obtained for the consolidated data over the 'aluminium over concrete' surface was

$$\Delta T = 1.17 \frac{\Delta T_\circ}{(U + 4.02U')^{0.17}} \tag{3.3}$$

The intensity of the minimum appears to depend less on the winds speed U than in the case of the concrete surface.

A scatter plot of the intensity of the minimum predicted from equation 3.3, versus the observed intensity of the minimum, for the consolidated data for the

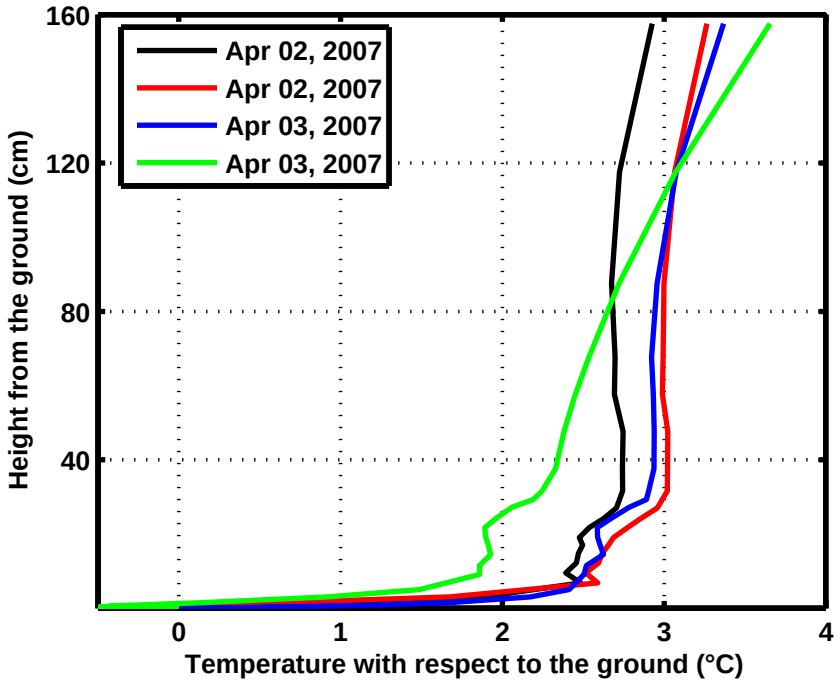

Figure 3.27: Temperature profiles obtained on the thermofoam surface (high ϵ_g, high β surface), showing that due to the rapid cooling of the surface, an inversion profile has developed over the observation surface, with the temperature minimum *at* the ground.

'aluminium on concrete' surface, is shown in figure 3.26.

3.4 Observations over the thermofoam surface (high ϵ_g, high β surface)

Though there are differences in ground cooling rate between different days in the concrete case itself, the differences are too small to show any marked change in the behavior of the minimum, especially considering there are many other variable factors which can mask any small changes. The effect of ground cooling rate is most dramatically shown up in observations over the thermofoam surface, which is a high ϵ_g, high β surface. The emissivity is almost the same as that of concrete, and

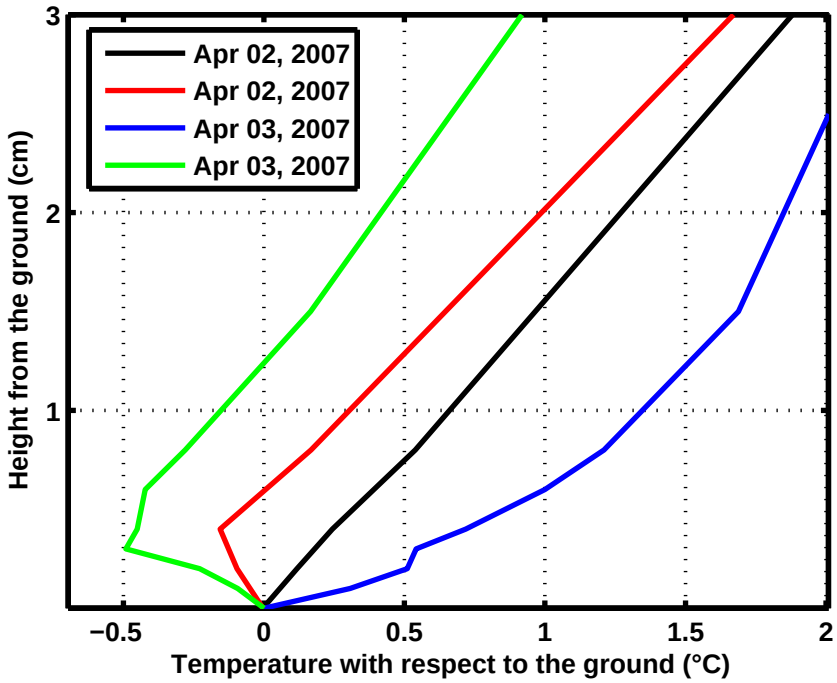

Figure 3.28: Magnified view of profiles shown in figure 3.27, showing that even on the rapidly cooling thermofoam surface, weak minima can sometimes form.

hence any differences (under similar conditions) are due to the cooling rate alone. This surface would correspond to natural surfaces over dry, loose soil or sand. The sand surface in a desert is a good example of such a high ϵ_g, high β surface.

Profiles obtained over this surface are shown in figure 3.27. The profiles are strikingly different from the base case. The profiles appear to be inversions, with the minimum temperature being at the ground. However, an inspection of these profiles very close to the ground (figure 3.28) reveals that two of these profiles, actually exhibit very weak minima, with both the intensity and height of the minimum being very low.

Both these minima occur on April, 03, 2007. In contrast, no minimum was formed throughout the observations on Apr, 02, 2007. The reason for the contrasting behavior on the two days can be seen from figure 3.29, where the time series

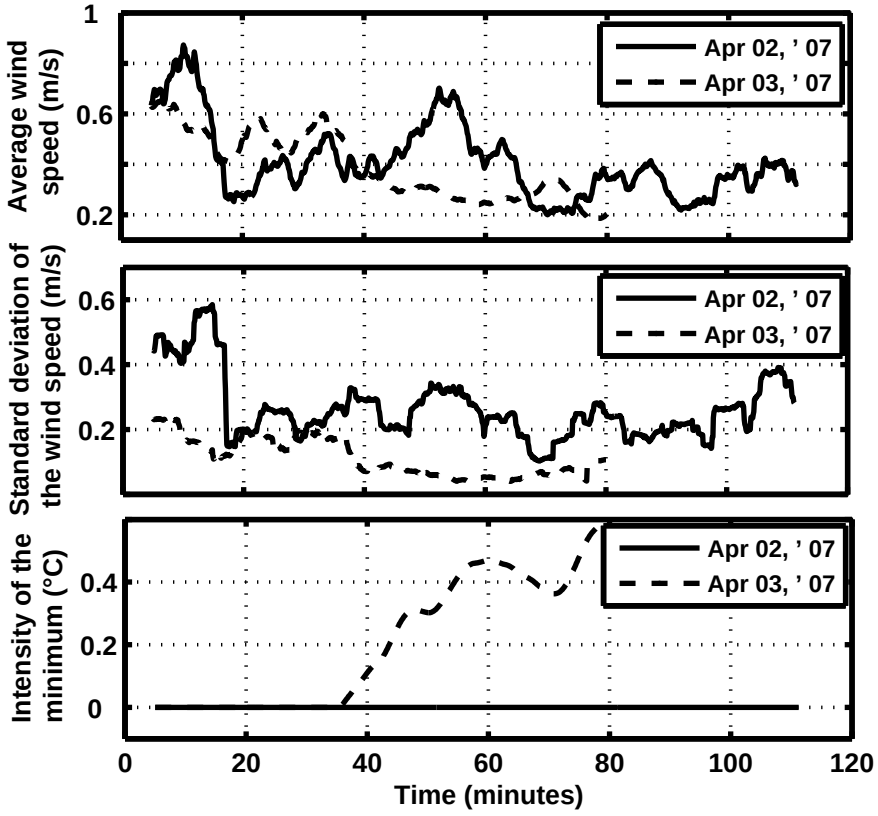

Figure 3.29: A comparison of the wind speed, turbulence levels (represented by the standard deviation of the wind speed) and intensity of the minimum for the observations made on two days (April 02, 2007 and Apr 03, 2007) over the thermofoam surface. The turbulence levels on April 03 are lower than on April 02.

data for average wind speed, standard deviation of the wind speed and intensity of the minimum is shown for observations obtained on both these days. It can be seen that throughout the observation period on April 03, the standard deviation of wind speed was lower as compared to that on April 02. At around 35 minutes on April 03, these standard deviation values started decreasing further and fell to values that were unusually low (compared with observations on this or any other surface). Around this time, the wind speed also decreased. Due to very low values

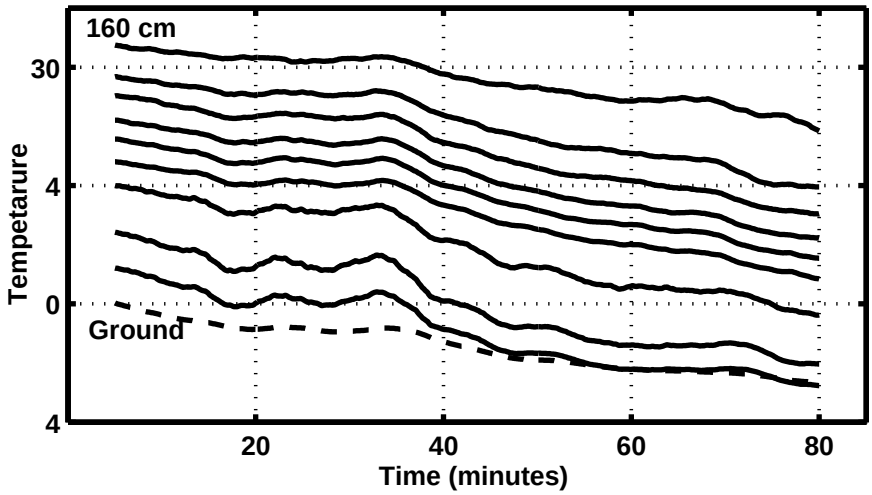

Figure 3.30: Time series of temperature data from observations made on the thermofoam surface on Apr 03, 2007. At around 40 minutes, the wind speed and turbulence levels fall to a low value (figure 3.29). The air layers above the ground cool relative to the ground, resulting in weak minima, which are shown in figure 3.31.

of the wind speed and turbulence levels, the minimum started forming at about 35 minutes. This can also be seen in figure 3.30, where the temperature traces at various heights during the observation period on April 03 is shown. The red trace is the ground temperature and the top most trace is that of the thermocouple at 160 cm (the highest observation station). As before, the traces have been suitably offset to avoid overlap. As the wind speed and turbulence levels fell at around 35 minutes after the start of the observations, the air layers just above the ground started cooling with respect to the ground, and eventually, fell a little below the ground. This can be seen in the temperature traces where, in spite of the offset, the first temperature trace above the ground (which is actually a trace of the thermocouple at a height of 5 mm) overlaps the temperature trace of the ground. Profiles at 30, 40, 45 and 60 minutes are shown in figure 3.31, where the development of the weak minimum can be seen. The intensity of the minimum eventually reached

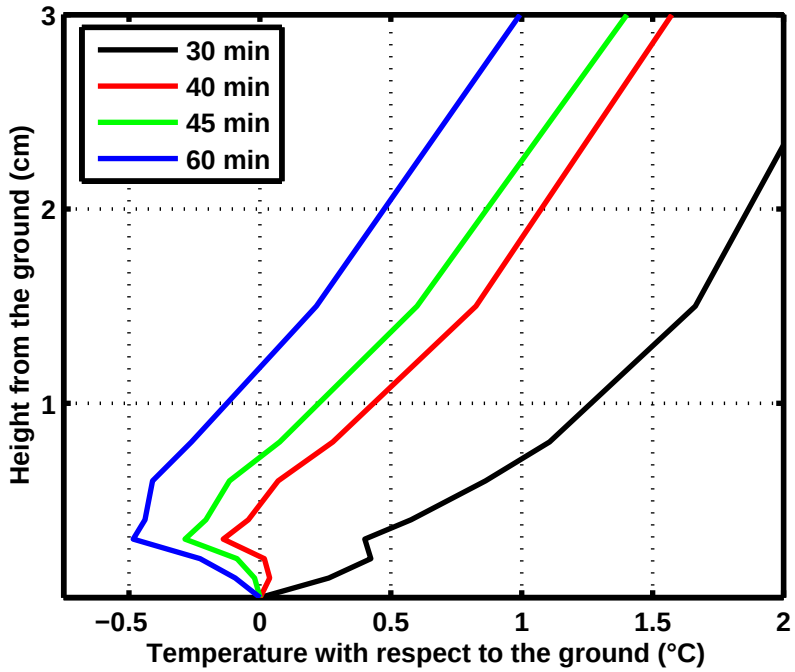

Figure 3.31: Profiles at different times corresponding to the data shown in figure 3.30. An unusually low value of the intensity of turbulent fluctuations (coupled with a low wind speed) results in a weak minimum over the thermofoam surface.

about 0.5 °C, with its height being around 5 mm.

The above observations are consistent with the predictions of the VSN model, according to which, both the height and intensity of the minimum should be lower for high cooling rate surfaces.

The gradients (in low wind conditions) during inversions appear to be much less as compared to the baseline case (concrete surface), as can be seen from figure 3.32.

After a break necessary to empty the data logger memory, a further period of observation was undertaken over the high emissivity, high cooling rate surface on April 03, 2007, which started a little before sunrise and continued till well after sunrise. This data set shows the evolution of the inversion developed over such

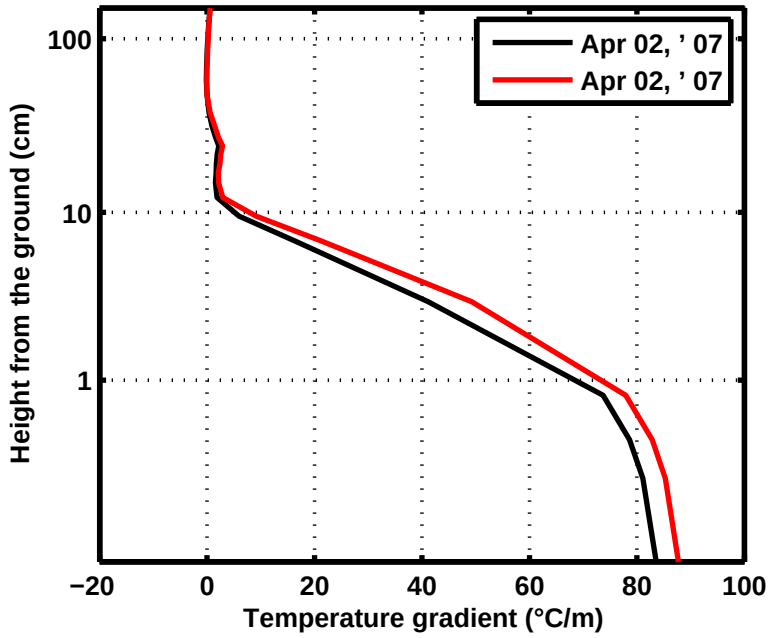

Figure 3.32: Typical near surface temperature gradients during inversions obtained over the thermofoam surface (high ϵ_g, high β surface). Besides being opposite in sign as compared to the concrete surface, they are also much lower in magnitude.

a surface during this period. Shown in figure 3.33 are the variation of ground temperature and down welling radiation over the period of observation. Profiles at different times corresponding to this observation period are shown in figure 3.34. Clearly, the ground responded to the increasing incoming radiation and warmed up faster than the air layers. Hence, as seen in the succession of profiles in figure 3.34, the inversion got progressively weaker, and tended to the usual day time profile. Here, profiles after 60 minutes are not shown as the thermocouples were not shielded, and the radiation errors will be quite high due to the direct solar radiation, but the trend towards development of the day time profile is clear.

As mentioned in section 2.1.1, Brunt's formula for ground cooling rate (see equations 1.1, 1.3), is not valid for the surfaces with high cooling rates, and finding

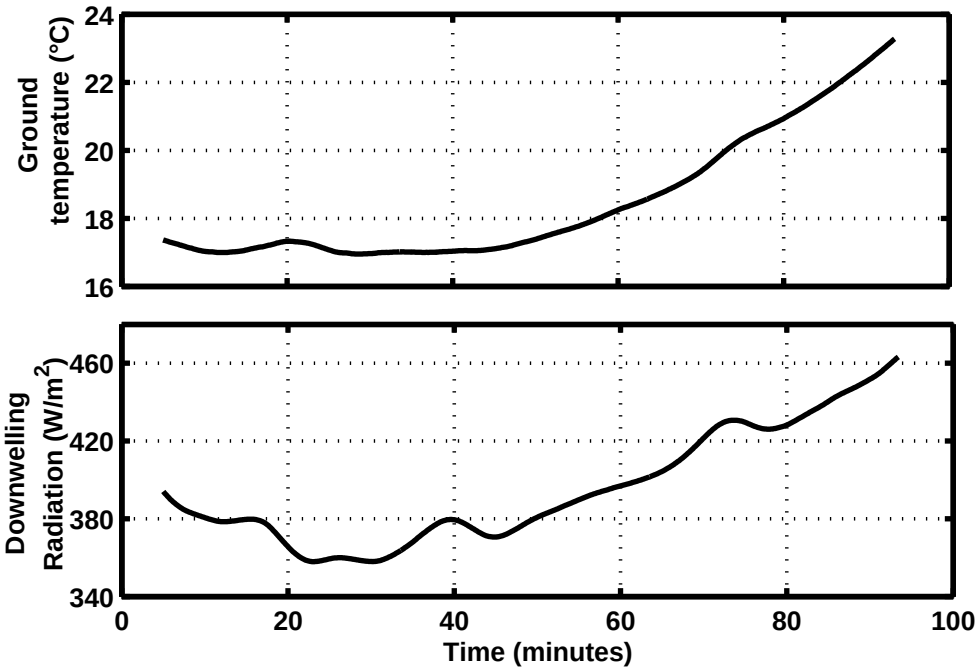

Figure 3.33: Increase in surface temperature and downwelling radiation (on thermofoam surface during measurements taken at sunrise.)

a β for such surfaces may not be meaningful. Nevertheless, for completeness, β values were estimated by identifying periods *within* an observational run, in which the plot of ground temperature versus $\sqrt{t}$ was more or less linear, and obtaining separate β values for each of those periods. A plot of ground temperature versus $\sqrt{t}$ over the thermofoam surface is presented in figure 3.35. This is from data obtained from observations in the early part of the night of April 03, 2007. The ground temperature changed in a very irregular manner. Periods for which a reasonable linear fit could be obtained are shown, along with the associated β values. β values obtained in this manner from all the observational runs on this surface range from -4 to 18 $K/\sqrt{hr}$. The negative sign indicates warming.

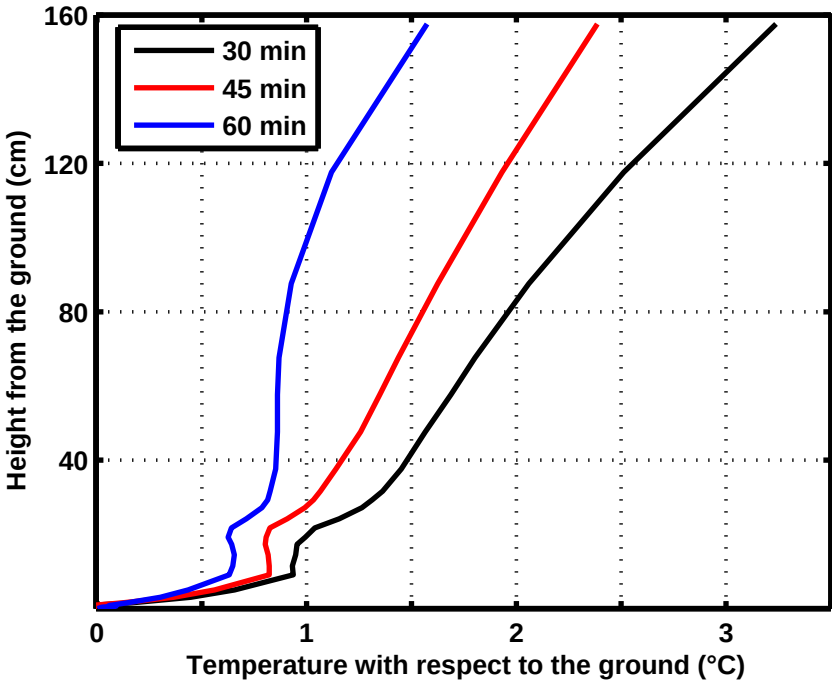

Figure 3.34: Profiles at different times over the thermofoam surface corresponding to the data shown in figure 3.33, showing how the inversion tends to a typical day time mixed layer.

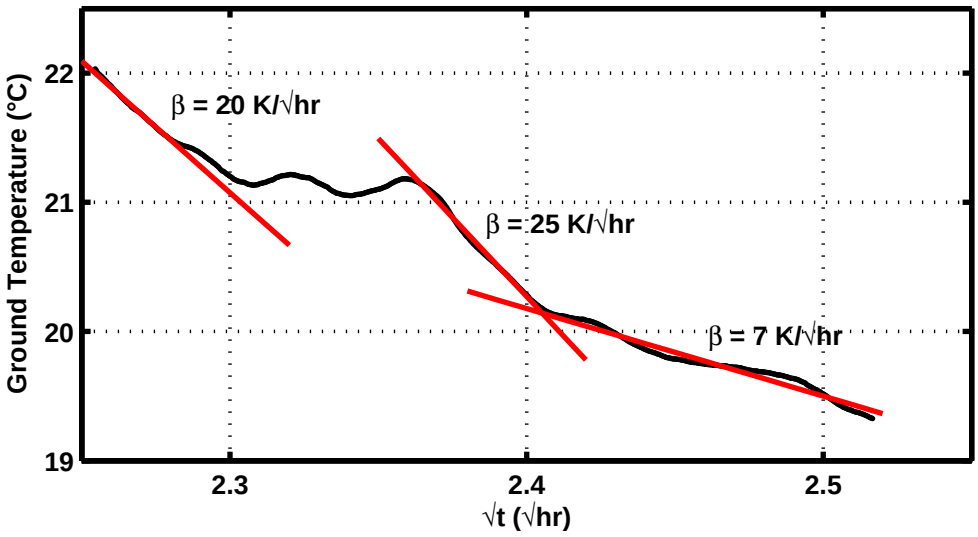

Figure 3.35: Plot of ground temperature versus $\sqrt{t}$ for the thermofoam surface. Taken from data obtained on April 03, 2007.

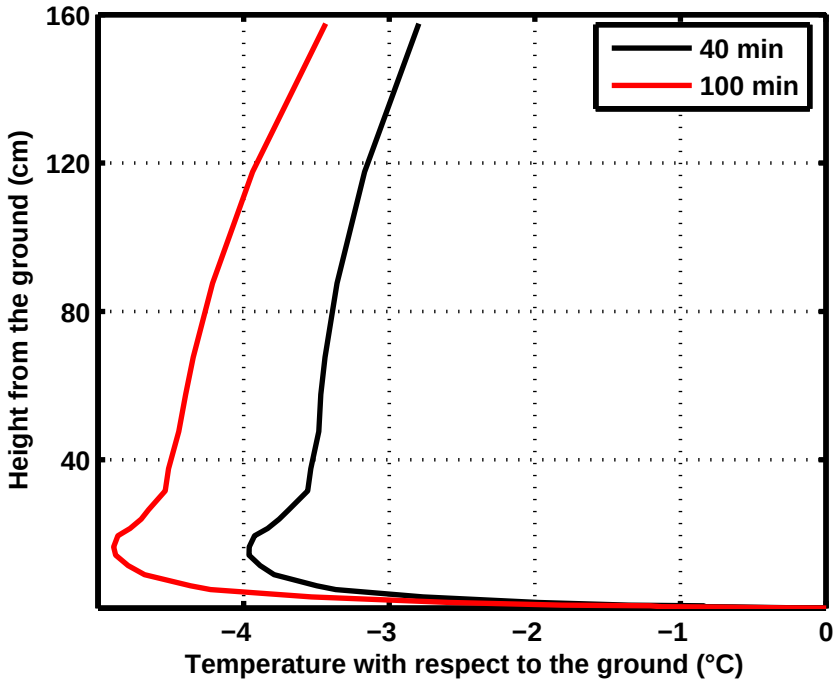

Figure 3.36: Profiles on the 'thermofoam with aluminium' surface (low ϵ_g, high β surface) surface, showing a moderate intensity of the minimum.

3.5 Observations over the 'thermofoam with aluminium' surface (low ϵ_g, high β surface)

Profiles obtained over the 'thermofoam with aluminium' surface (low ϵ_g, high β surface), are shown in figure 3.36. The profiles exhibit a clear minimum, with intensities only slightly lower than the base case. This surface has the same thermal inertia and conductivity as the thermofoam surface, on which inversion profiles or extremely weak minima were obtained. The significantly higher values of the minimum in this case are due to the low emissivity of the aluminium used to top the thermofoam.

As with the thermofoam surface, the ground temperature changes very irregularly with time. A plot of ground temperature versus $\sqrt{t}$ for the 'thermofoam with

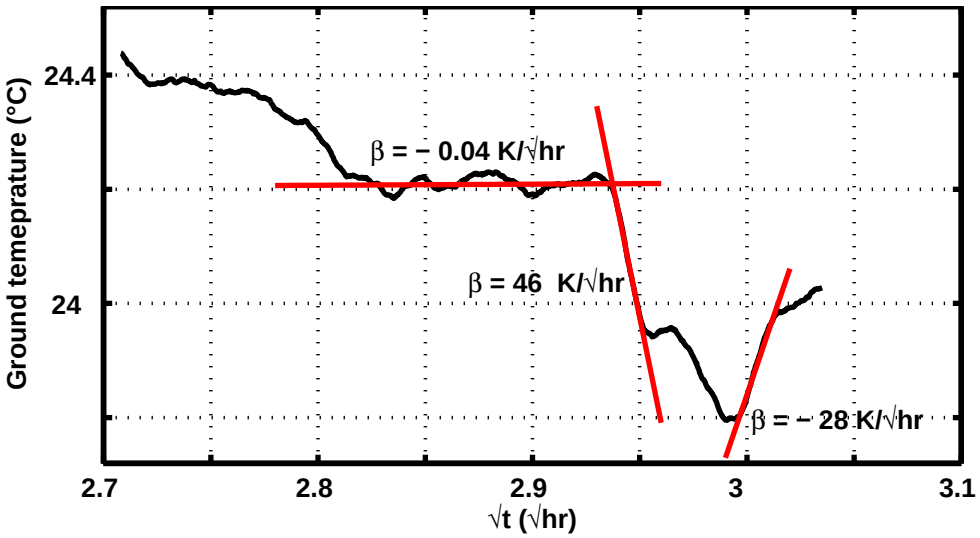

Figure 3.37: Plot of ground temperature versus Plot of ground temperature versus $\sqrt{t}$ for the 'thermofoam with aluminium' surface. Data was on obtained on April 07, 2007.

aluminium' surface is shown in figure 3.37, along with periods for which a linear fit could be obtained. Note the large warming period near the end. The β values for this surface range from -28 to 46 $K/\sqrt{hr}$, where, as before, the negative sign denotes warming.

3.6 Radiative flux divergence near the ground

According the VSN model, the radiative cooling causing the lifted minimum is due to a large radiative flux divergence in the so called 'emissivity sublayer' very close to the ground. For example, for ground emissivity = 0.8 and water vapor mixing ratio = 0.005, the flux divergence just above the ground is about 20 W/m^3, falling to about 5 W/m^3 at a height of 10 cm., and practically zero beyond a height of about 30 cm. above the ground. As in general, the observations are at least in qualitative agreement with the VSN model, it would be interesting to see if, as

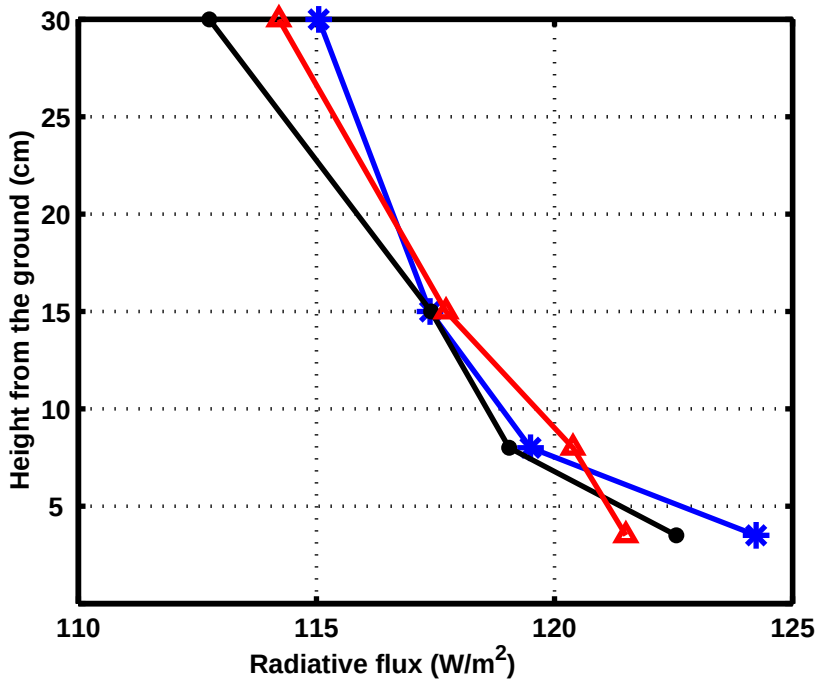

Figure 3.38: Typical near surface radiative flux profiles obtained using the large net radiometer. All the measurements either show no significant divergence or a small negative divergence, implying radiative warming.

predicted by the VSN model, there is indeed such a flux divergence close to the surface. Hence, radiation sensors were traversed close to the ground in order to try and measure the variation in radiative fluxes. A large number of such traverses were done on different occasions. Unfortunately, all the measurements indicated either negligible change in fluxes near the ground, or a radiative flux that decreased with height, which would imply radiative warming. For example, figure 3.38 shows radiation profiles obtained on Jan 07, 2005, using the net radiometer constructed using the larger thermoelectric module.

Assuming that the VSN model is correct in its essentials, one would surmise that there are some issues with measuring radiative flux profiles so close to the ground: like for example, that the radiometer itself influences the fluxes considerably. It

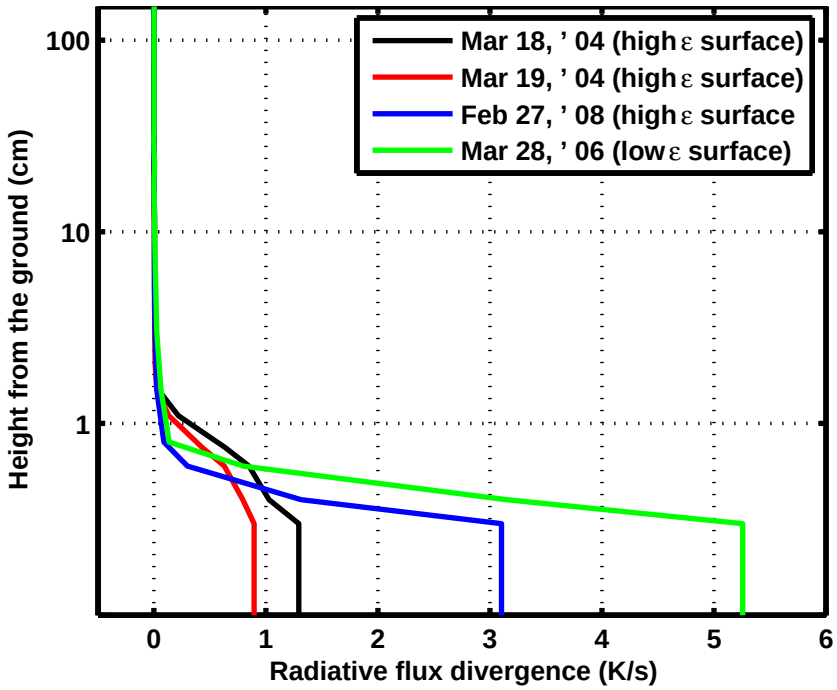

Figure 3.39: Typical near surface radiative flux profiles estimated from the data and the heat equation. The radiative flux divergence is negligible above even a couple of centimeters, which is possibly why they could not be measured with the net radiometers.

would still be nice if, by some means, even a rough idea could be obtained about the near surface divergence. High resolution, near surface temperature measurements are available from our field observations. These could be used along with the basic heat balance equation to get precisely such an estimate. The heat equation reads:

$$\rho c_p \frac{\partial T}{\partial t} = \kappa \frac{\partial^2 T}{\partial z^2} + \frac{\partial Q}{\partial z}$$

Here, T is the air temperature, t is the time, z is vertical coordinate measured from the ground, κ is the air conductivity, ρ is the air density and c_p is the specific heat capacity of air at constant pressure. $Q = \partial Q/\partial z$ represents the source term. Q can be split up into Q_r and Q_t representing the contributions of radiation and

convection respectively. When the is wind speeds are very small Q_t will be close to zero, and $\partial Q/\partial z$ will represent the infrared radiative flux divergence. If a curve can be fitted to the temperature data, then $\partial T/\partial t$ and $\partial^2 T/\partial z^2$ can be estimated, which immediately yields an estimate for the radiative flux divergence. Now,in the steady state of the minimum, $\partial T/\partial t$ is practically zero, and the heat equation reduces to a balance between the flux divergence $\partial Q/\partial z$ and $\kappa \partial^2 T/\partial z^2$. Hence, the problem boils down to estimating $\partial^2 T/\partial z^2$. As discussed in section 3.1, the SG filter may be used to obtain at least the order of magnitude of this quantity, and the radiative flux divergence then estimated.

Near surface divergences thus obtained on different days, expressed as a cooling rate by dividing out by ρc_p, are shown in figure 3.39. The divergence on March 18, 2004, March 19, 2004 and February 28, 2007 are over the concrete surface (high ϵ_g, high β surface), while that obtained on March 28, 2006 is over the 'aluminium on concrete' surface (low ϵ_g, low β surface). The near surface divergence over the concrete surface is thus typically around 1 K/s, with the region of significant divergence being a few centimeters. Data from other 'wind free' periods not shown here agrees with these estimates. The divergence over 'aluminium on concrete' surface is higher, being around 5 K/s. But as data over aluminium with low wind speeds could be obtained only on one occasion, this is perhaps only to be taken as indicative.

Thus, the estimates obtained here are at least one order of magnitude higher than that predicted by the VSN model, while the height below which the divergence is significant is much lower than the VSN model estimates.

These estimates indicate that the significant divergence is confined to less than a centimeter above the ground. This is probably why even with the small radiation probes used, we were unable to directly measure the near surface radiative flux

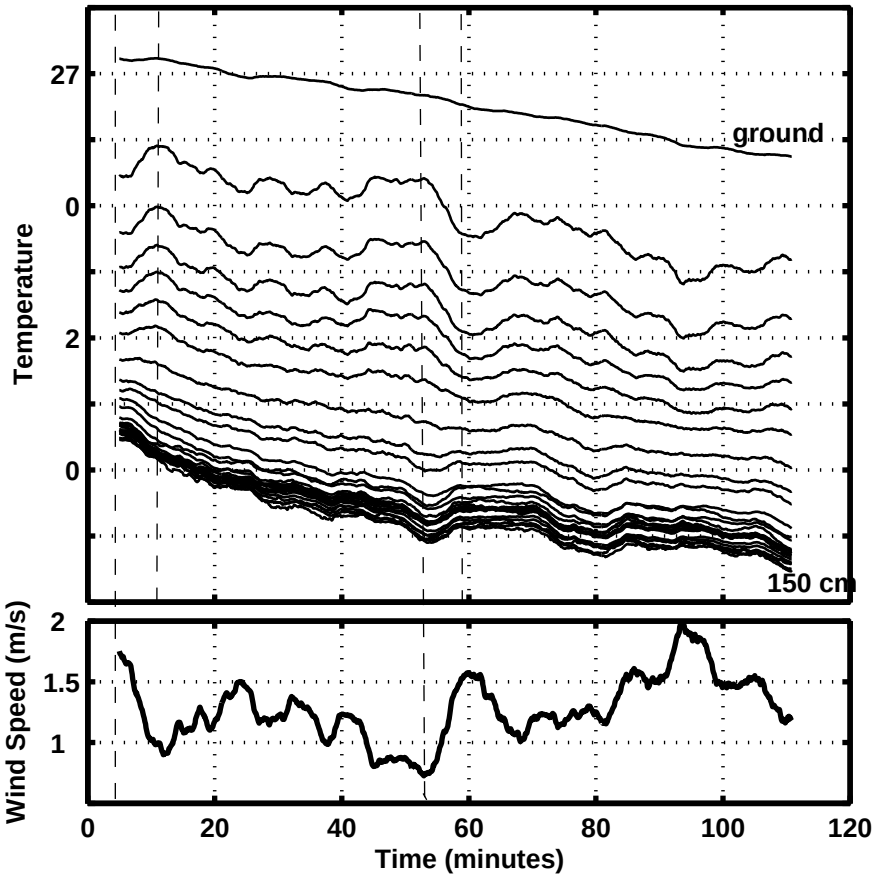

Figure 3.40: A typical example of fluctuations in air and ground temperature due to changes in wind speed.

divergence.

3.7 Temperature Fluctuations

We now turn to a few remarks on some temperature fluctuations observed in the field. Indeed, earlier in this chapter, it was noted that that the ground temperature often exhibited some temperature fluctuations, and it was remarked that this was due to changes in wind speed. Such fluctuations, as to be expected, are not confined

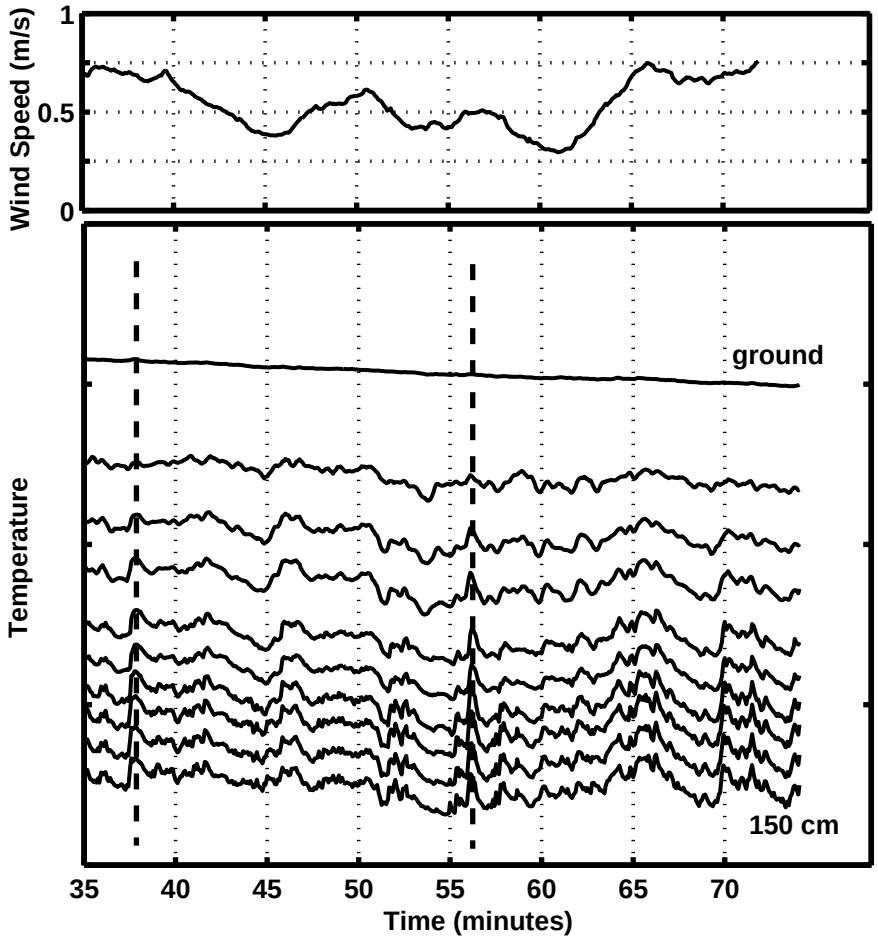

Figure 3.41: Small scale correlated temperature fluctuations on calm days, from data obtained on Mar18, 2004.

to the ground, but appear at all heights. A typical example is shown in figure 3.40. For example, at about 55 minutes, there is a sudden increase on wind speed. The higher air layers (above the minimum) warm up due to turbulent mixing in the inversion layer. But below the minimum, we have a decreasing temperature profile, and the increase in wind speeds causes the air layers and ground to cool. This short transient period is indicated between a pair of vertical lines at around 55 minutes. Just at the beginning (0 minutes), a fall in wind speed causes a transient in which

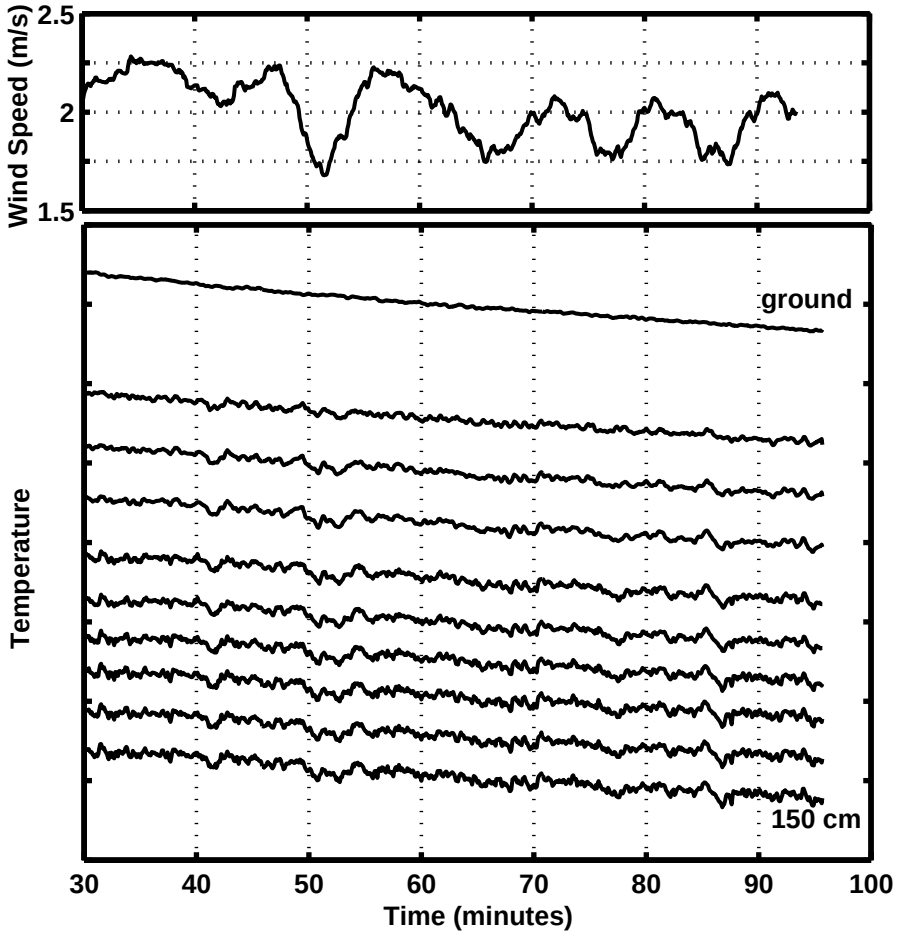

Figure 3.42: Absence of small scale temperature fluctuations on windy days, from data obtained on March 08, 2004.

the air layers near the ground warm up.

There are other smaller scale temperature fluctuations that occur only on calm days (wind speeds below 1 m/s). These temperature fluctuations occur at all heights (except very close to the ground) at more or less the same time, and are shown in figure 3.41. A couple of such fluctuations are indicated by vertical solid lines. Figure 3.42 shows the absence of such fluctuations (that stand out from the rest of the minor fluctuations) on windy days. As mentioned in the chapter

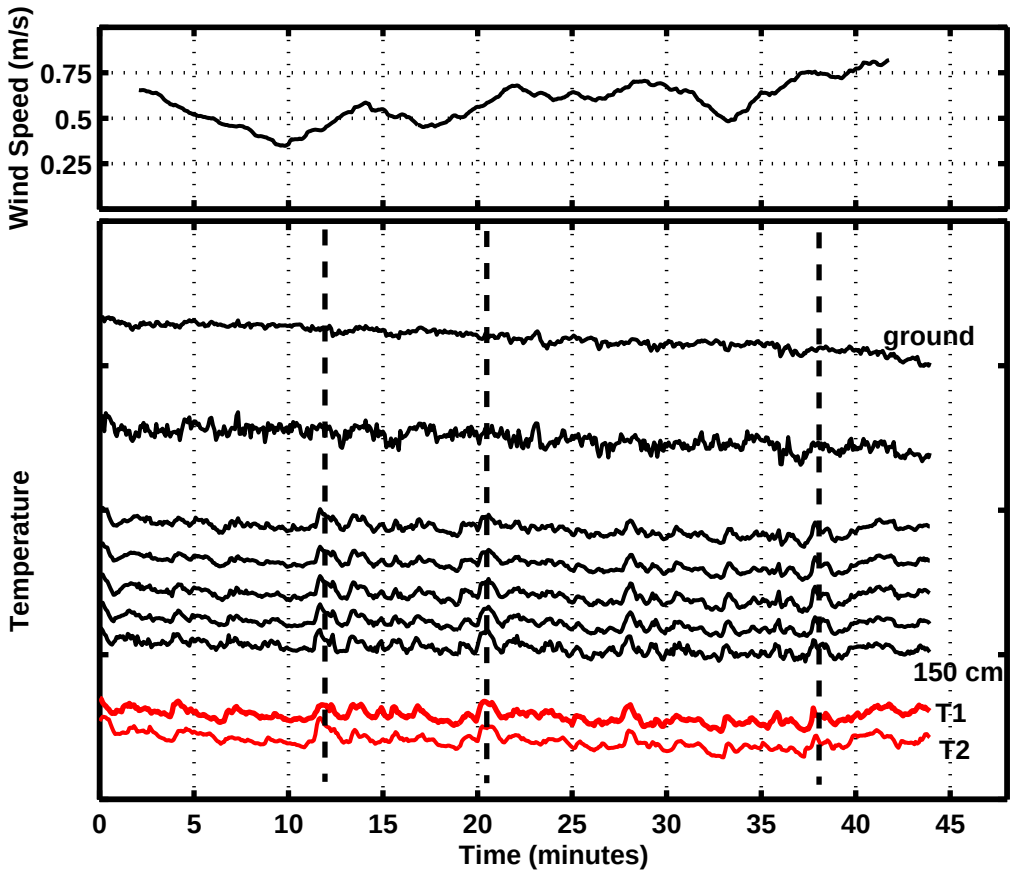

Figure 3.43: Small scale temperature fluctuations on a calm day, showing that the correlations occur simultaneously over a large area. Data obtained on June 23, 2004.

on the set up of the field observations, in order to investigate these fluctuations, two thermocouples at a height of about 15 cm. were kept on diametrically opposite sides of the mast about 8 meters apart. Thus, there were three temperature sensors at the same height: one on the mast and two others on opposite ends of the circular concrete patch. Results on a calm day with this arrangement are shown in figure 3.43. TC1 and TC2 indicate the temperature traces from the extra thermocouples kept on opposite sides of the patch. It is seen that the fluctuations are present in these too, and occur at the same time as the ones on the mast. As these fluctuations

occur almost simultaneously over such a large area, they are probably caused by some disturbance higher up in the atmosphere.

Summary

Observations were carried out over 4 surfaces: (1) Bare concrete (high emissivity, low cooling rate surface), (2) 'Aluminium on concrete' (low emissivity, low cooling rate surface, (3) Thermofoam (high emissivity, high cooling rate surface), and (4) 'Thermofoam with aluminium' (low emissivity, high cooling rate surface).

As its emissivity and cooling rates are comparable to that of compacted, bare soil, the observations over the concrete surface were taken as the baseline case against which the other observations could be compared. The intensity of the minimum is strongly affected by both wind speed and turbulence levels. The intensity decreases with an increase in either of these quantities. However, at all times, the profile obtained over concrete was of the lifted minimum type. Minimum with intensities reaching 7 °C were obtained over concrete at very low wind speeds and turbulence levels. The near surface temperature gradients during a lifted minimum (for low wind conditions) are very high, and are in fact the same order of magnitude as gradients during the the day.

On the thermofoam surface (high emissivity, high cooling rate surface), an inversion profile was obtained, with the minimum temperature occurring at the ground. The near surface gradients during such an inversion are much lower than those during a lifted minimum. However, there was a period during the observations in which the wind speeds and turbulence levels were unusually low. In this period, a lifted minimum profile was formed over this surface, but its intensity and height were very low as compared to the baseline case.

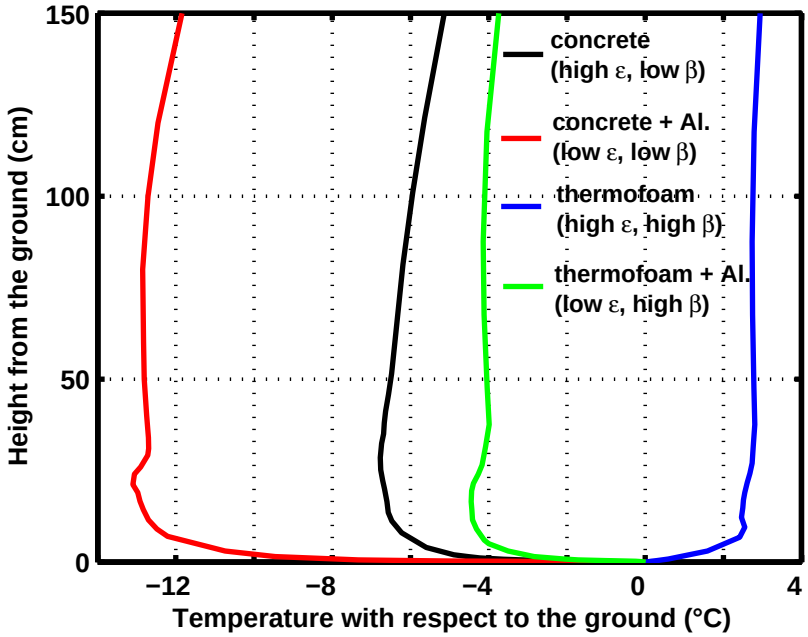

Figure 3.44: Representative temperature profiles over the four surfaces studied.

Observations over the surface consisting of 'aluminium on concrete' surface (low emissivity, low cooling rate surface), showed a dramatic increase in intensity of the minimum as compared to the baseline case. Under low wind conditions, minima with intensities reaching 13°C were obtained. The height of the minimum was not however, significantly different from the baseline case. The temperature gradients just above the surface were much larger than the baseline case.

Thus, the height of the minimum strongly depends on the ground cooling rate and is not affected much by the surface emissivity. The intensity of the minimum on the other hand is strongly affected by both the ground cooling rate and emissivity. The profiles and gradients under low wind conditions (wind speeds less than 0.3 m/s) for the various surfaces are shown in figures 3.44 and 3.45 respectively.

If ΔT represents the intensity of the minimum, and $\Delta T_\circ$ is the intensity of the minimum at the beginning of a given observational run, it was found that a

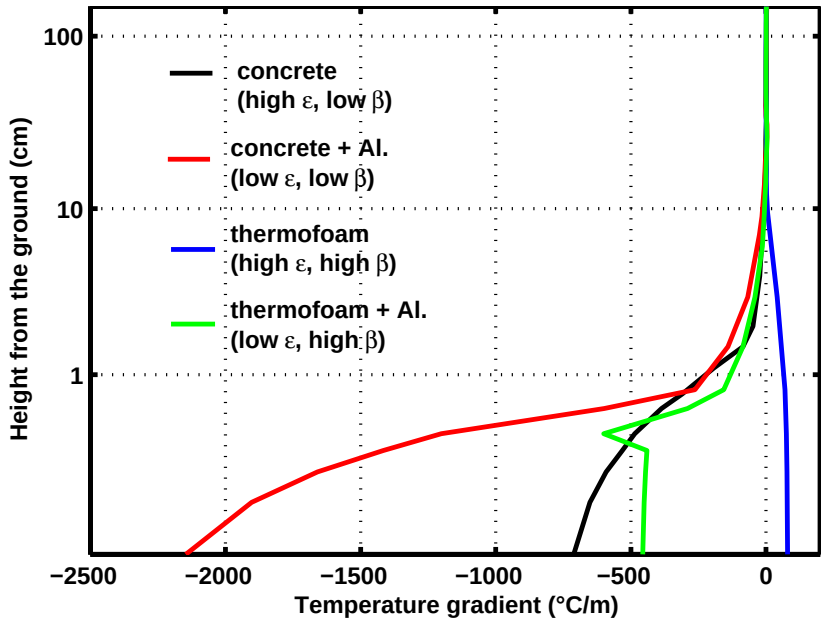

Figure 3.45: Representative temperature gradients over the four surfaces studied

simple functional relationship could be found between $\Delta T/\Delta T_\circ$ and the mean and standard deviation of the wind speed, that was valid *across* observational runs over a given surface. A scatter plot of the intensity predicted by the functional relationship and the observed intensity for the concrete and 'aluminium over concrete' surface are shown in figure 3.46. The intensity of the minimum depends less strongly on the wind speed for the 'aluminium over concrete' surface as compared to the concrete surface.

The predictions of the VSN model are in good agreement with the above observations. However, the VSN model predicts slightly lower values [†] for the intensity of the minimum and considerably lower values for the near surface temperature gradients than seen in the observations. Though the band model treats the radiation more realistically by including wavelength dependence, it predicts intensities of the minimum which are far lower than observed values.

[†]The observed cooling rates on concrete typically lie in the range 3 - 5 $K/\sqrt{hr}$. As the normal emissivity of concrete surface is 0.9, the hemispherical values can be assumed to be in the range 0.8 - 0.9. For this range of cooling rates and emissivity values, the VSN model (including only conduction and radiation) predicts intensities in the range 1 - 3.5 °C. For low wind speeds and turbulence levels (less than 0.3 m/s and 0.2 m/s respectively), the observed intensities are in the range of 4 - 8 °C

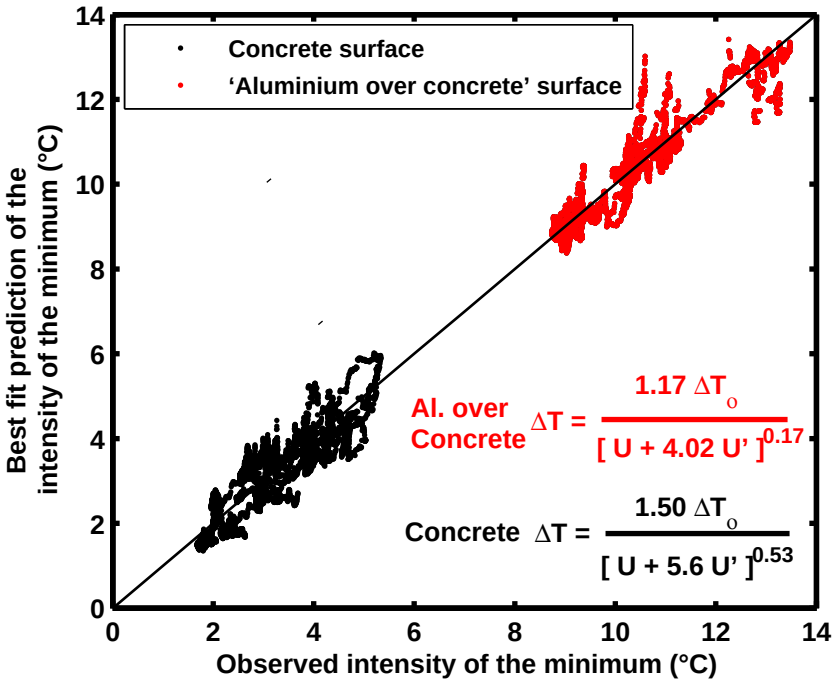

Figure 3.46: A scatter plot of predicted versus observed intensity of the minimum for consolidated data from observations over both the concrete (high emissivity, low cooling rate surface) and 'aluminium over concrete' surface (low emissivity, low cooling rate surface).

Even though humidity was monitored for all the observations (with the mixing ratio varying from 5 - 10 g/kg for the consolidated data), no systematic dependence of the lifted minimum on humidity could be demonstrated. This conclusion is also in agreement with the findings from the VSN model.

Using the temperature data obtained during very low wind conditions, the heat equation (with a source term) was used to estimate the radiative flux divergence near the ground. Expressed as a cooling rate (by dividing by ρc_p), the flux divergence just above the ground for the baseline case (concrete surface) is at least about 1 K/s. The flux divergence diminishes rapidly and is insignificant for heights greater than a few centimeters above the ground. The estimates thus obtained are almost two orders of magnitude higher than that predicted by the VSN model, while

the height below which the divergence is significant, is lower than the predictions of the VSN model by about one order of magnitude.

CHAPTER 4

LABORATORY EXPERIMENTS

Introduction

As mentioned before, one of the objectives of the present work is to examine the possibility of obtaining the lifted minimum in the laboratory. This would allow one to study the phenomenon in a more controlled manner than possible in field observations. The experimental set up could also be used for studying the more general problem of the influence of radiation on other forms of heat transfer.

This chapter is organized as follows: The literature related to the problem is surveyed in section 4.1. The experimental set up used to simulate the lifted minimum is described in section 4.2. The results from the laboratory experiments are presented and discussed in section 4.3. A summary of the results from the laboratory experiments concludes the chapter.

4.1 Literature Survey

Though there has been no previous work seeking to explicitly simulate the lifted minimum in the laboratory, there has been some work on the influence of radiation on convection and/or conduction. Goody (1956) considered the problem of the onset of instability in a horizontal layer of radiatively participating gas. A linear stability analysis was used to calculate the critical Rayleigh number (Rayleigh number at the onset of instability). The radiative heat transfer was calculated by a gray gas theory, in which the gas absorption coefficient is considered to be

independent of the wavelength. Work on this problem, on both the theoretical and experimental fronts, was continued by Gille & Goody (1964). On the theoretical side, a more realistic non-gray analysis was used for the radiative heat transfer. A coupled conduction-radiation was used to predict the temperature profile in and the heat transfer through the quiescent layer of gas before the onset of the convective instability. An approximate expression for the critical Rayleigh number was arrived at through a dimensional argument. Experiments were then conducted in horizontal layers of dry air and radiatively participating ammonia gas. The temperature profiles and heat transfer fluxes measured in the quiescent gas before the onset of instability, were found to compare well with the theoretical predictions. The maximum deviation from the linear conductive profile obtained was about 0.4 K. The critical Rayleigh numbers obtained for the ammonia gas were found to be significantly larger than those obtained for dry air. Though there were some discrepancies between the observed and predicted stabilizations, there was no doubt that the theory predicted the right kind of behavior. Though there have been quite a few papers after this on the theoretical aspects of the conduction-radiation problem and onset of instability in a radiating gas (Christophorides & Davis (1970), Arpaci & Gozum (1973), Crosbie & Viskanta (1971), Soufiani & Taine (1985)), the papers which also include experimental results have been rather less in number. Schimmel & Olsofka (1970) carried out experiments to understand the coupled conduction-radiation heat transfer in horizontal gas layers in the quiescent state before the onset of instability. Measurements were made in four gas mixtures: pure carbon dioxide, pure nitrous oxide, a mixture of carbon dioxide and nitrous oxide and a mixture of carbon dioxide and methane. Theoretical predictions for the coupled problem were made using three different radiation models: a gray gas model, a grayband model and an exponential wideband model. The predictions of

the wideband exponential model matched the measurements under all conditions tested, while the other two models performed rather poorly. Novotny & Olsofka (1970) extended the work by looking at the effect of mixing a non-participating gas with a participating gas. Agreement between a nongray analysis and the measurements were good for all the conditions considered. Hutchinson & Richards (1999) conducted experiments to determine the onset of thermal instability in horizontal layer of gas. Heat flux across the gas layers was measured both before and after the onset of instability and used to determine the critical Rayleigh number. The measurements showed a 7-20 % increase in the critical Rayleigh number for the radiatively participating carbon dioxide layer as compared to a non participating layer of dry air. A 20 % reduction in heat transfer after the onset of instability was observed in the carbon dioxide layer as compared with the dry air layer. The coupled conduction-radiation problem before the onset of convection was theoretically analyzed using a gray gas model. The heat fluxes thus predicted agreed with the measurements to within experimental uncertainty. The theoretical analysis also indicated that the distortion of the initial base state temperature profiles as a result of radiation in the quiescent carbon dioxide layers was extremely small (the maximum deviation reported being around 0.04 K).

4.2 Experimental Setup

The laboratory set up was basically designed to mimic, in simple way and to the extent possible, the basic features of the situation during a lifted minimum. With clear skies (one of the conditions for the formation of a lifted minimum), the effective 'sky' temperature is much lower than the temperatures in the inversion layer. Hence, the air layers near the ground can radiatively cool to the sky. In

this sense, the convective and radiative boundary conditions are decoupled, with the decoupling being effected by the inversion. The laboratory set up was designed to emulate this basic feature. With such a decoupling, the radiative boundary conditions can be set so that the effects of radiation on the base temperature profile are not swamped by conductive or convective effects. Then, the effect of radiation on the base temperature profile will become more readily apparent, and can be measured without the need for sophisticated instrumentation. It is because of the lack of such a decoupling that larger deviations from the linear profile than hitherto reported, are not possible in traditional set ups involving radiatively participating gases between two parallel plates. In fact, with conventional set ups, heating the top plate relative to the lower one for obtaining a stable stratification (similar to that present in the inversion layer at night) will result in a radiative *heating* near the bottom plate, precluding the radiative *cooling* associated with a lifted minimum. The laboratory set up with such a decoupling that allows one to obtain a radiative cooling near the bottom plate is described below. As this set up is discussed in detail in Tiwari (2006), only a brief overview is given here.

The schematic of the lab set up is shown in figure 4.1. The test section has a cross section of 80 cm by 80 cm, and a height of 10 cm. The air in this section corresponds to the air layers near the ground, and is where the temperature profile is measured. The bottom of the test section is a 5 mm. thick anodized aluminium plate. The temperature of this plate can be controlled, and sets the temperature of the bottom boundary of the test section. The side walls of the test section are made of 20 mm. thick thermofoam. This is to prevent near wall convection due to the hot air in the air circulation section. The top boundary of the test section is made of polyethylene with an average transmissivity of better than 80% in the far infrared (2 μm to 30 μm spectrum). The air circulation section encloses the test section.

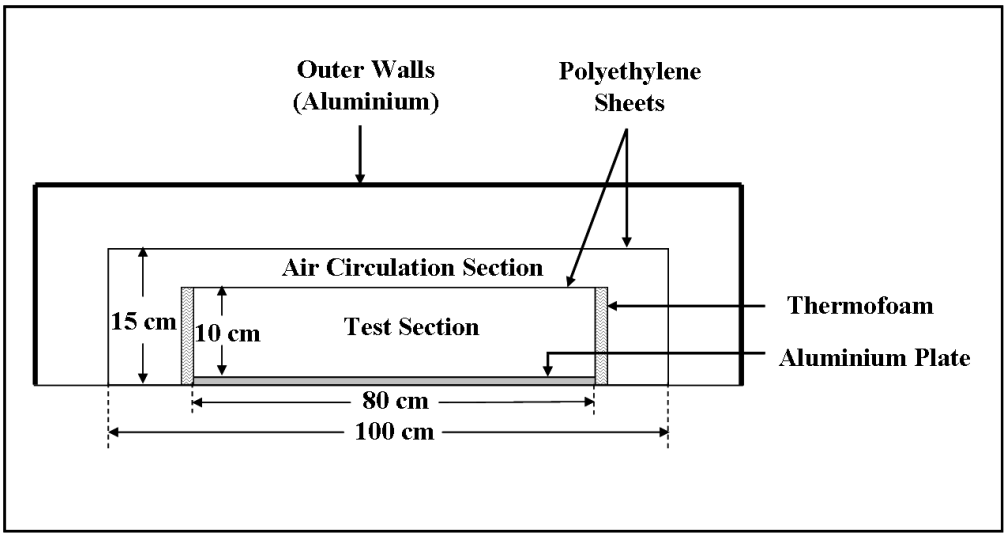

Figure 4.1: A schematic of the laboratory set up. The conduction or convection boundary conditions for the test section are fixed by controlling the temperature of the bottom aluminium plate and the temperature of the air being circulated in the air circulation section. The test section interacts radiatively with the outer walls (which can also be maintained at a desired temperature) through the transparent polythene walls of the test section and air circulation section.

This section is about 90 cm by 90 cm by 15 cm. The walls and top boundary of this section are made of polyethylene. With the help of a heater and blower unit, air at a desired temperature is circulated through this section. This fixes the temperature of the top boundary of the test section. Thus, by controlling the temperature of the bottom plate of the test section, and that the air being circulated through the air circulation section, an appropriate temperature differential (stable or unstable) can be set up across the test section. The air circulation section is enclosed on the four sides by aluminium walls (which are actually thin chambers), and on the top by an aluminium 'ceiling', (which in the current set up is actually a large, shallow aluminium tray, open on the top). Both the side chambers and the tray constituting the ceiling are provided with tubes, through which a fluid at a particular temperature may be circulated in order to maintain the walls and

ceiling at a desired temperature. For a typical lifted minimum scenario, these outer walls and ceiling will typically be kept at a temperature much lower than the temperatures of the top and bottom boundaries of the test section. These then simulate the low 'sky' temperatures during clear sky conditions at night. As air is being constantly circulated in the air circulation region, these outer walls do not significantly affect the temperatures set at the bottom and top of the test section. Thus, the air circulation section decouples the convective and radiative boundary conditions similar to what happens in a lifted minimum. A photograph of the set up is shown in figure 4.2.

Clearly, this set up can be used to investigate a variety of problems involving the effect of radiation on other modes of heat transfer in a participating medium. But in the present work, the set up is chiefly used for simulating the lifted minimum.

The temperatures were measured using thermocouples. For measuring the temperature profile in the test section, a stand similar to that used in the field to measure near surface temperatures was used. Thermocouples were also used to monitor the temperature of the bottom boundary (anodized aluminium plate), top boundary (polyethylene sheet) of the test section, outermost walls and ceiling, and various points in the air circulation region.

The set up has been described in rather ideal terms so far, and some practical issues must now be mentioned. As mentioned, the temperature of the outer walls and ceiling can be maintained by circulating a fluid through the tubes that they are provided with. But for these preliminary experiments, the temperature of these walls was lowered by simply using a mixture of water and crushed ice. The side chambers were filled with water and the ceiling (which is a large aluminium tray) also had a thin layer of water, and then crushed ice was dumped on the top as well as into the side chambers. The use of this simple procedure had two

Figure 4.2: A photograph of the laboratory set up. The front 'outer' wall has been removed to reveal the test section and air circulation section.

repercussions. As the ice water mixture was in full contact with the ceiling wall, the ceiling temperature could be lowered to about 278 to 280 K. But the ice floated on the surface of the water in the side chambers, and hence only the top region of the side walls had a temperature similar to the ceiling. Lower down, the side wall temperature could only be brought down to bout 295 K. However, as most of the radiation reaching the center of the test section was from the ceiling only, the side walls not being at a uniform temperature does not create any problems. To a good approximation, the temperature of the outermost boundaries (as far as radiative effects are concerned) can be taken to be that of the ceiling. The second effect of using ice was that the temperature of the ceiling (or side walls) could not be maintained at a fixed temperature. After the ice was dumped, the temperature of the outer walls and ceiling fell rapidly, and reached a low temperature. But soon, as the ice melted, the temperature would start rising slowly. To counter this, more ice was added at regular intervals so that the temperature of the outer boundaries was

maintained in a narrow band of 2-3 °C. This variation is quite small compared with the drop in temperature due to the addition of the ice, and as will be shown, this small variation does not radically affect conclusions reached. Another issue is that, the decoupling of the convective and radiative boundaries with the help of the air circulation region is not perfect, and the temperature of the air circulation region (and hence that of the top boundary of the test section) *is* affected by the lowering of the temperature of the ceiling and outer side walls. Thus, the temperature of the top boundary of the test section increases and decreases with the temperature of the outer walls and ceiling. Again, this effect is not so large as to disrupt the basic effect we wish to demonstrate. Moreover, by changing the power supplied to the heater-blower unit (either just as the ice is dumped, or at some other time), short periods (of about 5-15 minutes) can be obtained in which temperature of the top boundary of the test section does not change much. In fact, to compare the results across various experimental runs, only such 'steady state' periods will be used. Lastly, one would want that the top of the test section as well as the walls of the air circulation region be perfectly transparent to infrared radiation. But the polyethylene used in the experiment has an average transmissivity of only about 0.8. For the walls and ceiling of the air circulation section, this does not create much of a problem. However, as the top of the test section is not perfectly transparent to radiation, it interacts radiatively with the outer ceiling and the bottom of the test section. Hence, just as with a solid boundary surrounded by a radiatively participating gas, there is a jump in temperature near the top of the test section also, and this issue will be discussed later.

For further discussions, the following terminology will be used (see figure 4.3 The temperature of the bottom boundary of the test section (the top surface of the anodized aluminium plate) will be referred to as T_{bot}. The temperature just

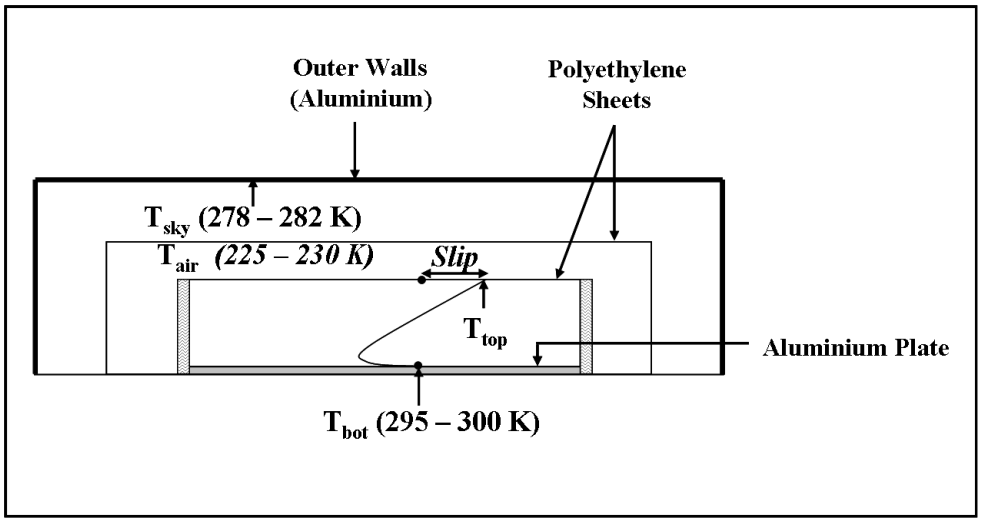

Figure 4.3: Terminology and symbols used in the discussion of results of the laboratory experiments. Also shown are typical temperature ranges for the bottom of the test section (T_{bot}), the air being circulated in the air circulation region (T_{air}) and the outer walls (T_{sky}) employed in most of the experiments in which the lifted minimum was simulated.

below the ceiling of the test section, as measured by the thermocouple nearest to the polyethylene sheet will be called as T_{top}, and with $\Delta T = T_{top}$ - T_{bot}. *slip* will refer to the temperature difference between the actual polythene temperature and T_{top}. The temperature of the outer ceiling will be called as T_{sky}.

4.3 Results from laboratory experiments

Shown in figure 4.4 is a typical temperature profile obtained in the laboratory, clearly showing the lifted minimum. Just as with the field data, the data are passed through a quadratic Savitzky-Golay filter, and in this plot both the original data points and the profile obtained after filtering are shown. In further plots only the filtered profile will be shown. One can clearly see the lifted minimum with a height of about 5 mm and an intensity of about 0.7 K. The temperature of the

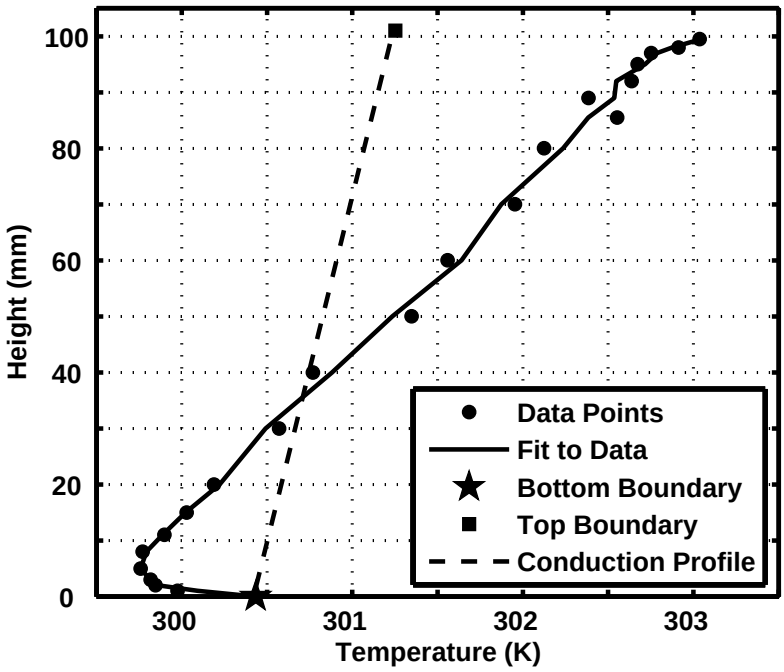

Figure 4.4: Temperature profile obtained in the laboratory showing the lifted minimum. T_{air} = 230 K, T_{sky} = 279 K. For comparison, the linear conductive profile is also shown as a dotted line. There is radiative cooling of the air layers near the bottom boundary, and radiative heating near the top boundary. Note the large deviation from the linear conduction profile, reaching a maximum of about 2 K just below the top boundary.

minimum point is lower than any the temperatures of the boundaries of the test section-a clear indication that the cooling is radiative, with the radiative sink being outside the test section. Another striking feature is the temperature slip (of about 1.5 K) at the top boundary: the temperature just below the top boundary (T_{top}) is higher than the temperature of the top boundary.

Shown in figure 4.5 is the time evolution of some of the variables, in the same experimental run from which the profile shown in figure 4.4 was obtained. The time shown in minutes on the X-axis is measured from the time that the data logging was started, and and the absolute value of the time is not of any significance. Ice was dumped into the side chambers and ceiling at around 165 min, and T_{sky}

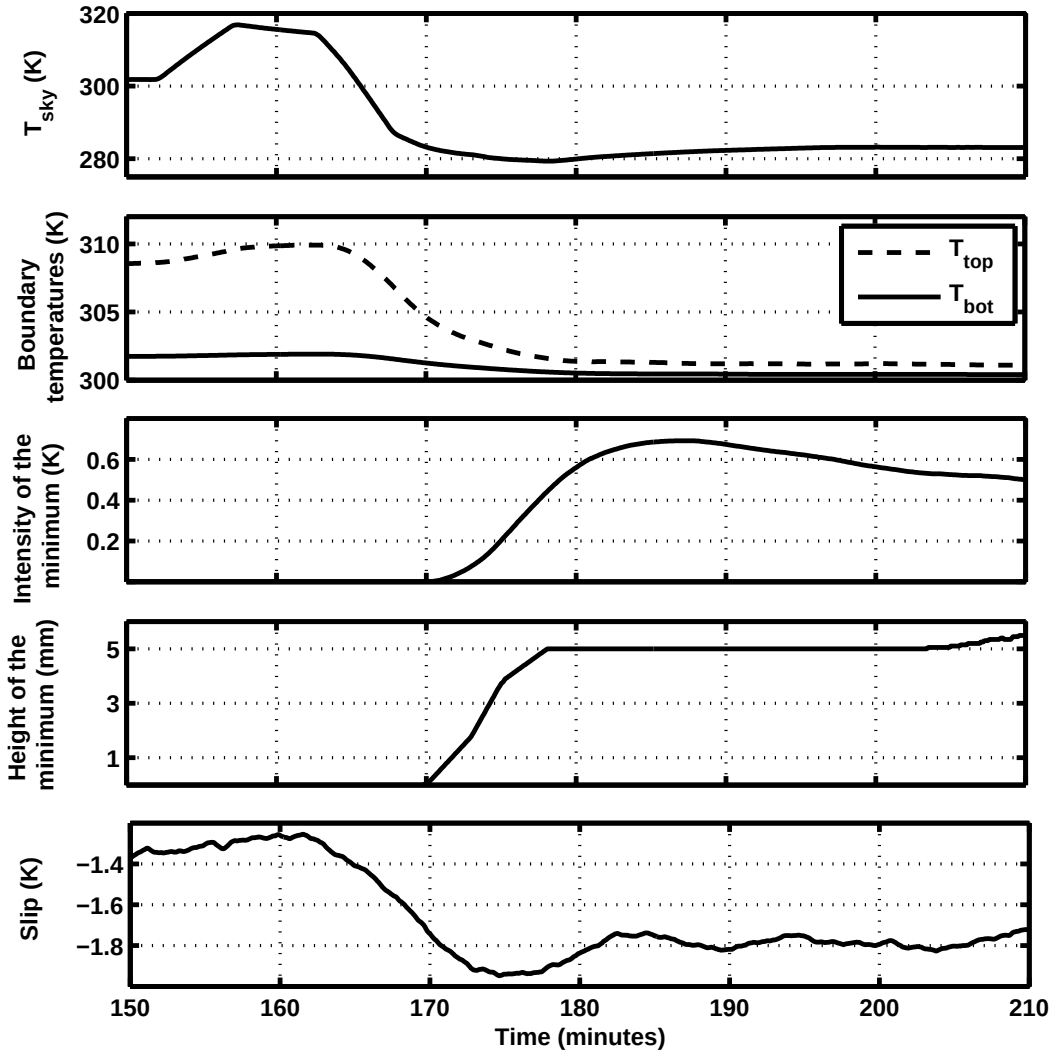

Figure 4.5: Time evolution of the height and intensity of the lifted minimum in the same experimental run from which figure 4.4 was presented. Ice was dumped on the outer walls at around 165 minutes, after which T_{sky} started decreasing. A minimum was immediately formed whose height and intensity increased. After about 190 minutes, there was a small drop in the intensity of the minimum due to a slow increase in T_{sky}.

immediately began decreasing. The small increase of T_{sky} prior to this is due to the fact that a little hot water was poured on the outer ceiling in order to see its effect on the *slip* value. The effect of this was not much, as the top boundary of the test section was already cooling to the bottom boundary. Data from another run will be shortly presented in which the effect of a high T_{sky} will be clearly seen. It was seen that as soon as T_{sky} started falling, the minimum started developing as indicated by an increase in intensity of the minimum from zero. The height of the minimum also started from zero and increased, indicating that, the lifted minimum is formed by a diffusive smearing of the radiative slip at the boundary, the radiative slip itself being formed due to a strong radiative cooling. Along with this, the value of *slip* also increased, indicating that the polyethylene sheet forming the top boundary of the test section was cooling radiatively faster than the air layers just below it. As mentioned before, the air circulation region, and consequently the temperature of the top boundary of the test section as well as T_{top} was affected by T_{sky}, and cooled along with T_{sky}. The mechanism to maintain the temperatureof the bottom plate ensures that T_{bot} is not much affected by T_{sky}.

4.3.1 Profiles with a High T_{sky}

An experimental run was carried out in which instead of ice, hot water was poured onto the outer ceiling, resulting in a high T_{sky}. Air at an ambient temperature (302 -303 K) was circulated through the air circulation section, so that, initially at least, there was no temperature difference between the top and bottom boundaries of the test section. The, T_{sky} was increased by pouring hot water onto the ceiling. The results of the experiment are shown in figures 4.6 and 4.7. As T_{sky} increased, T_{top} increased resulting in a stable stratification in the test section. The

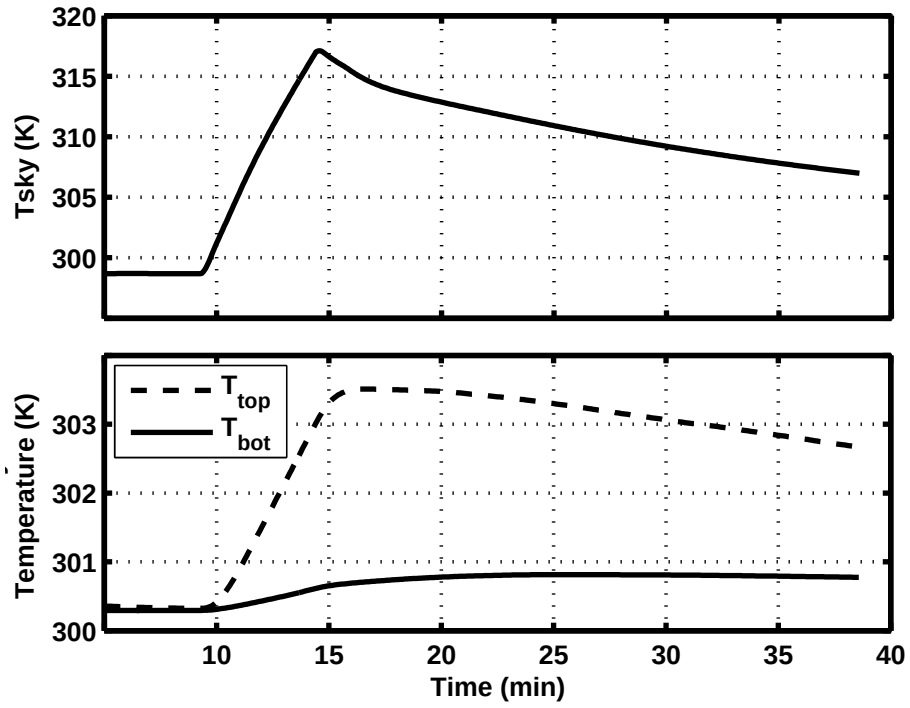

Figure 4.6: Time series of T_{sky}, T_{top} and T_{bot} from an experiment in which T_{sky} was *heated* instead of being cooled. Hot water was poured on the top 'wall' at around 10 minutes due to which both T_{sky} and T_{top} increased rapidly at first and then slowly cooled as the water cooled. T_{bot} was only slightly affected by T_{sky}. For this experiment, T_{air} = 302 - 303 K.

moment T_{sky} began increasing, the *slip* became positive, with the temperature of the polyethylene sheet being *higher* than that of the air just below it, as seen in the profile obtained at 15 min, shown in figure 4.7. The profile with a high T_{sky} is a 'S' shaped profile, with radiative heating near the bottom boundary and radiative heating near the top boundary. This is the kind of profile obtained in previous experiments (e.g Gille & Goody (1964)) involving a radiatively participating gas between two parallel plates. However, in the present experiments, the major radiative effect was not from the top plate or boundary, but due to T_{sky}. This results in a large deviation from the linear profile even for a relatively small temperature

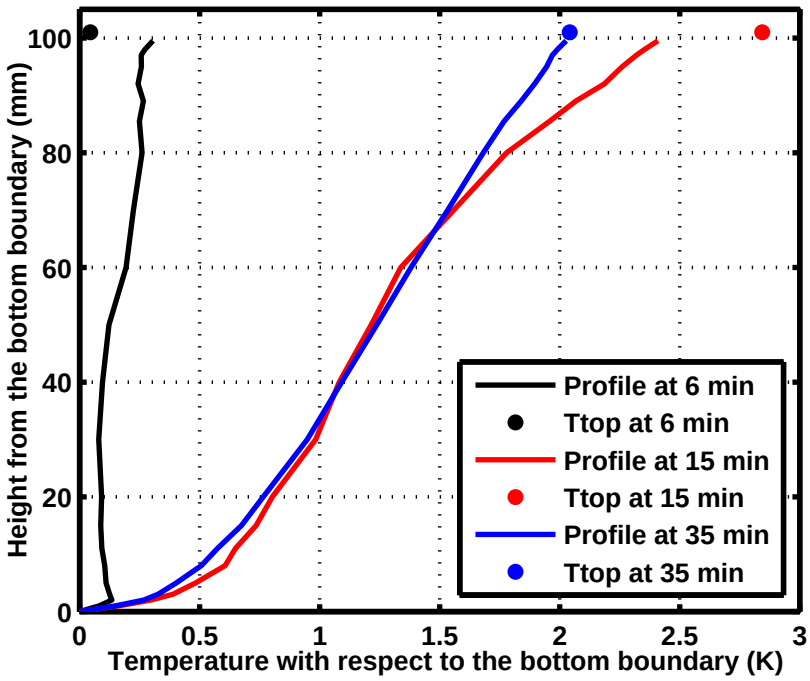

Figure 4.7: Profiles at different times for the case with high T_{sky} and a stable stratification in the test section. 'S' shaped profile similar to that is obtained with radiative heating near the bottom and cooling near the top of the test section.

difference in the test section. As T_{sky} slowly decreased, value of *slip* decreased, and eventually became zero at about 35 minutes.

4.3.2 Effect of radiative boundary condition

To observe the dramatic effect of radiation on the phenomenon, an experiment was performed in which as usual, a lifted minimum was obtained by maintaining a low T_{sky}. After the minimum had reached a more or less steady state, a large sheet of thermocole was inserted below the outer ceiling, but outside the air circulation section, so as to cut off the radiative interaction between the test section and the outer ceiling. After a short interval, this sheet was removed. The results of this run are shown in figure 4.8. The obstructing sheet was inserted at around 89 minutes.

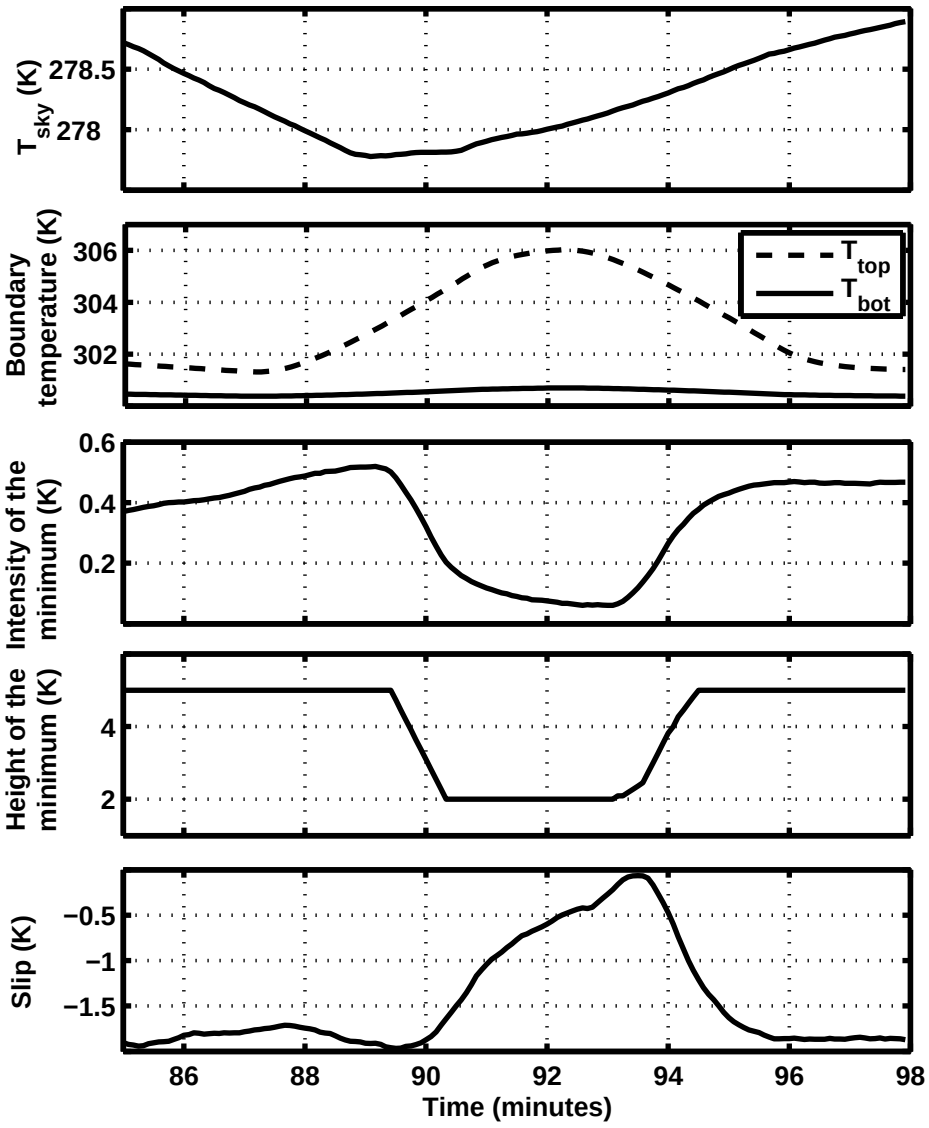

Figure 4.8: Time series data from an experimental run during which an opaque sheet was inserted just below the ceiling to cut off the radiation exchange with the test section. The sheet was inserted at 89 minutes upon which both the height and intensity of the minimum started decreasing. After the sheet was removed at 93.5 minutes, the intensify and height slowly build up again. T_{air} = 325 - 329 K.

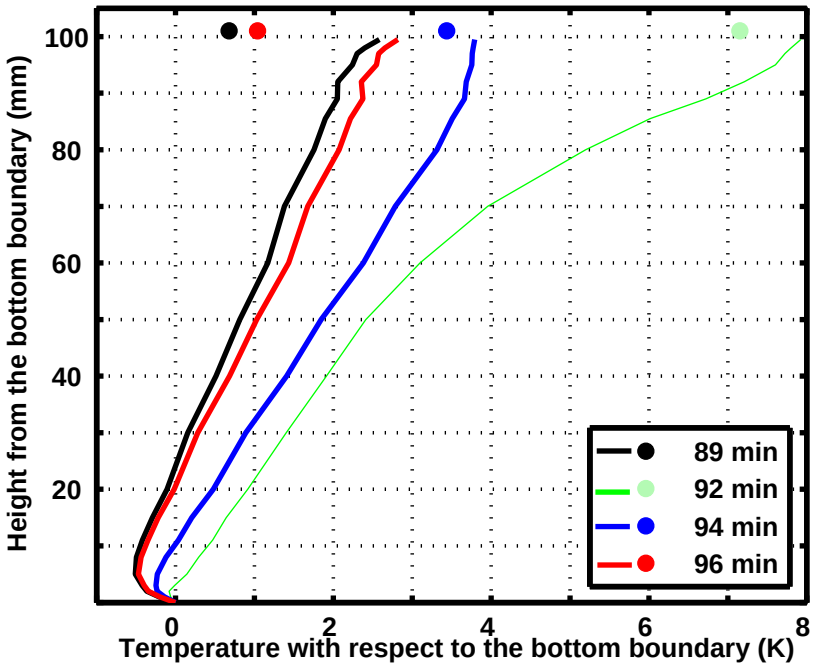

Figure 4.9: Profiles at different times for the experimental run in which an opaque sheet was inserted below the ceiling to cut of the radiation exchange with the test section. T_{sky} = 278 K, T_{air} = 325 - 329 K.

Immediately, both the height and intensity of the minimum started decreasing. The temperature jump at the top boundary of the test section also decreased rapidly, till it became zero at about 93.5 minutes. As the top ceiling was blocked both convectively and radiatively from the air circulation region, the temperature in that region increased, resulting in an increase in T_{top}. At 93.5 minutes, the obstruction was removed. Immediately, the height, intensity of the minimum as well as *slip* started increasing in magnitude. The height of the minimum regained its previous value within a minute, while the intensity and *slip* take a little more than a couple of minutes to regain their former values. The fact that the intensity was slightly less than its former value (before the radiative blocking) was due to the fact that by this time, T_{sky} had increased a bit. A few sample profiles in this period

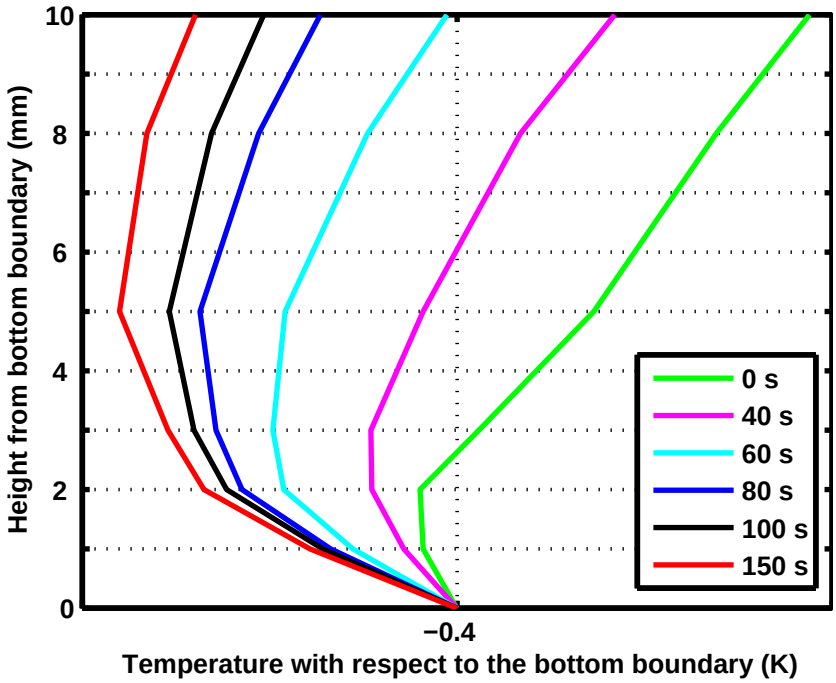

Figure 4.10: Near surface (below 1cm) profiles for the experiment in which an opaque sheet was inserted below the ceiling to cut of the radiation exchange with the test section. The profiles are shown at several instants after the obstructing sheet was removed showing the increase in height and intensity of the minimum.

showing the intensity and height of the minimum, as well as the temperature jump, are shown in figure 4.9. A closer view of the rapid reemergence of the minimum is shown in figure 4.10. In this figure, the time $t = 0$ seconds represents the time at which the thermocole sheet was removed.

4.3.3 Effect of a 'gust'

Another experiment was done in which, at first a lifted minimum was obtained. Then, a fan, placed near the edge within the test section, was turned on, kept running for a while, and then switched off. The results, shown in figure 4.11, indicate a rapid reemergence of the minimum. However, unlike the previous case

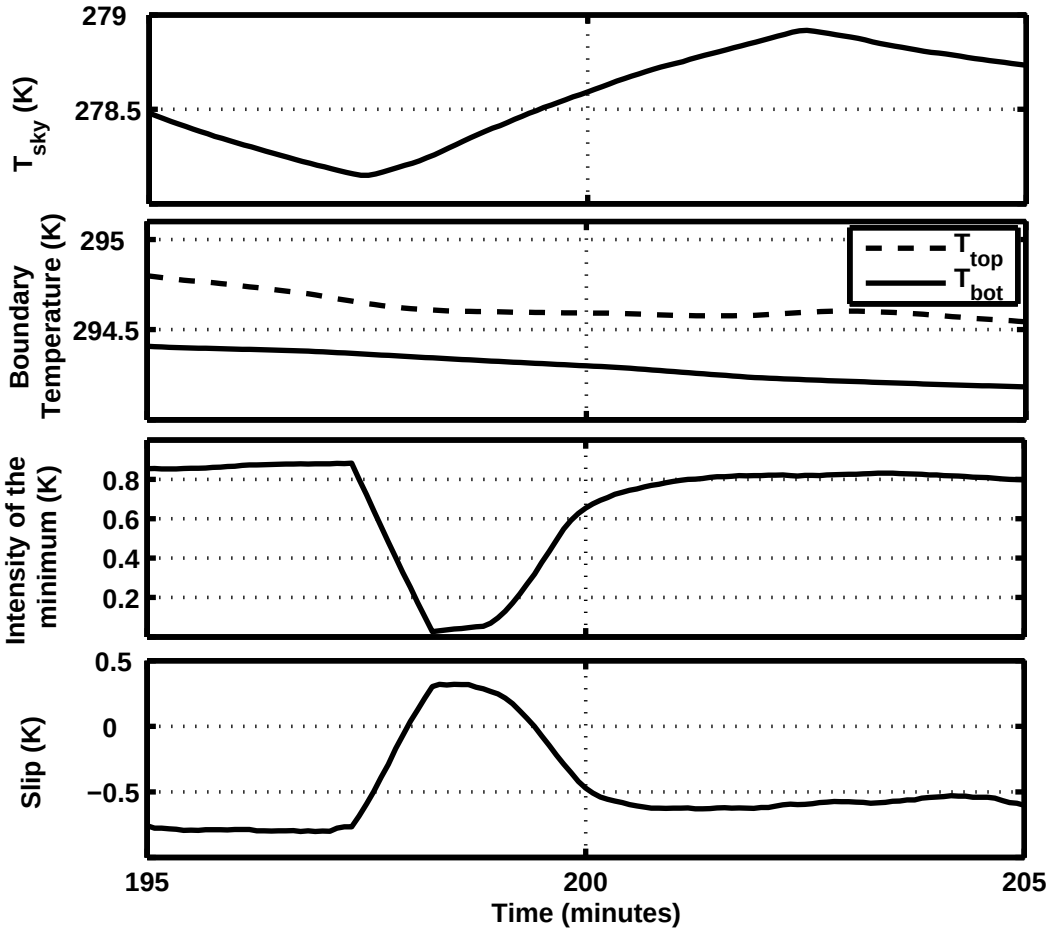

Figure 4.11: Time series data from the experimental run in which a fan was turned on for a while in the test section to cause mixing. The fan was switched on at about 197.5 minutes, whereupon the minimum was rapidly destroyed. It reemerged rapidly when the fan was switched off at about 199 minutes. T_{air} = 305 - 310 K

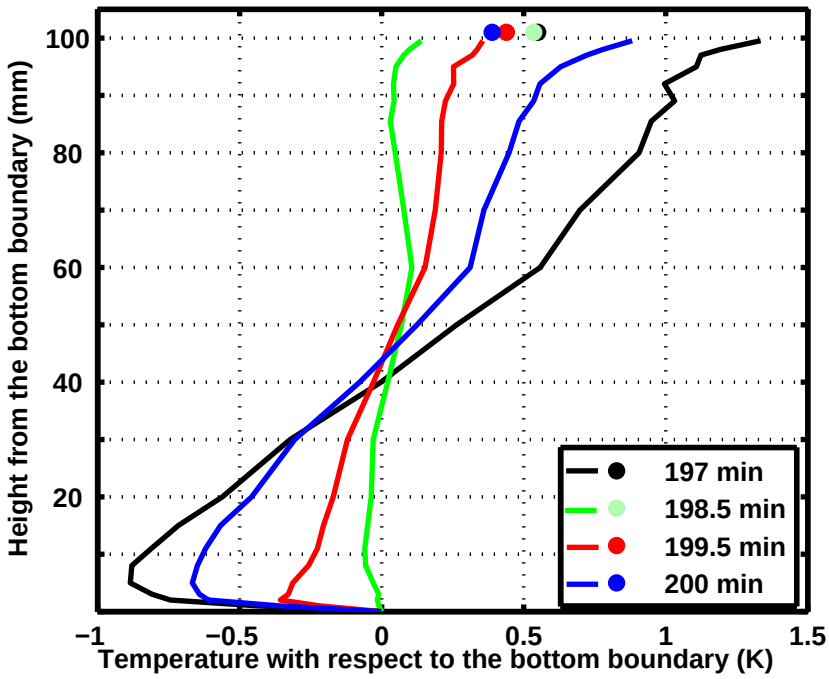

Figure 4.12: Profiles from the experimental run in which a fan was turned on for a while in the test section to cause mixing. $T_{sky} =$ 278 K, $T_{air} =$ 305 - 310 K

discussed in which the radiation is cut off, here, T_{top} is not affected, and hence when the fan is turned on, an almost isothermal profile is reached. Profiles at selected times corresponding to this experimental run are shown in figure 4.12.

4.3.4 Effect of emissivity

Some preliminary experiments were also done to study the effect of 'ground' emissivity on the lifted minimum. In the cases discussed so far, the bottom surface is anodized aluminium, with an emissivity of about 0.5, which for the present purposes, we shall refer to as a 'high emissivity' surface. For the low emissivity or reflective case, aluminium foil was spread over this plate, with a thin layer of oil between them to ensure good thermal contact. This resulted in a bottom boundary with a low emissivity of about 0.04. This surface shall be referred to as a 'low

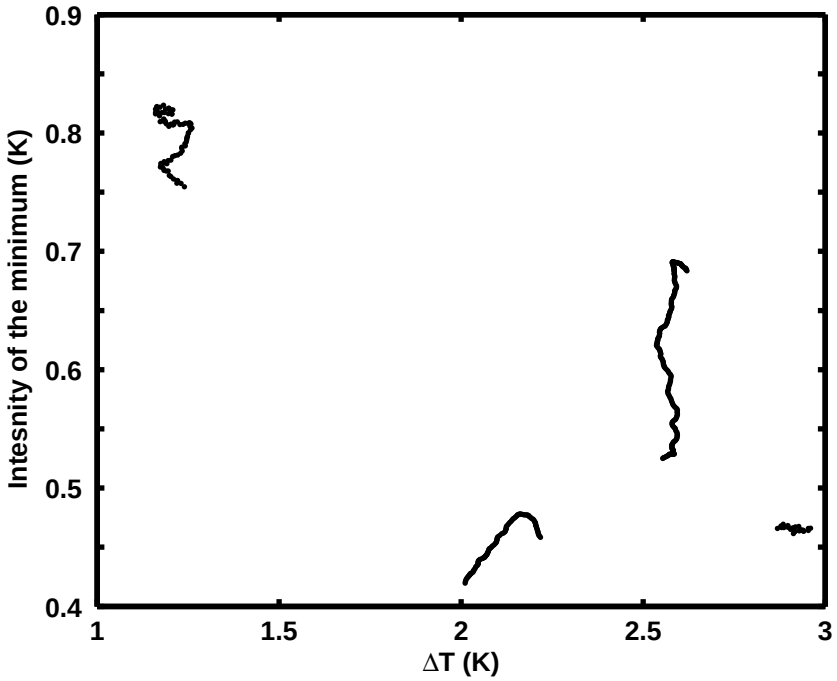

Figure 4.13: Plot showing the dependence of the intensity of the minimum on ΔT = T_{top} - T_{bot}. Each 'island' of points is from a separate experimental run. The intensity increases with decreasing ΔT. This is to be expected as a lower ΔT would imply a lower conductive flux, allowing for a stronger effect of radiation. The spread observed in each run is due to the effect of T_{sky}, which is not quite constant in an experimental run.

emissivity' surface. Before the effects of the low emissivity on the lifted minimum is discussed, a point must be discussed. In these preliminary experiments, there was no fine control over the temperatures. So, for example, as mentioned earlier, T_{sky} does not remain constant, and T_{top} tends to follow T_{sky}. Also whenever, in an effort to keep the value of T_{sky} within a small range, more ice is added to the outer ceiling or side walls, there is a sudden drop in T_{sky} (and T_{top}), along with a slower increase in intensity of the minimum. Again, because of this difficulty in finely controlling the temperatures, ΔT may not be the same in different experimental runs. Hence in order to compare the high and low emissivity cases, the main factors governing the lifted minimum must be understood so that a clear way to compare

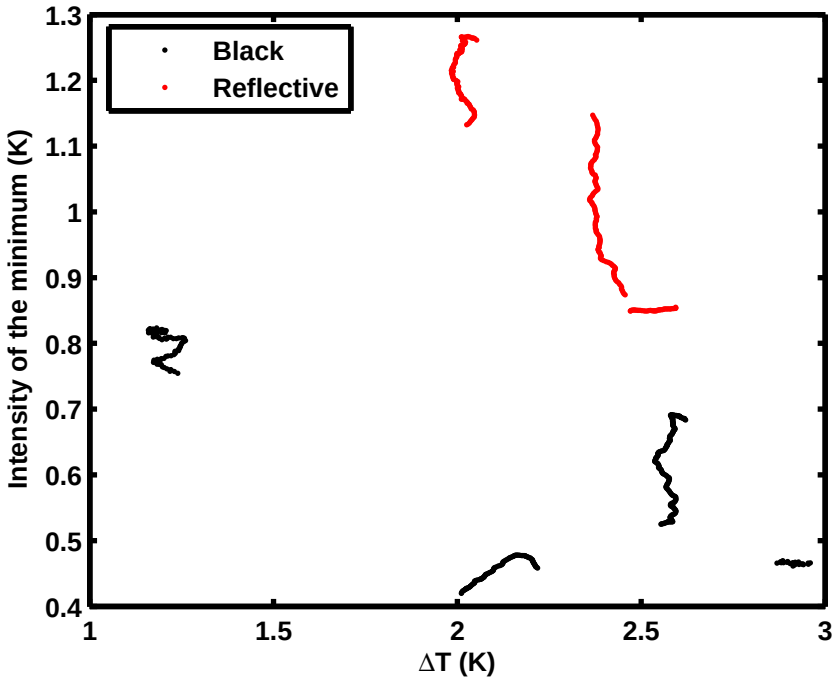

Figure 4.14: Plot showing the effect of emissivity on the intensity of the minimum. As in figure 4.13, intensity of the minimum is plotted against ΔT, with each 'island' of points representing a separate experimental run. The points in black are from runs with a non reflective surface, while the ones in red are from a reflective bottom surface. It is clear that for a given ΔT, the intensities are greater for the reflective case, in agreement with the field observations and the VSN model.

different runs may be established. This is done as follows: as mentioned before, by tweaking the power input to the heating unit, short times may be obtained in which T_{top} and hence ΔT does not change by more than 0.1-0.3 . Only such periods are selected for study. Within these periods, the time intervals just after adding ice in which there is a sudden change in T_{sky} and T_{top} are also avoided. So, we are left with short time intervals (of order of 5 - 15 minutes) in which a quasi steady state is achieved for all the quantities. If the minimum in such periods across different runs is compared, it is observed that though the small changes in T_{sky} that may occur within the period do have a small effect on the intensity of the minimum, the variable ΔT has the strongest influence on the intensity of the

minimum. Now, the conductive flux just above the minimum will have a strong impact on the minimum, with larger fluxes being associated with weaker minima. As the profile above the minimum is almost linear, this flux is well approximated by the temperature difference between the minimum point and T_{top}, which in turn, for minimum values within a small range as we have in our experiments is some definite fraction of $\Delta T = T_{top}$ - T_{bot}. So, it is not surprising that ΔT has such a strong influence on the intensity of the minimum. Shown in figure 4.13 is the scatter plot of ΔT versus intensity of the minimum from different runs for the high emissivity surface only. As mentioned, only quasi steady state data is considered. The correlation between ΔT on the minimum is clear. The small spread within each data set is due to the influence of a changing T_{sky}. Now, shown in figure 4.14 is a similar scatter plot, but involving data from low as well as high emissivity surface. The data points from the high emissivity cases are as before, indicated in black, while the red points indicate the low emissivity case. It is abundantly clear that for a given ΔT, more intense minima are produced over the low emissivity surface, in agreement with field observations and the VSN model.

Summary

If the lifted minimum can be simulated in the laboratory, it would allow for a more systematic study than possible through field observations alone.

In order to simulate the lifted minimum in the laboratory, a set up was fabricated which can mimic, in a basic way, the conditions under which the lifted minimum. A decoupling of the conduction/convection boundary conditions, similar to that occurring in the nocturnal surface layer, was a crucial feature of the set up. This allows one to have a stable temperature profile in a horizontal layer of

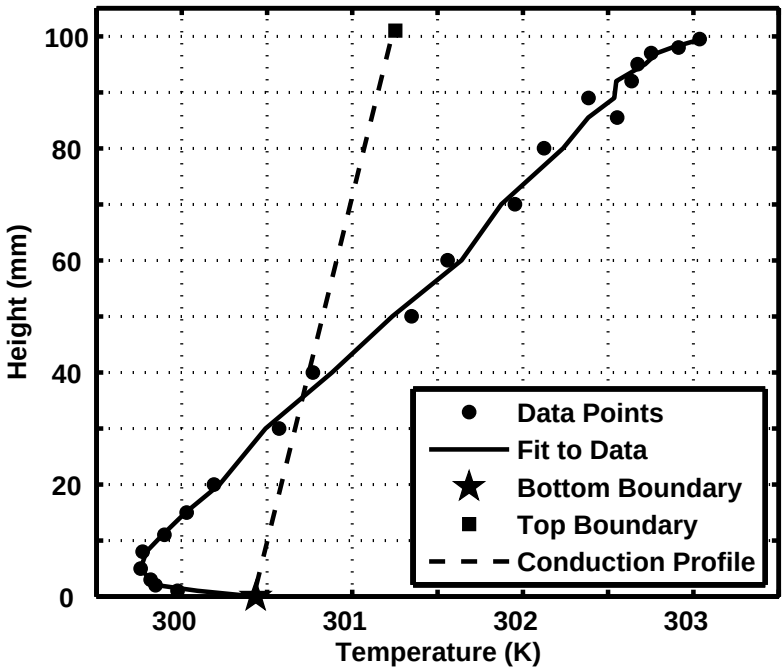

Figure 4.15: Temperature profile obtained in the laboratory showing the lifted minimum

gas, and yet have radiative cooling near the bottom boundary, which is necessary to produce a lifted minimum profile. The decoupling also allows one to have a stronger radiative effect on the base profiles (conductive or convective) than otherwise possible. This set up can be used to investigate fairly general problems concerning the effect of radiation on other forms of heat transfer. However, the present work is chiefly concerned with reproducing the lifted minimum.

Using appropriate boundary conditions in this set up, a lifted minimum profile was obtained in the laboratory. A typical laboratory profile is shown in figure 4.15. The profile was essentially a distortion of the linear, conductive profile due to radiative effects. The maximum deviation from the linear profile was much greater than reported in the literature on similar conduction-radiation experiments. A lower emissivity for the bottom boundary resulted in minima with higher intensi-

ties. This is consistent with the field observations as well as the predictions of the VSN model.

CHAPTER 5

CONCLUSIONS

The phenomenon called the 'Lifted Temperature Minimum' was investigated through field observations as well as laboratory simulations.

The field observations were carried out over four surfaces: (1) a surface with high emissivity and low cooling rate(2) a surface with low emissivity and low cooling rate, (3) a surface with high emissivity and high cooling rate, and (4) a surface with low emissivity and high cooling rate. In addition to observations of the vertical temperature profile, wind speed, humidity and net radiation were monitored.

The observations showed that wind speed and turbulence levels have a strong effect on the minimum, with the intensity of the minimum decreasing with an increase in either of these variables. However, even with the highest winds encountered during the observations (well above 2 m/s at a height of 20 cm above the ground), the lifted minimum persisted, though with a low intensity, and was not replaced by an inversion. The magnitude of temperature gradients just above the surface during a lifted minimum is surprisingly high. Typically, the magnitude of the gradients increase with increasing intensity of the minimum, and for low wind speeds, it is of the same order of magnitude as that of typical daytime gradients.

Minima with very high intensities (up to 13 °C) were obtained over the low emissivity, low cooling rate surface. Thus, lowering the surface emissivity results in an increase in the intensity of the minimum from about 6 °C to about 12 °C under low wind conditions. The near surface gradients were also higher than the baseline case.

Observations on the high emissivity, high cooling rate surface showed that,

typically, the lifted minimum was replaced by an inversion profile, in which the minimum temperature occurs on the ground. Under conditions of exceptionally low wind and turbulence levels, a minimum did form, but both its height and intensity were very small as compared to the baseline case.

Minima obtained over the low emissivity, high cooling rate surface had intensities slightly lower than the baseline case.

It was found that, for a given surface, a simple function involving only the average wind speed and standard deviation of the wind speed, was able to predict a suitably normalized intensity of the minimum that agreed well with observations. The normalization was done by dividing the intensities of the minimum obtained during an observational run, by the intensity observed at the beginning of that run. A comparison of the formulae showed that the intensity of the minimum obtained on the low emissivity, low cooling rate surface showed a lower dependence on wind speed that that obtained on the high emissivity, low cooling rate surface.

Thus, both the surface emissivity, as well as the surface cooling rate influences the phenomenon. The intensity of the minimum is strongly influenced by both these parameters. On the other hand, the height of the minimum strongly depends on the ground cooling rate, but is not affected much by the surface emissivity.

These results were compared with the VSN model (broad band flux emissivity model) and a band model that made predictions about the lifted minimum. The VSN model predicts that as the surface emissivity decreases, the intensity of the minimum should increase, though the height of the minimum is not affected much (except for emissivity values close to unity). An increase in ground cooling rate, on the other hand, reduces both the height and intensity of the minimum. Thus, the observations are qualitatively in agreement with the VSN model, though the model seems to slightly underestimate the intensity of the minimum. The band

model on the other hand, in spite of using a more refined model for the radiation, grossly underestimates the intensity of the minimum.

From the heat equation, and temperature data obtained during low wind conditions, the near surface radiative flux divergence was estimated. Expressed as a radiative cooling rate, the flux divergence just above the surface for the baseline case (concrete surface) was about 1 K/s. The radiative divergence rapidly decreases with height and is practically zero at heights of more than a few centimeters above the ground. The estimates thus obtained are almost two orders of magnitude higher than that predicted by the VSN model, while the height below which the divergence is significant, is lower than the predictions of the VSN model by about one order of magnitude. This probably accounts for the fact that the VSN model predicts lifted minima with slightly lower intensities and significantly lower near surface temperature gradients than that observed.

To simulate the lifted minimum in the laboratory, a set up was designed to mimic to the extent possible, the conditions under which the lifted minimum occurs in the field. An important feature of the set up is the decoupling of the radiation and conduction/convection boundary conditions, similar to that effected by the inversion at night. This decoupling allows one to maintain a stable temperature profile (temperature increasing with height) in a horizontal layer of gas, and yet have radiative cooling at the bottom of the layer, which is necessary to produce a lifted minimum. The decoupling also enables one to obtain a stronger effect of radiation on the base profiles than would be otherwise possible. Though the initial motivation was to simulate the lifted minimum in the laboratory, this set up can be used to study a wide range of problems involving the effect of radiation on conduction or convection.

Lifted minimum profiles were obtained as a deviation from a stable, linear

conduction profile, due to the effect of radiation. The experiments show a 'cold' radiative source is necessary for the formation of a lifted minimum. The deviation from the linear profile obtained was greater than previously obtained in such experiments. It was also found that a lower emissivity for the bottom boundary results in a more intense minimum, in agreement with field observations.

Appendices

A Relation between radiation and radiation sensor voltage

As far as heat transfer is concerned, the net radiation sensor, can be considered to be a one dimensional system, which is a very good approximation, except near the edges of the sensing element. Figure A-1 shows a schematic of the sensor. T_t and T_b are the temperatures of the top and bottom surfaces respectively of the thermopile (thermoelectric module). T_a is the ambient temperature. The polyethylene window is at a distance ℓ from the sensor surface (for both the upper and lower surfaces). k and λ are respectively the thermal conductivity of the thermoelectric module and air respectively. R$\downarrow$ and R$\uparrow$ are respectively the down welling and upwelling radiation, and $R_{net} \equiv R\uparrow - R\downarrow$.

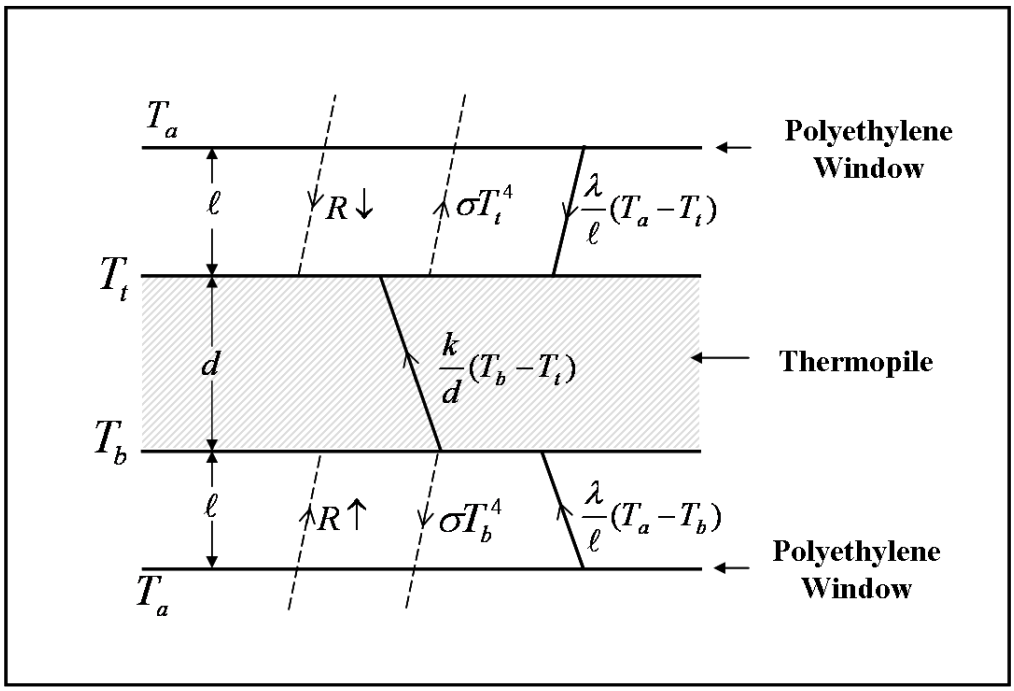

Figure A-1: Schematic of the radiation sensor indicating the heat fluxes involved in the energy balance.

In equilibrium, the energy balance for the upper surface of the sensor reads

$$R\downarrow + \frac{\lambda}{\ell}(T_a - T_t) + \frac{k}{d}(T_b - T_t) = \sigma T_t^4 \tag{A-1}$$

Similarly, the energy balance of the lower surface is

$$R\uparrow + \frac{\lambda}{\ell}(T_a - T_b) + \frac{k}{d}(T_b - T_t) = \sigma T_b^4 \tag{A-2}$$

Subtracting equation (A-1) from (A-2),

$$R_{net} \equiv (R\uparrow - R\downarrow) = \sigma(T_b^4 - T_t^4) + \frac{2k}{d}(T_b - T_t) + \frac{\lambda}{\ell}(T_b - T_t) \tag{A-3}$$

$\triangle T \equiv (T_b - T_t)$ is at most a few tenths of a Kelvin for usual values of net radiation, and hence is very small compared to T_t or T_b. Hence, we may use the approximation $T_b^4 - T_t^4 \simeq 4T_t^3 \triangle T$ in equation (A-3) to get

$$R_{net} = \triangle T(\frac{2k}{d} + \frac{\lambda}{\ell} + 4\sigma T_t^3) \tag{A-4}$$

Now, $2k/d$ is greater than 850 W/m^2K for both the thermoelectric modules, whereas λ/ℓ is around 9 W/m^2K , and $4\sigma T_t^3$ is less than 6.5 W/m^2K (for T_t less than 30°C). So, to a very good approximation,

$$R_{net} = \frac{2k}{d}\triangle T \tag{A-5}$$

Now,

$$S \propto \triangle T$$

$$\therefore S = C' \triangle T \tag{A-6}$$

where S is the Seebeck voltage developed across the module, and $\triangle T$ is the temperature difference across the module. C' is a constant of proportionality which depends on the Seebeck coefficient for each thermocouple and the number of thermocouple junctions. Using equation (A-5) in equation (A-6), we have

$$S = C' \frac{d}{2k} R_{net}$$

or

$$S = C R_{net} \tag{A-7}$$

Here C is the calibration constant for a given net radiometer.

Now, in the above derivation, it has been assumed that the ambient temperature at the lower and upper surfaces of the sensor is the same. This may not be true very close the ground (heights lower than 5 cm) in a lifted minimum, as the near surface gradients can be large. it has also been assumed that the polyethylene windows are at precisely the same distance from the upper and lower surfaces of the sensing element. Though the sensor has been constructed to have these distances equal, small differences in these distances can lead to an additional error in the net radiation measurements. To see these effects, the above derivation can be carried through making allowance for changing ambient temperature and slight differences in the distances of the two polyethylene windows from the respective surfaces of the sensing element. Instead of equation (A-4), we get

$$R_{net} = [\triangle T(\frac{2k}{d} + \frac{\lambda}{\ell} + 4\sigma T_b^3)] + [(\frac{\lambda}{\ell})(\frac{\delta}{\ell})(T_s - T_{ab})] + [\frac{\lambda}{\ell}E] \qquad \text{(A-8)}$$

Here(refer figure),

T_{at} is the ambient temperature just above the upper surface of the sensor and T_{ab} is the ambient temperature just below the lower surface of the sensor.

$$T_{at} - T_{ab} \equiv E$$

$$T_s = \frac{(T_B + T_t)}{2}$$

ℓ_t and ℓ_b are the distances of the upper and lower polyethylene windows respectively from the corresponding surfaces of the sensing element. Also,

$$\ell \equiv \frac{\ell_t + \ell_b}{2}$$

$$\delta \equiv \epsilon/2$$

,

Now, in equation(A-8), the term in the first square brackets is the same as that on the right hand side of(A-4). But there are two more terms (second and third square brackets). Now, δ for the sensor is better than 0.1 mm. Hence, $\delta/\ell \sim 0.034$. Hence, $(\lambda/\ell)(\delta/\ell) \sim 0.34$. $T_s - T_{amb}$ is around ± 4°C for the range of downwelling and upwelling radiation encountered in the tropics, and does not depend strongly on the ambient temperature. Hence, the term in the second square brackets is negligible ($\sim \pm$ 1.5 W/m^2). It also not change much with height (due to weak dependence on ambient temperature), and hence at worst it is an offset in the radiation profile measurements. The last term in square brackets, however

is not so straightforward. In a lifted minimum, $E = T_{at} - T_{ab}$, the difference in ambient temperatures across the sensor, is not constant with height and can be quite high near the ground surface, where temperature gradients are large. The difference across the sensor can be as high as 0.5°C at a height of 1 cm. above the ground, falling to about 0.3°C at 2 cm., 0.1°C at 3 cm. and negligible for greater heights. Hence the last term in square brackets will lead to an underestimation of the net radiation by about $5W/m^2$ at a height of 1 cm, $3W/m^2$ a a height of 2 cm., $1W/m^2$ at a height of 3 cm. and negligible thereafter. Hence, this can give rise to a spurious radiative flux divergence. The error due to this term does will not significantly affect the radiative flux profile measurements if the lowest traverse point is not too close to the ground (less than 2-3 cm.). In any case, the error arising due to this term must be borne in mind while interpreting radiative profile measurements using the described sensors in lifted minimum conditions.

B Radiation Sensor Calibration

As no standard facility to calibrate the radiation sensors was available, they were calibrated in a simple and direct way in our laboratory. In this appendix, the set up and procedure used to calibrate the radiation sensors is described.

A shallow, rectangular tray (about 45 cm by 45 cm), was positioned horizontally, a few feet above the laboratory floor. The underside of the tray was painted with black matte paint (with an emissivity of 0.9). The net radiometer was placed horizontally (parallel to the tray and floor surface), at some fixed distance below the tray (in the range of 5 to 20 cm), with the edges of the radiometer parallel to the edges of the tray. Hot water was poured into the tray. The temperature of the tray bottom was monitored by means of two thermocouples (with flattened beads, of the type used for ground temperature measurements in the field), stuck at different places on the underside of the tray.

Now, equation (A-7) reads

$$S = CR_{net}$$

where C is the radiometer specific calibration constant which is to be determined.

This may be rewritten as

$$S = C(R_{tray} + R_{else})$$

Here R_{tray} is the radiative flux from the tray bottom alone which is received by the sensor, and R_{else} is the radiative flux received by the sensor from everywhere else except the tray bottom

$$S = CR_{tray} + K \tag{B-1}$$

where

$$K = CR_{else}$$

Knowing the emissivities of the tray bottom and the sensor, the view factor between the sensor and the tray bottom, and the temperature of the tray, a good approximation to R_{tray} can be calculated. As the tray cools, R_{tray} keeps decreasing. Over the time of the experiment, R_{else} and hence K remains constant. Hence, the slope of a plot of S versus R_{tray} will yield the calibration constant C, assuming that the response is reasonably linear over the range of the experiment. Figure A-2 shows one such plot for a calibration experiment involving the bigger net radiation sensor. The sensor was placed 20 cm. below the bottom of the tray. A least squares linear fit (red line) shows that the response is reasonably linear (over the range of radiative fluxes in the experiment), yielding a calibration constant of 69 $\mu V/(W/m^2)$. Many calibration runs for each sensor were carried out with the sensors at different horizontal and vertical positions below the tray, and under different ambient temperature conditions. The result was that both the net radiation sensors were linear over the radiative flux range of our interest, with the calibration constants being 70 $\pm 3 W/m^2$ and 20 $\pm 3 W/m^2$ for the bigger and smaller sensors respectively.

As measurement of the radiative flux profile involves measuring *changes* in net radiation, rather than absolute values of the flux, this calibration method was deemed to be sufficient for the purpose.

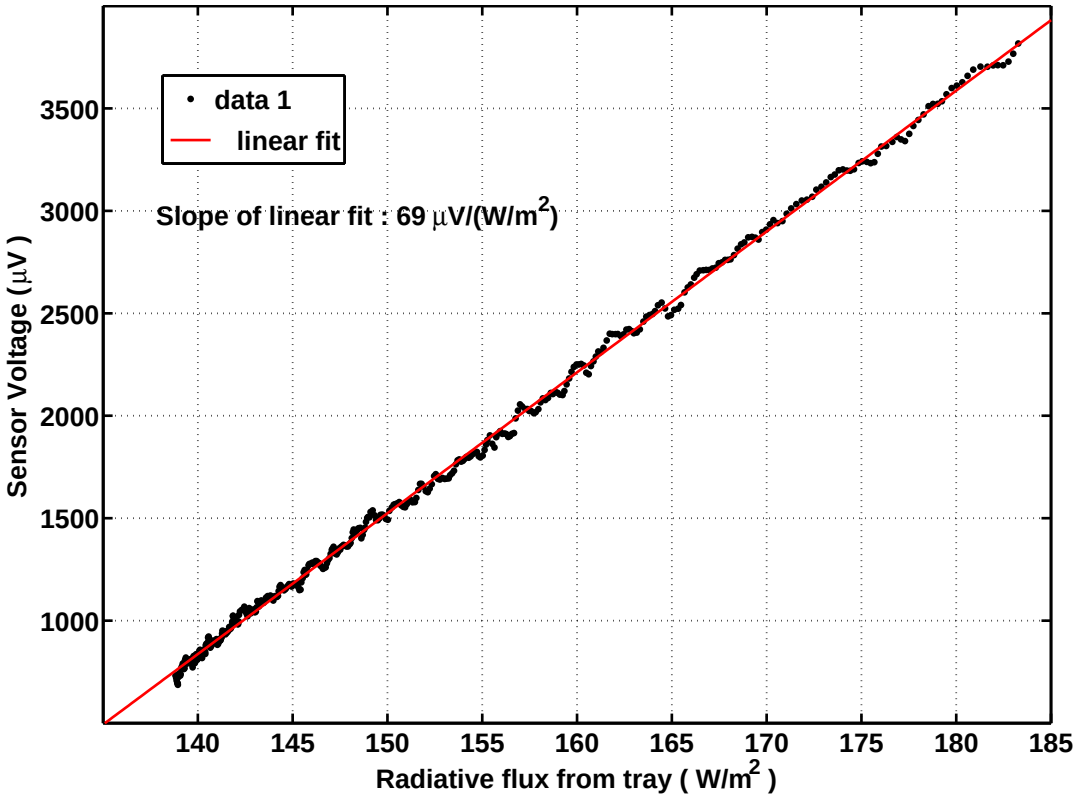

Figure A-2: A plot of sensor voltage versus radiative flux obtained from a single calibration run. The linear fit to the data is also shown.

References

Albani, F. 1951 Investigaciones sobre la distribución vertical de las temp. minimas en las capas de aire próximas al suelo. *Arch. Fitotécnico del Uruguay* **4**, 361–376.

Arpaci, V. S. & Gozum, D. 1973 Thermal stability of radiating fluids: the benard problem. *Physics of Fluids* **16** (5), 581–588.

Aschwanden, M. J. 2004 *Physics of the solar corona: an introduction*. Springer.

Brawand, H. & Kohnke, H. 1952 Micro-climate and water vapour exchange at the soil surface. *Proc. Soil Sci. Soc. Amer.* **16**, 195–198.

Brunt, D. 1941 *Physical and dynamical meteorology*. Cambridge University Press.

Christophorides, C. & Davis, S. H. 1970 The convective instability in a radiating fluid layer. *Physics of Fluids* **13** (2), 222–226.

Coantic, M. & Seguin, B. 1971 On the interaction of turbulent and radiative transfer in the surface layer. *Boundary Layer Meteorology* **3**, 152–177.

Crosbie, A. L. & Viskanta, R. 1971 Interaction of heat transfer by conduction and radiation in a nongray planar medium. *Warme und Stoffubertragung* **4**, 205–212.

Fleagle, R. G. & Badgley, F. I. 1952 The nocturnal cold layer. Atmospheric turbulence study at45-1. University of Washington.

Fritschen, L. J. & Gay, L. W. 1979 *Environmental Instrumentation*. Springer-Verlag.

Funk, J. P. 1960 Behaviour of freely exposed absobers in radiation fields. *J. Opt. Soc. Amer.* **50** (10), p.986.

Garratt, J. R. 1995 Observed screen (air) and gcm surface/screen temperatures: Implications for outgoing longwave fluxes at the surface. *J. Climate* **8**, 1360–1368.

Gille, J. & Goody, R. M. 1964 Convection in a radiating gas. *J. Fluid Mech.* **20** (1), 47–49.

Goody, R. M. 1956 The influence of radiative transfer on cellular convection. *J. Fluid Mech.* **1**, 424–435.

Hutchinson, J. E. & Richards, R. F. 1999 Effect of nongray gas radiation on thermal stability in carbon dioxide. *Journal of thermophysics and heat transfer* **13** (1).

Jenny, J. 1953 *Schweitz Gartnerztg* **56** (2).

Kondo, J. 1971 Effect of radiative heat transfer on profiles of wind, temperature and water vapour in the atmospheric boundary layer. *J. Met. Soc. Japan* **9**, 75–94.

Kondratyev, K, Y. 1972 *Radiation processes in the atmosphere*. WMO Note 359.

Lake, J. V. 1956a The temperature profile above bare soil on clear nights. *Q. Jl. R. Met. Soc.* **82**, 187–197.

Lake, J. V. 1956b Discussion on the paper of lake. *Q. Jl. R. Met. Soc.* **82**, 530–531.

Lettau, H. H. 1979 Wind and temperature profile prediction for diabatic surface layers including strong inversion cases. *Boundary Layer Meteorology* **17**, 443–464.

Liou, K. N. 1980 *An introduction to atmospheric radiation*. Academic Press.

Lützke, R. 1960 Unter welchen bedingungen hebt sich das nachtliche, temperatur minimum von der bodenoberflache ab? *Anggewandte Met.* **4**, 1–10.

Narasimha, R. & Vasudeva Murthy, A. S. 1995 The energy balance in the ramdas layer. *Boundary Layer Meteorology* **76**, 307–321.

Nijliks, H. & Moldau, H. 1960 On the nocturnal temperature minium over natural surfaces. In *Studies in Atm. Phy.*. Inst. Atm. Phy. Acad. Sci. Estonia S. S. R.

Novotny, J. L. & Olsofka, F. A. 1970 The influence of a non-absorbing gas in a raddiation-conduction interaction. In *AIAA 5th Thermophysics Conference*.

Oke, T. R. 1970 The temperture profile near the ground on calm clear nights. *Q. Jl. R. Met. Soc.* **96**, 14–23.

Ragothaman, S., Narasimha, R. & Vasudeva Murthy, A. S. 2001 The dynamical behaviour of the lifted temperature minimum. *Il Nuovo Cimento* **24C**, 353–375.

Ragothaman, S., Narasimha, R. & Vasudeva Murthy, A. S. 2002 Evolution of nocturnal temperature inversions - a numerical study. *Il Nuovo Cimento* **25C**, 147–163.

Ramanathan, K. R. & Ramdas, L. A. 1935 Derivation of angstorm's formula for atmospheric radiation and some general considerations regarding nocturnal cooling of air layers near the ground. *Proc. Ind. Acad. Sci.* **1**, 822–829.

Ramdas, L. A. & Atmanathan, S. 1932 The vertical distribution of air temperature near the ground at night. *Beit. Zur Geophys.* **37**, 116–117.

Ramdas, L. A. & Malurkar, S. L. 1932 Theory of extremely high lapse rates of temeprature very near the ground. *Ind. J. Phys.* **6**, 495–508.

Raschke, K. 1954 A sturdy thermoelectric psychrometer for microclimatic measurements. *Proc. Ind. Acad. Sci.* **39 A**, 98–107.

Raschke, K. 1957 Über das nächtliche temperaturminimum über nackten boden in poona. *Met. Rundschau.* **10**, 1–11.

Savitzky, A. & Golay, M. J. E. 1964 Smoothing and differentiation of data by simplified least squares procedures. *Anal. Chem.* **36**, 1627–1639.

Schimmel, W. P., N. J. L. & Olsofka, F. A. 1970 Interferometric study of radiation-conduction interaction. In *Proceedings of the 4th International Heat Transfer Conference*, , vol. 3. Elsevier.

Soufiani, A., H. J. M. & Taine, J. 1985 Validity of band model calculations for co_2 and h_2o applied to radiative properties and condcutive-radiative transfer. *Journal of quantitative spectroscopy and radiative transfer* **33** (3).

Szakály, J. 1957 Temperature minimum above the bare soil during the night. *Idöjárás* **61**, 31–82.

Tiwari, P. 2006 laboratory simulation of lifted temeprature minimum.

Varghese, S. 2003b Band model computation of near-surface logwave fluxes. PhD thesis, Jawaharlal Nehru Centre for Advanced Scientific Research, Bangalore, India.

Varghese, S., Vasudeva Murthy, A. S. & Narasimha, R. 2003a A fast, accurate method of computing near-surface logwave fluxes and cooling rates in the atmosphere. *J. Atmos. Sci.* **60**, 2869–2886.

Vasudeva Murthy, A. S., Srinivasan, J. & Narasimha, R. 1993 A theory of the lifted temperature minimum on calm clear nights. *Phil. Trans. R. Soc. Lond.* **344A**, 183–206.

Warner, J. X. & Ellingson, R. G. 2000 A new band radiation model for water vapour absorption. *J. Atmos. Sci.* **57**, 1481–1496.

Yamada, M. & Takahashi, H. 2004 Frost damage to *Hemerocallis esculenta* in a mire: relationship between flower bud height and air temperature profile during calm, clear nights. *Can. J. Bot.* **82**, 409–419.

Zdunkowski, W. 1966 The nocturnal temperature minimum above the ground. *Beitr. Phys. Atmos.*. **39**, 247–253.